

THE ROLE OF CUMULUS CONVECTION  
IN THE  
DEVELOPMENT OF EXTRATROPICAL CYCLONES

by

MARTIN STEVEN TRACTON

B. S., University of Massachusetts  
(1966)

S. M., Massachusetts Institute of Technology  
(1969)

SUBMITTED IN  
PARTIAL FULFILLMENT  
OF THE REQUIREMENTS FOR THE  
DEGREE OF DOCTOR OF PHILOSOPHY

at the  
MASSACHUSETTS INSTITUTE OF  
TECHNOLOGY

May, 1972

Signature of Author . . . . .

Department of Meteorology, May 5, 1972

Certified by . . . . .

Thesis Supervisor

Accepted by . . . . .

Chairman, Departmental Committee  
on Graduate Students

<sup>Lindgren</sup>  
**WITHDRAWN  
FROM  
MIT LIBRARIES**  
1972



Room 14-0551  
77 Massachusetts Avenue  
Cambridge, MA 02139  
Ph: 617.253.5668 Fax: 617.253.1690  
Email: docs@mit.edu  
<http://libraries.mit.edu/docs>

## **DISCLAIMER OF QUALITY**

Due to the condition of the original material, there are unavoidable flaws in this reproduction. We have made every effort possible to provide you with the best copy available. If you are dissatisfied with this product and find it unusable, please contact Document Services as soon as possible.

Thank you.

**Some pages in the original document contain pictures, graphics, or text that is illegible.**

**Two pages numbered 61.**

THE ROLE OF CUMULUS CONVECTION  
IN THE  
DEVELOPMENT OF EXTRATROPICAL CYCLONES  
by  
MARTIN STEVEN TRACTON

Submitted to the Department of Meteorology on 5 May 1972  
in Partial Fulfillment of the Requirements for  
the Degree of Doctor of Philosophy.

ABSTRACT

The goal of this study is to determine whether cumulus convection plays a role in the development of extratropical cyclones, and if it does, to determine the nature of that role. The basic approach is to ascertain whether there is a systematic relationship between the observed extent and degree of convective activity accompanying cyclogenesis and the departure of actual storm evolution from that predicted by large-scale dynamic models.

On the basis of intensive analysis of the two storms initially chosen for study, the following hypothesis was formulated, and the balance of the investigation directed primarily towards ascertaining its validity:

In some instances of extratropical cyclogenesis, cumulus convection plays a crucial role in the initiation of development through the release of latent heat in the vicinity of the cyclone center. In such cases, dynamical models which do not adequately simulate convective precipitation, especially as it might occur in an environment that is unsaturated, will fail to properly forecast the onset of development.

Evidence either to support or refute the hypothesis was derived, in part, from detailed analysis of seven additional storms and cursory examination of twelve others. In addition, both qualitative and quantitative aspects of the physical mechanisms involved were considered. Although possibly not conclusive proof of the hypothesis, the evidence does indeed support it.

The case in support of the hypothesis is presented in terms of four arguments: i) in some storms, there was a coincidence in time between the initial development and the occurrence of convective showers in the vicinity of the low center. Almost invariably, the environment in which the convection occurred was unsaturated; ii) in those cases in which the initial development was

accompanied by convective showers in the vicinity of the low center and the environment in which the convection occurred was unsaturated, the dynamic prognoses systematically failed to properly forecast the onset of development, apparently because of the models' failure to predict the convective rainfall; iii) the importance of the latent heat release by cumulus convection to the initiation of development of some extratropical cyclones, which is implied by the apparent source of the systematic error, is physically plausible and quantitatively reasonable; and iv) there appears to be no defensible alternative explanation for the observed systematic error.

The nature of the error in predicting the initiation of cyclogenesis, namely, a lag in forecasting the time of the onset of development, suggests that the release of latent heat by cumulus convection initiates cyclogenesis, in some cases, prior to the time when it would occur if larger-scale motions and processes alone were operative.

Significant shower activity occurred in the center of storms generally only during the early phases of their life history. Convective activity which was not in the immediate vicinity of the low center did not appear crucial either to the initiation of development or to the trend of continued development following the onset of cyclogenesis.

Thesis Supervisor: Frederick Sanders  
Title: Professor of Meteorology

To my wife, Bette

## ACKNOWLEDGMENTS

The author gratefully acknowledges Professor James Austin and Dr. Pauline Austin for their advice and encouragement throughout his stay at M.I.T. Thanks are expressed also to the author's thesis adviser, Professor Frederick Sanders.

Special mention is given to Steven Ricci and Isabele Cole for their assistance in drafting the figures. In addition, the author extends his sincere appreciation to Dr. Robert Houze for his expert guidance in the final preparation of the figures. Thanks also go to the author's wife, Bette, for the typing of the manuscript.

Finally, but most appreciatively, the author acknowledges his wife for her love, patience, understanding (and typing skill), without which this thesis would not have been possible.

---

Financial support during the author's tenure at M.I.T. came in the form of an NSF Traineeship, a Teaching Assistantship, and a Research Assistantship supported in part by the National Severe Storms Laboratory (NOAA) Grant No. E22-22-70 (G) and by the National Science Foundation Grant No. A27908X.

TABLE OF CONTENTS

<u>TITLE</u>	1
<u>ABSTRACT</u>	2
<u>DEDICATION</u>	4
<u>ACKNOWLEDGMENTS</u>	5
<u>TABLE OF CONTENTS</u>	6
<u>LIST OF TABLES</u>	8
<u>LIST OF FIGURES</u>	9
<u>CHAPTER I. INTRODUCTION</u>	17
1a. Background and Statement of Problem	17
1b. Basic Approach	19
1c. Formulation of the Hypothesis	21
<u>CHAPTER II. METHODS OF ANALYSIS</u>	24
2a. Choice of Cases	24
2b. General Procedure	25
2c. Methods Utilized in Analysis of the Convective Activity	25
2d. General Aspects of the Models	32
2e. Suitability of the Models as Tools for this Investigation	36
2f. Evaluation of Forecasts	37
<u>CHAPTER III. ARGUMENTS I AND II: COINCIDENCE IN TIME BETWEEN CONVECTION AND INITIAL DEVELOPMENT; SYSTEMATIC ERROR IN THE NUMERICAL PROGNOSSES</u>	40
3a. Introduction	40
3b. Detailed Case Studies	45
3c. Results of cursory Examination of Twelve Additional Cases	61
<u>CHAPTER IV. ARGUMENT III: PHYSICAL PLAUSIBILITY AND QUANTITATIVE REASONABLENESS</u>	63
4a. Introduction	63
4b. Physical Plausibility	63
4c. Quantitative Reasonableness	66

<u>CHAPTER V.</u>	ARGUMENT IV: ALTERNATIVE SOURCES OF THE SYSTEMATIC ERROR	71
<u>CHAPTER VI.</u>	SUMMARY AND CONCLUSIONS	74
<u>TABLES</u>		80
<u>FIGURES</u>		85
<u>APPENDIX A.</u>	DETERMINATION OF THE INITIALIZED VALUES OF CENTRAL PRESSURE	146
<u>APPENDIX B.</u>	METHOD UTILIZED IN OBTAINING SOLUTIONS OF THE QUASI-GEOSTROPHIC OMEGA AND VORTICITY EQUATIONS	149
<u>BIOGRAPHICAL SKETCH</u>		154
<u>REFERENCES</u>		155



LIST OF TABLES

<u>Table</u>		<u>Page</u>
1	Symbols utilized in radar charts.	80
2	Models considered for the initial times relevant to the nine detailed case studies.	81
3	Characterization of the initial development of the nine detailed case studies.	82
4	Characterization of the initial development of the twelve storms for which a cursory examination was made.	83
5	Computed deepening rates.	84

## LIST OF FIGURES

<u>Figure</u>		<u>Page</u>
1	Location of hourly rainfall stations, tipping-bucket gauges, and weather radars.	85
2	Surface-radar chart, 4 Feb. 1971.	86
3	Precipitation cross sections for Charleston, S. C., and Pensacola, Fla., 11 Nov. 1968.	87
4	Surface-radar charts, 11 and 12 Nov. 1968.	88
5	Precipitation cross sections for New York, N. Y., 12 Nov. 1968, and Montgomery, Ala., 11 Nov. 1968.	89
6	Precipitation cross sections for Tulsa, Okla., and Lehigh, Okla., 4 Feb. 1971.	90
7	Horizontal domain of integration and the vertical structure of NMC-PE, FNWC-PE, and LFM operational forecast models.	91, 92
8	Surface-radar charts, 4 and 5 Feb. 1971.	93
9	Observed central pressure vs. time, 4-6 Feb. 1971.	94
10	Surface-mean relative humidity charts, 4 and 5 Feb. 1971.	94

<u>Figure</u>		<u>Page</u>
11	Precipitation cross sections for Tulsa, Okla., and Lehigh, Okla., 4 Feb. 1971.	95
12	Precipitation cross section for Springfield, Mo., 4 Feb. 1971.	95
13	Precipitation cross section for Memphis, Tennessee, 4-5 Feb. 1971.	96
14	Observed and forecast central pressure vs. time in terms of departure from initial value at 12Z 4 Feb. 1971.	97
15	FNWC-PE and NMC-PE 12-hour precipitation forecasted from 12Z 4 Feb. 1971.	97
16	Observed and forecast central pressure vs. time in terms of departure from initial value at 00Z 5 Feb. 1971.	98
17	FNWC-PE and NMC-PE 12-hour precipitation forecasted from 00Z 4 Feb. 1971, and 12-hour observed precipitation, 00Z - 12Z 5 Feb. 1971.	98
18	Surface-radar charts, 1 and 2 April 1970.	99
19	Observed central pressure vs. time, 1-3 April 1970.	100
20	Surface analyses, 1-2 April 1970.	101

<u>Figure</u>		<u>Page</u>
21	Tipping-bucket traces for Cairo, Ill., 1 April 1970; Evansville, Ind., 1-2 April 1970; and Louisville, Ky., 2 April 1970.	102
22	Surface-mean relative humidity charts, 1 and 2 April 1970.	103
23	Observed and forecast central pressure vs. time in terms of departure from initial values at 12Z 1 April 1970 and 00Z 2 April 1970.	104
24	NMC-PE 12-hour precipitation forecasted from 12Z 1 April 1970 and 00Z 2 April 1970.	105
25	Observed central pressure vs. time, 11-13 Nov. 1968.	106
26	Surface-radar charts, 11 and 12 Nov. 1968.	107
27	Precipitation cross section for Pensacola, Fla., 11 Nov. 1968.	108
28	Precipitation cross section for Bruns- wick, Ga., 11 Nov. 1968.	108
29	Precipitation cross section for Charleston, S. C., 11 Nov. 1968.	109

<u>Figure</u>		<u>Page</u>
30	Precipitation cross section for Cape Hatteras, N. C., 12 Nov. 1968.	109
31	Surface-mean relative humidity charts, 11 and 12 Nov. 1968.	110
32	Observed and forecast central pressure vs. time in terms of de- parture from initial values at 00Z and 12Z 11 Nov. 1968 and 00Z 12 Nov. 1968.	111, 112
33	NMC-PE 12-hour precipitation fore- casted from 00Z and 12Z 11 Nov. 1968 and 00Z 12 Nov. 1968.	113
34	Surface-radar charts; 2, 3 and 4 March 1971.	114
35	Observed central pressure vs. time, 2-4 March 1971.	115
36	Surface-mean relative humidity charts; 2, 3 and 4 March 1971.	115
37	Precipitation cross section for Macon, Ga., 3 March 1971.	116
38	NMC-PE 12- and 24-hour sea-level pressure charts generated from 12Z 2 March 1970.	117

<u>Figure</u>		<u>Page</u>
39	Observed and forecast central pressure vs. time in terms of departure from initial values at 12Z 2 March 1971, 00Z and 12Z 3 March 1971, and 00Z 4 March 1971.	118
40	NMC-PE 12-hour precipitation forecasted from 12Z 2 March 1971 and observed precipitation for 12Z 2 March to 00Z 3 March 1971; NMC-PE 12-hour precipitation forecasted from 00Z and 12Z 3 March 1971.	119
41	Surface analyses, 12 Feb. 1971.	120
42	Surface-radar charts, 12 Feb. 1971.	121
43	Precipitation cross section for Foreman, Ark., 12 Feb. 1971.	122
44	Surface-mean relative humidity charts, 12 and 13 Feb. 1971.	123
45	Observed central pressure vs. time, 12-14 Feb. 1971.	124
46	NMC-PE 12-hour sea-level pressure chart from 00Z 12 Feb. 1971 and verifying surface analysis.	125
47	NMC-PE 12-hour precipitation forecasted from 00Z 12 Feb. 1971.	126

<u>Figure</u>		<u>Page</u>
48	Observed and forecast central pressure vs. time in terms of departure from initial values at 12Z 12 Feb. and 13 Feb. 1971.	127
49	Surface-radar charts, 23 March 1969.	128
50	Observed central pressure vs. time, 23-24 March 1969.	128
51	Precipitation cross section for Lake Bridgeport, Texas, 23 March 1969.	129
52	Surface-mean relative humidity charts, 23 March 1969.	129
53	Observed and forecast central pressure vs. time in terms of departure from initial values at 00Z and 12Z 23 March 1969.	130
54	NMC-PE 12-hour precipitation forecasted from 00Z 23 March 1969 and observed precipitation for 00Z to 12Z 23 March 1969.	131
55	Observed central pressure vs. time, 26-28 Feb. 1971.	132
56	Surface-radar charts, 26 Feb. 1971.	132
57	Precipitation cross section for Minneapolis, Minn., 26 Feb. 1971.	133

<u>Figure</u>		<u>Page</u>
58	Observed and forecast central pressure vs. time in terms of departure from initial values at 00Z and 12Z 26 Feb. 1971	134
59	Surface-radar chart, 26 Feb. 1971.	135
60	Observed central pressure vs. time, 25-27 Dec. 1970.	136
61	Observed and forecast central pressure vs. time in terms of departure from initial values at 12Z 25 Dec. and 00Z 26 Dec. 1970.	137
62	Observed central pressure vs. time, 25-27 Jan. 1971.	138
63	FNWC-PE and NMC-PE 12-hour sea-level pressure forecasts from 12Z 25 Jan. 1971 and verifying surface analysis.	139, 140
64	Observed and forecast central pressure vs. time in terms of departure from initial values at 12Z 25 Jan. 1971 and 00Z 26 Jan. 1971.	141
65	500 mb height and vorticity at time of initial development of Case VII and Case IV.	142
66	Vertical structure of model utilized in solution of the omega and vorticity equations.	143



Figure

Page

67	NMC-PE 24-hour 500 mb forecasts from 12Z 1 April 1970 and verifying 500 mb analysis.	144
68	Comparison of operational (NMC) manually drawn sea-level pressure analysis with the NMC objective analysis for 00Z 24 March 1969.	145
69	Same as Fig. 68, except for 00Z 4 March 1971.	145

## CHAPTER I

### INTRODUCTION

#### 1a. Background and Statement of Problem

It has been well established that cumulus convection plays a vitally important role in the development and maintenance of tropical cyclones. From an observational standpoint, Riehl and Malkus (1961) have demonstrated that the important dynamic and thermodynamic processes of a hurricane are highly concentrated in deep cumuli within the storm's core. From a theoretical and numerical modeling point of view, Charney and Eliassen (1964), Kuo (1965), Ooyama (1969), and others have shown that tropical cyclones are forced circulations driven by the release of latent heat in organized convection. In addition, the intense vertical currents of convective cells significantly influence the cyclonic-scale circulation through the vertical transports of heat, momentum, and moisture.

Cumulus convection also frequently occurs in association with the development of extratropical cyclones. This is evident from the presence of convective showers as revealed by radar observations, recording raingauge data, and/or surface synoptic reports. In mid-latitudes, unlike the tropics, however, the fundamental mechanism of cyclogenesis is the baroclinic instability of the meandering westerlies (Charney, 1947; Eady, 1949). Extratropical cyclones thus have

as their basic source of energy the large-scale temperature contrast between air masses. Consequently, the importance of cumulus convection with respect to the larger-scale baroclinic processes in the evolution of mid-latitude storms is not clear, a priori, and has not yet, in fact, been established observationally or theoretically.

One aspect where convection might play a role in extra-tropical cyclogenesis is in the diabatic process of latent heat release. It has been established that this process per se is often an important contributing factor in overall storm development. Aubert (1957), for example, found released latent heat tended to lower the heights of isobaric surfaces in the lower troposphere and raise them in the upper troposphere. These changes resulted in deepening of the low-level cyclone and acceleration of the rate of movement. Danard (1964, 1966) demonstrated the release of latent heat could contribute significantly to the rate of generation of kinetic energy. Furthermore, Danard showed that the positive contribution of heating to generation of available potential energy is normally greater than the negative effect arising from the enhanced vertical motion. Consequently, cyclogenesis is not merely accelerated through the influence of condensational heating, but the difference in the kinetic energies between final and initial states is greater.

In these and other investigations of this question, little if any consideration is given to the fact that, for whatever difference it might make in either the total amount of condensation or in the temporal and spatial distribution thereof, much of the precipitation

accompanying an extratropical storm may be produced by convective updrafts rather than by the more gradual slope ascent characteristic of larger-scale baroclinic processes (Tracton, 1969).

In addition to the release of latent heat, other possibly more subtle influences of convection in extratropical storm development might be the vertical transports of such quantities as heat, momentum, and moisture. These processes are significant in tropical cyclogenesis, and there is no reason to believe that they may not be of some importance in the development of extratropical cyclones.

The goal of this thesis is to determine whether cumulus convection plays a role in the evolution of extratropical cyclones, and if it does, to determine the nature of that role. It is felt this question warrants consideration because of its importance to a complete understanding of the complex phenomenon of cyclogenesis and its implications to numerical weather forecasting.

#### 1b. Basic Approach

A direct and comprehensive analysis, either descriptive or dynamic, of the interactive role of cumulus convection and large-scale baroclinic development would be exceedingly difficult, if at all physically or economically feasible. Observationally, a very dense network of stations would be required to describe the interactions of convective and larger-scale motions and processes. Existing meso-scale networks, such as that operated by the National Severe Storms Laboratory in Oklahoma, have areal coverages which are small

compared to the domain of a cyclone and, furthermore, they are fixed geographically. From a theoretical standpoint, the problem is analytically intractable. Numerical integration of the governing equations wherein the cumulative effects of convection on the synoptic-scale development are parameterized is possible; however, the computational and physical complexities of a dynamic model designed explicitly for investigation of the role of cumulus convection in extratropical cyclogenesis would be numerous. Moreover, it is often as difficult in a numerical model as in the real atmosphere for one to keep track of all possible interactions and their consequences.

Thus, an indirect approach was adopted for this investigation wherein it was sought to determine whether there is a relationship between the extent of convective activity within extratropical cyclones, as ascertained from conventional meteorological data, and the departure of actual storm evolution from that predicted by operational forecast models. In so far as these models do not incorporate or adequately formulate the effects of sub-grid-scale convection, the emergence of a consistent relationship in the analysis of several storms would indicate that cumulus convection systematically alters the course of synoptic-scale development from that which would be expected if larger-scale processes alone were operative. The nature of such a relationship would, of course, reflect the nature of the role of convection in extratropical cyclogenesis and guide consideration of the physical mechanisms involved.

1c. Formulation of the Hypothesis

At the outset of this study, the role of convection in the evolution of extratropical cyclones was not assumed, nor was it explicitly assumed that convection indeed played a role. Rather, the approach was to dive into myriads of data, forecasted and observed, to see if anything physically plausible would emerge. Initially, two storms were chosen for analysis; the intense cyclogenesis along the East Coast of the United States, 11-13 November 1968, and the less dramatic but nevertheless major development over the central United States, 22-23 March 1969. The observed degree and extent of convective activity associated with each storm was ascertained to the fullest extent permitted by the data and methods of analysis outlined in Section 2c. An extensive analysis was then made of the difference between the forecast and actual evolution of the storms.

In both cases, the numerical prognoses (the National Meteorological Center's primitive equation model, NMC-PE) did forecast cyclogenesis in terms of deepening the central pressure and intensifying the cyclonic circulation of the sea-level system. The forecasts, however, were not without errors. The most notable with respect to possible implications of the role of convection was the failure in the November case to properly forecast the initiation of development. More specifically, the model lagged behind the real atmosphere in forecasting the onset of development. The observed initiation of cyclogenesis was accompanied by intense convective showers

in the unsaturated environment of the cyclone center. Since the large-scale processes which the model purports to represent require saturation in order to produce precipitation, the forecasts failed to predict the release of latent heat associated with the convection.

The initial development of the March storm was also accompanied by convective showers in the vicinity of the low center. In this case, however, the environment was sufficiently near saturation so that the rainfall and concomitant latent heat release were predicted, and the onset of development was properly forecast.

The analyses of these two cases therefore suggested that the release of latent heat by cumulus convection may be, at least in some instances, a critical factor in the initiation of cyclogenesis.

There were, in both cases, many errors in the detail and magnitude of the forecast patterns, other than the lag phenomenon in the November storm. These errors, however, did not appear to be related to differences or similarities in the extent and degree of the convective activity associated with the storms. Moreover, it was evident from detailed analysis of the cases that if there are indeed systematic errors in the numerical prognoses of cyclogenesis other than the lag phenomenon, they would either likely be obscured by the noise of other physical or computational limitations of the model, or a prohibitively large number of storms would have to be analyzed for their existence to become apparent. Prohibitive here is defined in terms of the difficulty and cost of acquiring data and the time necessary for analysis of each case.

At this point in the study, therefore, the following hypothesis was formulated, and the balance of the investigation directed primarily towards ascertaining its validity.

In some instances of extratropical cyclogenesis, cumulus convection plays a crucial role in the initiation of development through the release of latent heat in the vicinity of the cyclone center. In such cases, dynamical models which do not adequately simulate convective precipitation, especially as it might occur in an environment that is unsaturated, will fail to properly forecast the onset of development.

Seven storms in addition to those discussed above were analyzed in detail with respect to their bearing on the hypothesis, and cursory examination was made of twelve others. Also, to complement these basically empirical considerations, theoretical diagnostic calculations were performed to assess quantitatively the influence of latent heat release on surface development.



CHAPTER II

METHODS OF ANALYSIS

2a. Choice of Cases

Nine storms were analyzed in detail for this investigation. In no instance was a storm chosen for analysis because of any prior specific knowledge of the performance of the numerical prognoses or the degree of convection associated with the observed cyclogenesis. Criteria for selection were the intensity of actual development, availability of numerical forecasts, and sufficient data to determine the extent of convective activity from the structure of precipitation patterns.

A storm for which there was a 12-hour period having an average surface deepening rate of at least one millibar per hour was considered an intense development. Cases were restricted, except for that of 25-27 December 1970, to storms that developed over the relatively data-rich eastern two thirds of the United States or to storms that remained close enough to the Atlantic Coast so that a major portion of the precipitation either fell over land or was within the range of land-based radar. Primary interest in the 25-27 December 1970 case, a storm whose major development was well out over the Atlantic, was a comparison of the NMC-PE forecasts to those available from test runs of the limited area fine mesh version of this model (LFM). Emphasis on storms of the 1970-1971 winter season reflects operational implementation in September, 1970, of the Fleet Numerical Weather

Central's primitive equation model (FNWC-PE). (A brief description of the general aspects of the models appears in Section 2d.)

## 2b. General Procedure

For each storm, the actual course of the synoptic-scale development was traced via NMC sea-level pressure analyses at 3-hour intervals. It was found that in most instances the central pressure served as an adequate indicator of the degree of cyclogenesis; however, note was made of situations where development was manifested more by an increase in the intensity of the cyclonic circulation, assessed qualitatively, than by a decrease of central pressure.

The extent and degree of convective activity accompanying the observed development were deduced from precipitation patterns in the manner described below. The methods of analysis which were employed permitted depiction of the macroscale distribution and magnitude of convection with respect to the surface cyclone. Once this picture was clear, a comparison was made between the forecast and actual evolution of the storm (see Section 2f).

## 2c. Methods Utilized in Analysis of the Convective Activity

It is assumed that significant convection occurs only in regions of convective precipitation. Lapse rates in excess of the dry adiabatic, necessary to sustain convection without condensation, are infrequent. In addition, the influence of non-precipitating cumuli,

through latent heat release or otherwise, is likely to be small compared with that of cells which produce rain.

The extent and degree of convective shower activity accompanying development of a storm was deduced from composite analysis of weather radar data, tipping bucket rain-gauge traces, hourly rainfall amounts, and surface-synoptic reports. The weather radar observations are those of the National Oceanic and Atmospheric Administration's network of WSR-57's. The location of the radars and areal coverage of this network over the eastern two thirds of the United States is shown in Fig. 1. Radar data are available in three forms: i) summary charts of the nationwide distribution of precipitation echoes, ii) data sheets that contain the record of observations at individual stations, and iii) film records of the actual plan-position indicator (PPI). The summary charts enable one to depict the broad features of the distribution and character of the precipitation pattern about the storm in question. Fig. 2, for example, is a composite of the radar chart and the simplified surface analysis for 12Z 4 February 1971. The meanings of the symbols used on the radar charts appear in Table 1. It is seen from Fig. 2 that there is a solid line (squall line) of thunderstorms extending southward from the low along the cold front. The line is embedded in a more general region of scattered to broken thundershowers which extends and broadens somewhat north of the low. In the extreme northwestern area of the precipitation, some freezing rain is indicated.

An important feature of the radar data is the reported heights of the top of cells. In Fig. 2, the maximum top reported is

that of a 39,000 foot high cell located in the squall line. Generally speaking, the greater the height of the cells, the more intense is the convection.

The radar charts are generally available at 3-hour intervals. In the two storms analyzed initially for this investigation (11-13 November 1968; 23-24 March 1969), time resolution of one hour or less was obtained by constructing composite charts from the data sheets of individual radar stations. In addition, the PPI films for selected stations were examined to clarify the verbal and symbolic description of the echo patterns. In the subsequent case studies, however, after formulation of the hypothesis, the radar charts at 3-hour intervals were considered adequate.

A more refined and quantitative picture of the extent and degree of convective activity than that obtained by radar was ascertained from surface measurements of rainfall. Two types of data were utilized: hourly precipitation amounts and tipping-bucket records of the continuous temporal variation of rainfall rate. Of these, the tipping-bucket data is more definitive in delineating the presence and intensity of convective showers; however, as can be seen from Fig. 1, the density of stations reporting hourly totals is much greater than that for tipping-bucket gauges.

In the analyses of the first two storms, tipping-bucket records were obtained for all stations shown in Fig. 1 where there was precipitation. In the subsequent detailed case studies, though, only data for those locations thought pertinent to consideration of the

hypothesis were utilized; however, records from the entire network of hourly reporting stations were surveyed.

The tipping-bucket gauges record precipitation with a time resolution of about one-quarter minute. As can be seen from comparison of Figs. 3 and 5, this is sufficient to differentiate between rather steady stratiform rain and rainfall fluctuating rapidly in space and time as is characteristic of convective showers. The duration of individual showers over a gauge depends upon their speed and horizontal dimensions and is on the order of several minutes. Peak precipitation rates, which may be considered a measure of the intensity of convection, usually are greater than  $.3 \text{ in hr}^{-1}$  and may often exceed  $2 \text{ in hr}^{-1}$ .

From the spacing of shower peaks on the tipping-bucket traces, it is evident that cells generally occur in groups and are separated by continuous precipitation. Quantitative radar studies (Austin and Houze, 1972) show these cell arrays, or mesoscale areas as they are termed, reflect organization of the convection into areas or bands whose dimensions range from  $10^2 \text{ km}^2$  to more than  $10^4 \text{ km}^2$ , as would be the case for an extensive squall line. The continuous precipitation that is observed between cells likely represents condensate produced in convective updrafts that is spread by divergence from near the top of the layer containing the cells (Melvin, 1968). Alternatively, however, this so-called mesoscale component of the precipitation may reflect stable ascent of some saturated layer between the cells. Both mechanisms may contribute to some extent, but the

relative contribution of each is not known because of uncertainty in the nature of the mesoscale circulations involved. In any event, it is clear that the mesoscale precipitation is intimately related to the occurrence of convection. Therefore, for the purposes of this investigation, the precipitation that falls both between and beneath the shower peaks is considered to be convectively produced.

Since the tipping-bucket gauges are geographically fixed, they in effect record the instantaneous precipitation rate along line segments which connect successive positions of the station with respect to moving features of the surface system. For example, Fig. 3a is the raingauge trace of Charleston, South Carolina, for the period 19Z -23Z 11 November 1968. The line segment with respect to the low center and fronts along which the precipitation cross section applies is shown schematically. Fig. 3a shows that between 21Z and 2230Z Charleston experiences a series of heavy showers, which place this convective activity just to the north-northwest of the low. Peak shower intensities are about  $3 \text{ in hr}^{-1}$  with .46 in and .84 in of rain recorded at Charleston between the hours of 21Z and 22Z and between 22Z and 23Z, respectively. In comparison, the raingauge record at Pensacola, Florida, between 09Z and 12Z 11 November 1968 (Fig. 3b) is indicative of the presence of convective showers, but the activity is much more subdued than that exemplified by the Charleston trace. In this case, the peak shower intensities of  $.8 \text{ in hr}^{-1}$  and the one-hour precipitation amounts of .15 in and .35 in between 10Z and 11Z and between 11Z and 12Z, respectively, characterize the convective

activity just north of the low some twelve hours earlier in the storm's development than does the Charleston record. It should be noted that in both situations the radar charts (Fig. 4) and surface synoptic reports serve only to indicate in a qualitative manner that there are showers and thunderstorms in the vicinity of the low center at the times considered.

As further illustrations in the use of tipping-bucket data, the traces of Montgomery, Alabama, between 09Z and 13Z 11 November 1968 and that of New York City from 19Z to 23Z 12 November 1968 are presented in Fig. 5. With reference to Fig. 3b, one can see that at the same time the Pensacola trace indicates shower activity in the vicinity of the low center, the Montgomery record shows steady, exclusively non-convective rainfall some 150 miles to the north. The New York City gauge (Fig. 5a), on the other hand, is indicative of light purely stratiform precipitation near the storm center some 24 and 36 hours later, respectively, from when the area was sampled by the Charleston and Pensacola gauges.

The same approach used in consideration of the tipping-bucket records can be applied to stations which report just the cumulative one-hour precipitation amounts. Because the network of tipping-bucket gauges is relatively sparse, these data are used both to check and supplement the tipping-bucket observations. Although the intensity of individual showers cannot be determined, the magnitude of the convection can be assessed in terms of the hourly totals<sup>1</sup>. Fig. 6a,

---

<sup>1</sup> There is, of course, some uncertainty in assessing the hourly precipitation data because of the inherent time smoothing involved. It is possible, for example, that the sum of the reported totals for two successive hours actually all fell in a time span of one hour (or less). Such possibilities were considered in the storm analyses.

for example, presents a histogram of the successive one-hour rainfall amounts recorded during a series of thunderstorms at Tulsa, Oklahoma, between 10Z and 15Z 4 February 1971 (see also radar chart Fig. 2). Fig. 6a shows this histogram is, in effect, a cross section through the center of the storm. As the low passes over Tulsa between 12Z and 15Z, the one-hour rainfall amounts peak at .80 in. In comparison, the largest one-hour precipitation amount recorded during the same interval of time at Lehigh, in southeastern Oklahoma, is .36 in (Fig. 6b). In this case, the cross section is through the cold front and its accompanying squall line. Although the intensity of individual showers in this sector of the storm may be as great or greater<sup>2</sup> than those occurring in the low center, the degree of convective activity in terms of the net amounts of convective rainfall being produced is significantly less. As will be seen in the discussion of the case studies (Section 3b), at a later stage in the development of this storm, the convection in the squall line is much heavier while there is virtually no precipitation in the vicinity of the low center.

From the above discussion it should be clear that through judicious analysis of radar and raingauge data, a fairly detailed picture of the extent and degree of convective activity accompanying development of a particular storm can be obtained. In the actual analyses, a description was compiled of the distribution and magnitude of

---

<sup>2</sup> The radar echo tops (Fig. 2) suggest the intensity of the squall line showers is greater than those in the vicinity of the low center.



convection on essentially a continuous basis as the storm evolved, i. e., time resolution of 1 to 3 hours. It should be emphasized here that no attempt was made to keep track of individual convective cells. Rather, concern was with the macroscale distribution and magnitude of convection with respect to the developing cyclone. The goal of this thesis is, of course, to determine whether the convection so described plays a role in the overall storm development.

#### 2d. General Aspects of the Models

Three dynamical forecast models were used in this investigation: i) the six-layer primitive equation model of the National Meteorological Center (NMC-PE), ii) the limited area fine mesh version of the NMC-PE (LFM), and iii) the five-layer primitive equation model of the Fleet Numerical Weather Central (FNWC-PE). The basic features of the NMC-PE have been described by Shuman and Hovermale (1968) while Howcroft (1970) has discussed the LFM. The routine programming and physical adjustments made in the operational procedures at NMC are documented in a series of publications entitled Technical Procedures Bulletins and in the semi-annual publication Numerical Weather Prediction Activities. The principal aspects of the FNWC-PE have been described by Kesel and Winninghoff (1970).

The NMC-PE became operational in June, 1966, while the FNWC-PE was implemented in September, 1970. Forecasts are

generated twice daily from the nominal times of 00Z and 12Z. The LFM forecasts utilized were test runs of this model made prior to its operational implementation in October, 1971. Table 2 summarizes, for the nine storms analyzed in detail, the models which were considered for each of the relevant initial times.

For the first two storms analyzed in this study, the NMC-PE data were obtained from copies of NMC's so-called "B-3" magnetic tapes. These tapes contain the grid point values of both the objective analyses of the initial state and the forecasts through 36 hours. Primarily because it was found that extraction of the relevant data from the tapes was quite time consuming and expensive, the contoured forecast charts that are transmitted routinely over facsimile were, with some exceptions, used in the subsequent case studies. The exceptions were certain forecasts for the cases of 1-3 April 1970 and 2-4 March 1972, which were retrievable only from the appropriate tapes. Contour charts of the NMC-PE quantitative precipitation forecasts are not transmitted over facsimile. They are, however, archived at NMC by Russel Younkin, from whom copies were obtained. The FNWC-PE forecasts were in the form of contour charts that were obtained directly from the Fleet Numerical Weather Central, Monterey. The LFM data, which were supplied by NMC, were contoured computer printouts of the grid point values.

Each of the models integrates the primitive (hydrostatic), hydrodynamic and thermodynamic equations and includes such physical

effects as orography, solar and terrestrial radiation, sensible heat flux between the atmosphere and oceans, and moisture prediction with the feedback of latent heat. The respective horizontal and vertical domains of integration are shown in Fig. 7. The NMC-PE and FNWC-PE are hemispheric models with a horizontal grid spacing of 380 km (at  $60^{\circ}\text{N}$ ), while the LFM encompasses the general area of North America with grid points separated by 190 km. Vertical variations in the FNWC-PE are represented in Philips (1957) sigma-coordinate system in which pressure is normalized with the underlying terrain pressure. The vertical coordinate in the NMC-PE and LFM is a slight generalization of Philips' system. The one more level of vertical resolution in the NMC-PE and LFM reflects explicit consideration of a planetary boundary layer (50 mb in depth) that the FNWC-PE does not recognize.

Consideration of the forecasts of more than one model, when possible, was motivated by a desire to both check and augment any deductions gleaned from one model's prognoses alone. The equation systems and basic physics of the LFM are the same as those of the NMC-PE; the principal differences are the areal coverage and the horizontal grid spacing. Thus any inconsistency in the deductions drawn from the forecasts of these two models would likely reflect either the lesser truncation error in the LFM or the more refined specification of initial conditions. Differences between the NMC-PE and FNWC-PE forecasts could reflect any one of a number of physical and computational dissimilarities. Particular interest, however, was

on any difference in the forecasts that might reflect a difference in the method of parameterizing small-scale convection. The NMC-PE (and LFM) utilizes the so-called "convective adjustment" scheme wherein the lapse rate is adjusted to the moist adiabatic when it is forecast to exceed that value and at the same time the grid column is forecast to be saturated. In effect, the lapse rate is neutralized through an upward transport of heat. There is no specific allowance, however, for the convective rainfall that can occur in an unsaturated environment<sup>3</sup>. In essence, the "convective adjustment" in the NMC-PE (and LFM) is more a mechanism for preventing the computational instability that would result without such adjustment than a meaningful attempt to incorporate convection. The FNWC-PE, on the other hand, more explicitly considers convection through use of a parameterization scheme adapted from that utilized in the Mintz Arakawa General Circulation Model. In this scheme, energy parameters are used in conjunction with measures of the total upward convective mass flux, as well as entrainment, to determine a specific convective component of precipitation and the vertical redistribution of heat and moisture. This parameterization scheme does give the FNWC-PE the capability to simulate convective precipitation that can occur in an unsaturated environment; however, the lack of

---

<sup>3</sup> The NMC-PE and LFM can predict precipitation prior to the time when grid-scale saturation is forecast, since saturation in the models is defined in terms of a threshold value of relative humidity of between 80 and 100 per cent. The motivation in utilizing a reduced saturation criteria is primarily to account for the stable (stratiform) precipitation which can occur before grid-scale saturation, rather than to make any meaningful attempt to simulate convective precipitation in an unsaturated environment.

sufficient vertical resolution in the model limits its ability to represent the frequent pre-convective outbreak condition of a mixed moist layer topped by an inversion with potentially very unstable air above.

2e. Suitability of the Models as Tools for this Investigation

The NMC-PE, LFM, and FNWC-PE are assumed to be the best dynamical prognoses currently available for describing the evolution of the cyclone-scale circulation corresponding to a particular set of case studies. Despite their relatively high degree of theoretical sophistication, however, these models, with or without proper consideration of sub-grid-scale convection, are far from perfect representations of the real atmosphere. Therefore, it is not clear, a priori, whether they are suitable tools for use in an investigation of this type. The models do have inherent in them the fundamental mechanisms of cyclogenesis, and each has indeed on occasion demonstrated an ability to forecast the development of intense storms; however, errors in the timing, magnitude, and spatial detail of the forecast patterns on occasions when cyclogenesis is forecast and the complete failure to predict development in other situations may reflect any one or a combination of various physical, dynamical, or computational limitations<sup>4</sup> other than inadequate treatment of convective processes.

---

<sup>4</sup> Examples are lack of horizontal and vertical resolution, insufficient initial data, artificial boundary conditions, and initializing and smoothing procedures.

The question, then, is if convective activity does indeed play a role in cyclogenesis, would inadequate simulation of some feature of the observed convection lead to a systematic error that would emerge from the noise inherent in other failings of the models. As will be shown in the following sections, there does appear to be such a systematic error, so that, a posteriori, the use of the models as tools is justified.

## 2f. Evaluation of Forecasts

The predicted storms are described primarily in terms of the central pressure of the sea-level system<sup>5</sup>. In most situations, this served as an adequate measure of the degree of development, but as with the actual storms, note was made of those occasions where

---

<sup>5</sup> Charts of the FNWC-PE sea-level pressure forecasts are contoured in increments of 4 mb, with maxima and minima in the pressure field appropriately identified and labeled with their respective numerical values. The computer printouts of the LFM sea-level pressure prognoses are contoured in increments of 4 mb, as were the printouts generated of the NMC-PE forecasts extracted from the "B-3" tapes. Both the LFM forecasts and those NMC-PE prognoses which were obtained from the tapes allow essentially an unambiguous determination of the predicted central pressures. Charts of the NMC-PE sea-level pressure forecasts are contoured only in 8 mb intervals. The location of maxima and minima are identified, but the numerical values are often either not printed or are unreadable. Consequently, there was some uncertainty in assigning a value to the predicted central pressures of those NMC-PE forecasts for which only the contour charts were available. The approach adopted in such cases was to subjectively extrapolate the pressure gradient on the basis of: i) synoptic experience, ii) experience gleaned from examining contour charts that do have the value of central pressure printed on them, and iii) experience obtained by comparing, when possible, contour charts with computer printout of the B-3 data for the corresponding forecast. It is felt that in no instance does the uncertainty (maybe 1-3 mb) affect the validity of the discussions that follow.

the intensity of the circulation, assessed qualitatively, was more representative. In evaluation of the performance of forecasts, emphasis was on the departure between predicted and actual changes, rather than on the absolute difference between observed and forecast at some given time. This is especially pertinent with regard to the hypothesis where, for example, the absolute error in a 36-hour forecast of central pressure is less important than comparison of the temporal evolution of the actual and predicted development.

It should be noted that the numerical prognoses are through 24 or 36 hours from the initial time (either 00Z or 12Z) with generally two or more successive initial times considered for each case. Since the output of the numerical forecasts from some given initial time is in 12-hour increments, comparison is with the net 12-hour observed changes between the nominal times of 00Z and 12Z. Another point to note is that the initial 12-hour forecast changes of central pressure are reckoned from the minima of pressure of the objectively analyzed fields of sea-level pressure from which the prognoses are generated. Because of the inherent smoothing that occurs in the objective analyses of data to a rather coarse grid, the initialized values of central pressure were generally somewhat greater (1-5mb) than the lowest pressures indicated on the corresponding manually analyzed surface charts that were used to trace the actual storm development. For several of the case studies (Table 2), the actual objective analyses were not available,

so that it was necessary to estimate the initialized values of central pressure on the basis of experience gained in comparison of the manually produced surface charts with the corresponding objective analyses. This matter is discussed further in Appendix A.

In addition to development of the sea-level pressure system, other potentially relevant items such as precipitation and 500 mb forecasts were examined.



CHAPTER III

ARGUMENTS I AND II: COINCIDENCE IN TIME BETWEEN  
CONVECTION AND INITIAL DEVELOPMENT;  
SYSTEMATIC ERROR IN THE NUMERICAL PROGNOSSES

3a. Introduction

The principal observations and deductions of this investigation will be discussed with reference to the following hypothesis:

In some instances of extratropical cyclogenesis, cumulus convection plays a crucial role in the initiation of development through the release of latent heat in the vicinity of the cyclone center. In such cases, dynamical models which do not adequately simulate convective precipitation, especially as it might occur in an environment that is unsaturated, will fail to properly forecast the onset of development.

The hypothesis was formulated at an early phase of this study as a statement of provisional conjecture, based upon intensive analyses of two case studies. The aim of the investigation thereafter was directed primarily towards ascertaining the validity of the hypothesis. Further evidence either to support or refute the hypothesis was derived from detailed analysis of seven additional storms, cursory examination of twelve others, and both qualitative and quantitative consideration of the physical mechanisms involved. The purpose of the discussions in this and the following two chapters is to summarize

the evidence and show that, although it may not be conclusive proof of the hypothesis, it does provide sufficient support to elevate its stature from mere conjecture to an assertion which may be accepted as highly probable.

The case in support of the hypothesis may be summarized in terms of the following four arguments:

- I. In some storms, there was a coincidence in time between the initial development and the occurrence of convective showers in the vicinity of the low center. Almost invariably, the environment in which the convection occurred was unsaturated<sup>6</sup>.
- II. In those cases in which the initial development was accompanied by convective showers in the vicinity of the low center and the environment in which the convection occurred was unsaturated, the dynamic prognoses systematically failed to properly forecast the onset of development, apparently because of the models' failure to predict the convective rainfall.
- III. The importance of the latent heat release by cumulus convection to the initiation of development of some extratropical cyclones, which is implied by the apparent source of the systematic error, is physically plausible and quantitatively reasonable.

---

<sup>6</sup> A saturated region is defined here as one in which the mean surface to 500 mb relative humidity, as on the operational charts received over facsimile, is in excess of 90 per cent. It is noted that the concept of saturation and nonsaturation is in and of itself unimportant. What is important is the fact that while saturation is a necessary condition for significant stratiform precipitation, heavy convective rainfall may occur in an environment which is unsaturated.

- IV. There appears to be no defensible alternative explanation for the observed systematic error.

In this chapter, Arguments I and II will be discussed and then documented through descriptions of the case studies. Discussion of Arguments III and IV are presented in the two following chapters.

In order to facilitate the discussion of Arguments I and II, Table 3 presents for each of the nine storms analyzed in detail, a dichotomous characterization of the initial development with respect to the following: i) the occurrence or nonoccurrence of convective showers in the vicinity of the low center, ii) saturation or nonsaturation of the environment of the center of the storm, iii) prediction or non-prediction of the convective rainfall, if it occurred, and iv) adequate or inadequate forecast of the onset of development. Discussion of the results of cursory examination of twelve additional storms is presented in Section 3c.

With regard to Argument I, Table 3 shows that the initiation of development of six of the nine storms was accompanied by convective shower activity in the vicinity of the low center. Of these, in only one case was the environment of the low saturated. It follows, of course, that the initial development of three of the nine storms was not accompanied by shower activity. Furthermore, since the environment about the center of these storms was also unsaturated, there was little or no stratiform precipitation and, hence, latent heat release was not a factor in the initiation of their development.

With reference to Argument II, Table 3 indicates that in each of the five cases where the initial development was accompanied by showers in an unsaturated environment, the dynamical prognoses failed both to predict the convective precipitation and to adequately forecast the onset of development. In the one storm in which convection occurred in an environment that was saturated, the precipitation and the concomitant release of latent heat were predicted, as was the initiation of development. Also, the onset of development was properly forecast in those cases where there was no convection. Hence, the dynamical prognoses systematically failed to predict the onset of cyclogenesis in those storms in which the initial development occurred in association with convective shower activity in an unsaturated environment. Furthermore, the apparent source of the systematic error was the failure of the models to simulate the rainfall produced by cumulus convection in an environment which was unsaturated.

It should be noted that significant shower activity occurred in the center of the storms generally only during the early stages of their life history. Following an initial period of development, which lasted anywhere from 6 to 36 hours, the convection became dissociated from the low center. Forecasts which were generated subsequent to the actual onset of cyclogenesis but prior to the dissociation process were consistent with the notion of the importance of convection in the low center to the initial development in that when the precipitation was predicted, so too was the trend of continued development.

An additional significant point relevant to Arguments I and II is that convective activity appeared to be important to the onset or continued development of the storms only when it occurred in the immediate vicinity of the low center. That is, only when the convection occurred in the low center was there a consistent contemporary relationship between it and the observed storm evolution or was there a systematic error in the numerical prognoses.

In order to further scrutinize and document Arguments I and II, a brief discussion of the nine detailed case studies is presented. The illustrative material pertinent to Argument I includes the following:

i) plots of central pressure versus time (central pressure plotted generally at 3-hour intervals<sup>7</sup>), ii) composite charts of the mean surface to 500 mb relative humidity and simplified surface analysis (12-hour intervals), iii) selected composite charts of the radar echo patterns and simplified surface analysis, and iv) selected tipping-bucket traces and histograms of 1-hour rainfall amounts, together with schematic diagrams to indicate the line segments with respect to the low center along which the precipitation cross sections apply. The illustrative material relevant to Argument II includes: i) plots of the observed and forecast values of central pressure versus time (central pressures plotted at 12-hour intervals

---

<sup>7</sup> In situations where there was no definite minimum in the pressure field prior to development, the pressure at the point along the trough axis from which the low center ultimately developed was assigned as the value of central pressure. With some exceptions which will be discussed, it is felt that the indicated changes of central pressure are an adequate measure of the degree of development.

in terms of the departure from the value at the initial time), and  
ii) precipitation forecasts for relevant cases (cumulative 12-hour totals with track of forecast low superimposed). Note is made that the actual forecast charts of sea-level pressure and the appropriate initial and verifying analyses will be presented only when visual inspection thereof is more enlightening than consideration of central pressure alone. Also, the isohyal analyses of actual precipitation amounts will be presented for comparison only when either it is not clear from the discussion of the observed 1-hour precipitation amounts that the forecast 12-hour amounts are negligible or it is readily apparent that significant amounts of rainfall were predicted.

### 3b. Detailed Case Studies

#### Case I - February 4 to 5, 1971

During the 18-hour period prior to 12Z Feb. 4, a low-pressure system moved without developing from New Mexico to central Oklahoma. Through 09Z Feb. 4, there was no significant convective activity in association with this system. The 09Z composite surface-radar chart (Fig. 8) does show the presence of a small area of light showers to the south of the low along the cold front, but to this point, inspection of the hourly rainfall data indicated negligible amounts of precipitation were produced. Between 09Z and 12Z, as shown by the radar observations (Fig. 8), however, and more precisely between 11Z and 12Z, as was indicated by hourly precipitation data, there was

an explosive increase in the extent and degree of shower activity.

Shortly after 12Z, the low began to deepen (Fig. 9).

During the initial period of development between 12Z and 18Z Feb. 4, the radar observations display a line of thundershowers (i. e., a squall line) which extended south of the low and which was embedded in a more general area of scattered to broken showers and thunderstorms that extended and broadened somewhat to the north of the low. It is evident from the composite surface-mean relative humidity charts (Fig. 10) that the convection occurred in an unsaturated environment. As an indication of the magnitude of the shower activity, the rainfall histograms of Tulsa and Lehigh, Oklahoma, are presented in Fig. 11. The Tulsa histogram, which represents a cross section through the low center between 11Z and 15Z, indicates a peak 1-hour rainfall amount of .80 in. In contrast, the largest 1-hour total deposited as the squall line passed over Lehigh was .36 in. The 1-hour amounts north of the storm were similarly less. Thus, although the intensity of individual showers, as implied by the radar echo tops, was greatest in the squall line, the degree of convection in terms of the net amounts of rainfall that were being produced was greatest in the center of the storm. The only available tipping-bucket gauge relevant to the immediate discussion was that of Springfield, Missouri (Fig. 12), which indicates that the intensities of showers in the center of the low between 15Z and 18Z were generally from .50 to 1.0 in  $\text{hr}^{-1}$ , though one peak was in excess of 2.0 in  $\text{hr}^{-1}$ . Subsequent to 18 Z Feb. 4, the storm continued to intensify as it tracked northeastward towards the

Great Lakes. As can be seen clearly from the series of surface radar charts (Fig. 8), however, the convective activity began to spread eastward away from the center of the storm between 18Z and 21Z. By 00Z Feb. 5, there was virtually no precipitation in the vicinity of the low center. The squall line, though, became more extensive and, as exemplified by the Memphis histogram (Fig. 13), was producing more precipitation than it had been prior to 00Z Feb. 5.

At this point, it is desirable to note that the configuration of the shower activity during the initial phase of development of this storm is characteristic of each storm in which the onset of development was accompanied by an outbreak of convection. More specifically, reference is made, first, to the radar echo pattern shown, for example, by the 12Z surface-radar chart and, second, to a maximum in the convectively produced amounts of rainfall within the center of the storm. It is also noted that with one exception (Case V), the dissociation of significant shower activity from the center of the storm occurred, as in this case, while the storm was continuing to intensify.

One can see from Fig. 14 that neither the NMC-PE or FNWC-PE prognoses generated from 12Z Feb. 4 properly forecast the initiation of development. The models did forecast cyclogenesis in the sense that significant deepening was predicted between 12 and 24 hours after the initial time, but it is clear from Fig. 14 that each lagged behind the real atmosphere in the onset of development. Fig. 15 shows that during the 12-hour period immediately following 12Z Feb. 4, when the observed initial development occurred, both models produced negligible amounts of precipitation ( $< .25$  in).



It is noted that both the NMC-PE and FNWC-PE prognoses generated from 00Z Feb. 5, which was after the shower activity became dissociated from the low center, properly forecast the continuation of development in the 12-hour period immediately following the initial time (Fig. 16). The degree of the forecast development, which was about the same in both cases, was less than observed, but there was no lag in the trend of continued development. What is important in this regard is that while the FNWC-PE predicted a significant fraction of the precipitation that occurred in association with the squall line, the NMC-PE produced negligible amounts (Fig. 17). The implication, therefore, which was corroborated by the other case studies, is that there was no systematic error in the numerical prognoses related to the occurrence of cumulus convection other than when it occurred in the center of the storms during the initial phase of development. It should be emphasized that this does not necessarily rule out the possibility that extensive shower activity at the periphery of the storm plays some role in the detail or magnitude of the actual storm evolution, since the approach employed in this investigation may not have been adequate to deduce such a role. What can be said, though, is that convective activity which was not in the immediate vicinity of the low center did not appear to be crucial either to the continuation of development following the onset of cyclogenesis, as illustrated here, or to the actual initiation of development, as will be explicitly discussed with reference to Case VII.

Case II - April 1 to 3, 1970

At 12Z April 1, an inverted trough extended northward from central Texas through Oklahoma. The composite surface-radar charts (Fig. 18) indicate that at this time there was an area of broken light showers, with a few thunderstorms embedded to the north-northwest of the trough axis; however, there was no precipitation in the interior of the trough itself, as was the case through 18Z. Between 12Z and 18Z some surface development occurred in terms of the appearance of a minimum of pressure (2-3 mb deepening along the trough axis) and a slight increase of the circulation about the trough, but the actual onset of cyclogenesis did not occur until the 6-hour period following 18Z (Fig. 19). As can be seen from the 21Z April 1 and 00Z April 2 surface-radar charts (Fig. 18), the initiation of development coincided with an outbreak of extensive shower activity in the center of the low.

It is interesting to note that the storm deepened 6 mb between 18Z and 21Z April 1, but that there was little further decrease of central pressure during the 3-hour period thereafter. What occurred, rather, as illustrated by Fig. 20, was that between 21Z and 00Z, the low center was in the process of redeveloping northeastward such that, although there was virtually no net change of central pressure, the observed 3-hour pressure falls of 4-5 mb along the Illinois-Kentucky and Indiana-Kentucky borders were developmental components of the isallobaric field. The contemporary relationship which existed between the shower activity and the redevelopment and continued deepening of the

low thereafter through about 06Z is clearly demonstrated by the tipping-bucket traces of Cairo, Illinois; Evansville, Indiana; and Louisville, Kentucky (Fig. 21). Peak intensities of the showers within the new low center were well in excess of  $2.0 \text{ in hr}^{-1}$ , with 1-hour totals generally greater than .50 in and often in excess of 1.0 in (Louisville recorded 1.73 in between 04Z and 05Z April 2). Except for the extreme southern portion of the squall line, these amounts were considerably greater than those reported elsewhere in association with the storm.

Following 06Z April 2, as the storm continued to intensify, the heaviest shower activity became dissociated from the low center. What shower activity there was in the center of the storm was much subdued from that prior to 06Z (1-hour amounts less than .20 in).

With reference to the series of surface-mean relative humidity charts (Fig. 22), one can see that through 00Z April 2, although the area to the north of the low was saturated, the environment of the low center itself was not. By 12Z April 2, however, the region about the center of the storm had become saturated.

Inspection of Fig. 23 indicates that the 12-hour NMC-PE prognoses generated from 12Z April 1 completely failed to predict the observed initial development. Some deepening (3 mb), however, was forecast between 12 and 24 hours after the initial time, and major development followed during the 12-hour period thereafter. Thus, although the model did predict cyclogenesis, the onset of development was not properly forecast. As can be seen from Fig. 24a, although precipitation was forecast to the north of the low between 12 Z April 1

and 00Z April 2, none was predicted in the unsaturated environment of the low center itself. The forecasts generated from 00Z April 2 (Fig. 23b), which was prior to when significant convection became dissociated from the low center, did predict the continued trend of development, without lag. As shown by Fig. 24b, the model also forecast substantial amounts of precipitation in association with the forecast center of low pressure during the 12 hours immediately following the initial time.

Case III - November 11 to 13, 1968

At 00Z November 11, a weak low-pressure area was located in the vicinity of Galveston, Texas. During the 12-hour period prior to this time no precipitation was associated with this system as it drifted across Texas without developing. In the 12-hour period following 00Z, the low deepened slowly (Fig. 25) as it tracked eastward along the Gulf Coast to a point just to the southeast of Pensacola, Florida. The 06Z and 12Z surface-radar charts (Fig. 26), plus the tipping-bucket trace of Pensacola (Fig. 27), serve to illustrate that the initiation of development was accompanied by an outbreak of shower activity.

Between 12Z and 18Z Nov. 11, the storm began to track northeastward towards the central Atlantic Coast. It is interesting to note that during this period there was little or no further development (Fig. 25), and as illustrated by the 15Z surface-radar chart (Fig. 26), the shower activity in the central region of the storm dissipated. The radar observations indicate some light showers to the northwest of the low and an area of thunderstorms to the southeast, but there was no

activity in the center of the storm. At about 18Z, however, as exemplified by the surface-radar charts and the rainfall histogram of Brunswick, Georgia (Fig. 28), heavy showers reappeared in the low center, and development recommenced shortly thereafter (Fig. 25).

The tipping-bucket trace of Charleston, South Carolina, and rainfall histograms of Cape Hatteras, North Carolina (Figs. 29 and 30), illustrate that shower activity remained in the central region of the storm through about 06 Z Nov. 12. During the 3-hour period thereafter, as the storm continued to intensify while moving northward along the Atlantic Coast, significant convection spread eastward away from the low center.

It can be seen from the series of surface-mean relative humidity charts (Fig. 31) that although the area to the north and northwest of the storm was saturated, the immediate environment of the low center through 00Z Nov. 12 was not. By 12Z Nov. 12, the area about the low had become saturated.

It is evident from Fig. 32a that the NMC-PE failed to properly forecast the initiation of development. The predictions generated from 00Z Nov. 11 erroneously filled the low through 24 hours after the initial time. Not until the 24 to 36-hour forecast period was the onset of cyclogenesis predicted. It is noted also that the forecasts generated from 12Z Nov. 11 (Fig. 32b) lagged behind the real atmosphere in the continuation of development. That is, no further deepening was forecast until 12 to 24 hours after the initial time. Figs. 33 a-b

show that neither the prognoses generated from 00Z or 12Z Nov. 11 forecast the heavy convective rainfall observed in the center of the storm during the 12-hour period immediately following their respective initial times. The prognoses from 00Z Nov. 12 (Fig. 32c) did forecast, without lag, the observed continuing development, and did forecast significant amounts of precipitation in association with the predicted low center (Fig. 33c).

Case IV - March 2 to 4, 1971

At about 15Z March 2, showers and thunderstorms developed along the entire length of a stationary front that extended from southern Texas to the southeast Atlantic Coast (Fig. 34). Between 15Z March 2 and 00Z March 3, the inverted trough which was situated about the front began to deepen, and a nascent wave cyclone developed in southern Mississippi, where, as can be seen from the 00Z surface-radar chart, the most intense convection had become concentrated.

During the 24-hour period following 00Z March 3, the low developed slowly (Fig. 35), but steadily, as it tracked northeastward to the coast of North Carolina. The tipping-bucket trace of Macon, Georgia (Fig. 37), and the 00Z March 4 surface-radar chart (Fig. 34) illustrate the fact that there was extensive convective activity in the vicinity of the low center for this entire period.

Between 00Z March 4 and 00Z March 5, the storm intensified explosively while it moved northward along the Atlantic seaboard to New England. Radar data and ship observations indicate,

however, that significant shower activity became dissociated from the center of the storm shortly after 00Z March 4.

Fig. 36 shows that the environment about the storm center was unsaturated through 12Z March 3, but had become saturated by 00Z March 4.

One can see from the NMC-PE sea-level pressure charts which were generated from 12Z March 2 (Fig. 38) that the model did not deepen the inverted trough or produce an incipient center of low pressure until 12 to 24 hours after the initial time (see also plot of forecast and observed central pressures vs. time, Fig. 39a). That is, the prognoses lagged behind the real atmosphere in the onset of development. Comparison of the observed and predicted precipitation between 12Z March 2 and 00Z March 3 (Fig. 40a) shows that, although the model did forecast some precipitation in the northeast and southwest portions of the trough, it did not produce any rainfall corresponding to that observed in association with the development of the incipient low.

Both the FNWC-PE and NMC-PE forecasts from 00Z and 12Z March 3 predicted the continuation of development, without lag (Figs. 39b and 39c, respectively). As can be seen from Figs. 40b and 40c, the NMC-PE also forecast significant precipitation in association with the low center<sup>8</sup> during the 12-hour periods immediately

---

<sup>8</sup> With regard to the NMC-PE forecast from 00Z March 3, it is noted that the environment about the actual low center was unsaturated through 12Z March 3; however, with the reduced saturation criteria of 90 per cent, the model did saturate the region about the low in the 12-hour period after 00Z March 3, and hence, was able to produce precipitation.

following the respective initial times. The FNWC-PE precipitation forecasts were not available and, therefore, one can only speculate that this model also simulated the convective rainfall.

It is noted that both models predicted major development to occur in the first 12-hour period following the initial time of 00Z March 4 (Fig. 39d), although the magnitude of that development was not as great as observed. (No precipitation forecasts available for either model.)

#### Case V - February 12 to 13, 1971

Between 00Z and 09Z Feb. 12, a well-defined nascent cyclone developed from a general area of low pressure that at 00Z was situated over Texas and Oklahoma. Although during this period, while the storm drifted across southern Arkansas, there was virtually no net change of central pressure<sup>9</sup>, there was a definite increase in the cyclonic circulation (Fig. 41). The initiation of development, as can be seen from the 06Z surface-radar chart and rainfall histogram of Foreman, Arkansas (Figs. 42 and 43, respectively), was accompanied by an outbreak of significant shower activity in the vicinity of the low center. It can be inferred, in addition, from the 00Z Feb. 12 surface-mean relative humidity chart (Fig. 44) that the environment in which the storm first developed was unsaturated.

---

<sup>9</sup> There was approximately 1-2 mb deepening between 00Z and 09Z Feb. 12, if account is taken of the normal diurnal tendencies.



The surface-radar charts (Fig. 42) serve to illustrate that significant convection became dissociated from the center of the storm by 12Z Feb. 12. Thereafter, although the area was saturated (Fig. 44), there was little or no precipitation, either stratiform or convective, within the low center for the balance of the storm's life history.

It should be noted that unlike Cases I-IV and Case VI, development did not continue, either in terms of a decrease of central pressure (Fig. 45) or an increase of the cyclonic circulation during the dissociation of the convective activity from the center of the storm. In fact, there was little further development until about 03Z Feb. 13, when the low began to develop rapidly as it tracked northeastward towards Pennsylvania. Apparently, when the convection became dissociated from the low center, large-scale motions and processes alone were not yet conducive to further development.

It can be seen from comparison of the 12-hour NMC-PE sea-level pressure chart generated from 00Z Feb. 12 with the initial and verifying analyses (Figs. 41 and 46) that the model failed to predict the onset of development. The model did not, in fact, produce a minimum of pressure corresponding to the observed storm until 24 to 36 hours after the initial time. Fig. 47 illustrates that negligible amounts of precipitation were forecast between 00Z and 12Z Feb. 12, when the observed initiation of development occurred.

Each of the models available for the initial time of 12Z Feb. 12 forecast some deepening between 12Z Feb. 12 and

00Z Feb. 13 and, with the exception of the LFM (for reasons not readily apparent), predicted more significant development, as was observed, during the 12-hour period thereafter (Fig. 48a); however, although the FNWC-PE prognoses generated from 00Z Feb. 13 forecast the continuation of development without lag, the NMC-PE forecast from 00Z Feb. 13 did not predict further development until 12 to 24 hours after the initial time (Fig. 48b). The failure by the NMC-PE to properly forecast the continued development cannot be ascribed to the occurrence of convective showers, but it is emphasized here that this particular forecast was the only case in which this situation was encountered.

#### Case VI - March 23 to 24, 1969

Between 00Z and 06Z March 23, an ill-defined minimum in the pressure field drifted slowly across the Texas Panhandle without developing. The radar observations (Fig. 49) indicate that during this interval of time there was some shower activity in association with the low, but only light amounts ( $< .10$  in) were recorded by hourly rainfall stations.

During the 6-hour period following 06Z, the low began to deepen (Fig. 50), and, as illustrated by the 12Z surface radar composite (Fig. 49) and the rainfall histogram of Lake Bridgeport, Texas (Fig. 51), the onset of development was accompanied by an explosive increase in the extent and degree of convection. Between 15Z and 18Z, while the storm was continuing to intensify, significant shower activity became dissociated from the low center.

It can be seen from the surface-mean relative humidity charts (Fig. 52) that the area about the low at 00Z March 23 was quite dry. At 12Z, however, shortly after the major outbreak of convective activity, the environment of the storm center was indeed saturated.

Fig. 53 indicates that the NMC-PE prognoses from 00Z March 23 forecast the initiation of development, as was observed, during the first 12 hours following the initial time. The model also predicted during this same interval of time significant amounts of precipitation in association with the forecast center of low pressure (Fig. 54).

It is noted that the prognoses generated from 12Z March 23 (Fig. 53) predicted the continuation of development, without lag, and also forecast substantial amounts of precipitation in association with the forecast low.

#### Case VII - February 26 to 27, 1971

Between 06Z and 12Z Feb. 26, a weak low-pressure system began to develop (Fig. 55) as it tracked north-northeastward from central Nebraska towards eastern Minnesota. The radar-surface charts of 12Z and 18Z Feb. 26 (Fig. 56) show that some light showers were associated with the initial development, but as exemplified by the tipping-bucket trace of Minneapolis, Minnesota (Fig. 57), the activity can be considered negligible. The peak intensity of the shower at Minneapolis was just  $.35 \text{ in hr}^{-1}$  with only  $.08 \text{ in}$  of rainfall recorded in the hour during which the shower occurred (17Z - 18Z).

In terms of the net 12-hour changes of central pressure, the onset of development did not actually occur until between 12Z Feb. 26 and 00Z Feb. 27 (Fig. 58). In fact, the low filled 2 mb during the 12-hour period prior to 12Z Feb. 26. Fig. 58a shows that both the FNWC-PE and NMC-PE prognoses generated from 00Z Feb. 26 predicted this trend of events. Twenty-four hours after the initial time there was a large error in the absolute difference between the predicted and observed values of central pressure; however, what is significant is that there was no lag in prediction of the initial development, or in other words, the time of the onset of cyclogenesis was properly forecast. The same is true for the prognoses from 12Z Feb. 26 (Fig. 58b). Although the magnitude of the predicted initial development was not as great as that observed, the models did forecast the onset of development during the 12-hour period immediately following the initial time.

As an illustration of the apparent unimportance to the initiation of development of convective activity which occurs at the periphery of the storm area, reference is made to the following: the expanded areal coverage of the 12Z Feb. 26 surface-radar chart presented in Fig. 59 illustrates that there was extensive and obviously intense shower activity in the southern United States which was not directly associated with the development of this storm. That is, the convection appeared well before the onset of cyclogenesis and persisted through the later stages of development. Both the NMC-PE and FNWC-PE prognoses generated from 00Z Feb. 26 did adequately forecast the convective rainfall between 12 and 24 hours after the initial

time (i. e., the period during which the onset of development occurred), but the 12-hour forecasts from 12Z Feb. 26 produced negligible amounts of precipitation during that same period. It is noted, however, that both models in the forecasts generated from 00Z and 12Z Feb. 26 properly forecast the onset of development. The implication, therefore, which was corroborated by other case studies, is that convective activity on the periphery of the storm area was not crucial to the initiation of development.

Case VIII - December 25 to 27, 1970

The initial development of this storm occurred between 15Z and 18Z Dec. 25 (Fig. 60) when what had been an innocuous minimum in the pressure field drifted eastward from the border of North and South Carolina across the Atlantic Coast. Thereafter, the storm intensified to near hurricane proportions as it tracked north-eastward to a position just south of Nova Scotia at 00Z Dec. 27.

The center of the storm was within range of the radar at Cape Hatteras, North Carolina, until 00Z Dec. 26, and through that time, there was no indication of shower activity. The extent and degree of any convection there might have been about the center of the storm following 00Z is not known (no pertinent ship observations available).

Fig. 61 clearly indicates that the models did forecast the onset of development, as was observed, between 12Z Dec. 25 and 00Z Dec. 26, and predicted the trend of continued development in the 12-hour

period thereafter. It is noted that the models did not predict significant precipitation in the vicinity of the forecast low center between 00Z and 12Z Dec. 26. Hence, if there was any precipitation about the actual storm center during this period, it was not crucial to the continuation of development subsequent to 00Z.

### Case IX - January 25 to 26, 1971

Between 12Z and 15Z Jan. 25, a minimum of pressure appeared in the southeastern extremity of a broad cyclonic area that extended from Idaho to Iowa. Development commenced shortly thereafter (Fig. 62) as the low moved eastward towards the Great Lakes. The only precipitation accompanying the initiation of development was some inconsequential light snow to the north of the low center.

It can be seen from the charts of the FNWC-PE and NMC-PE 12-hour forecasts generated from 12Z Jan. 25 (Fig. 63), that both models produced well-defined 1000-mb cyclones (see also plot of forecast vs. observed central pressure, Fig. 64a). The predicted storms are not as deep as the observed, but the onset of development was indeed forecast. It is noted, also, that the prognoses forecast the continued development subsequent to 00Z Jan. 26 (Fig. 64b).

### 3c. Results of Cursory Examination of Twelve Additional Cases

In order to augment the nine detailed case studies, a cursory examination was made of twelve additional storms. Each of the twelve cases, as were the nine storms analyzed in detail,

was an intense cyclogenesis which occurred over the eastern two thirds of the United States or western Atlantic.

Data utilized in analysis of the convective activity were restricted to the "SM" surface synoptic reports and 6-hour precipitation totals received over teletype at M.I.T., and to radar charts received over facsimile. These data alone are not sufficient to describe the detailed distribution and magnitude of convection accompanying a storm's development; however, one can deduce from these data whether there was significant shower activity in the vicinity of the low center during the initial development.

Emphasis on storms of the 1971-1972 winter season reflected operational implementation of the LFM in October, 1971. Only NMC-PE and/or LFM forecasts were considered and were in the form of contour charts received over facsimile. The LFM precipitation forecasts are received over facsimile, but NMC-PE precipitation forecasts are not. However, prediction or nonprediction of rainfall can be inferred from whether or not the model produced saturation about the forecast center of low pressure (relative humidity forecasts are received over facsimile).

The results of the analysis of the twelve storms are presented in Table 4. In those cases where the forecasts of both models were available, the conclusions to be drawn from each were consistent with one another. It can be seen that the initial development of six storms was accompanied by an outbreak of convective showers in the vicinity of the low center. Of these, in five cases the environment

of the low was unsaturated, the convective precipitation was not adequately simulated, and the initiation of development was not properly forecast. In the one storm in which the convection occurred in a saturated environment, the precipitation was predicted, as was the initiation of development. In the six other storms, there was little or no precipitation, either convective or stratiform, in association with the initial development and, in each case, the onset of cyclogenesis was properly forecast.



CHAPTER IV

ARGUMENT III: PHYSICAL PLAUSIBILITY AND  
QUANTITATIVE REASONABLENESS

4a. Introduction

In this chapter, attention is focused upon Argument III: the importance of latent heat release by cumulus convection to the initiation of development of some extratropical cyclones, which is implied by the apparent source of the systematic error, is physically plausible and quantitatively reasonable.

4b. Physical Plausibility

The importance of latent heat release to the development and maintenance of extratropical cyclones has been well established. Danard (1964), for example, has shown that the release of latent heat amplifies the upward motion and thereby increases the low-level convergence. As a result, the sea-level ( or 1000-mb) system tends to intensify and move with the center of heaviest precipitation. However, Danard, as have others who explicitly considered the question (e. g., Bullock and Johnson, 1971; Petterssen, 1956), expressed the belief that condensational heating does not play a role in the initiation of cyclogenesis, but rather that it effects the subsequent growth. The underlying idea behind this premise is that significant precipitation

in association with intense extratropical storms does not occur until after development has commenced and large-scale cloud systems have been formed; in other words, after broadscale saturation has been achieved.

Heavy convective rainfall, though, can occur in an unsaturated environment. Moreover, as was documented in the previous chapter, the initial development of some storms does indeed coincide with an outbreak of shower activity prior to large-scale saturation. It is therefore physically plausible that the released latent heat, through enhancement of the upward motion, plays an important role in the onset of cyclogenesis.

It is noted that the mechanism which is generally ascribed to the initiation of cyclogenesis, when the release of latent heat is not taken into account, is the superposition of a region of positive vorticity advection in advance of an upper-level trough over a low-level baroclinic (frontal) zone along which the thermal advection is discontinuous (Petterssen, 1956). Prior to development, when the vorticity advection is well to the rear of the surface front, the induced vertical motion is opposed by the distribution of horizontal advective cooling. When the region of positive vorticity advection has advanced so that the opposing influence of thermal advection beneath it is weaker or nonexistent, an imbalance is created and development commences<sup>10</sup>.

---

<sup>10</sup> Surface frictional effects must also be considered. That is, the magnitude of the vorticity advection must be sufficient to offset the opposing influence of friction as well as cold advection.

In each of the storms analyzed in this investigation, the development did occur in association with the advance of an upper trough towards a low-level frontal system. As exemplified by Fig. 65, however, in those storms in which the onset of cyclogenesis was accompanied by convective showers, the vorticity advection over the incipient low center during the initial stage of development was, qualitatively speaking, less than in the other cases. It would appear, therefore, that an outbreak of convective showers creates the imbalance necessary for development to commence prior to the time when vorticity advection alone would initiate development<sup>11</sup>. From another point of view, it is recalled that the error in prediction of the initial (or continued) development was manifest not in a complete failure to predict the occurrence of cyclogenesis, but rather in a lag in the forecast of the onset of development. Thus, it can be inferred that the convective release of latent heat initiates cyclogenesis prior to the time when it would have occurred if only the larger-scale baroclinic processes were operative. In effect, the release of gravitational instability by small-scale convection triggers the baroclinic instability associated with the large-scale temperature contrast between air masses.

---

<sup>11</sup> Close inspection of the figures Petterssen (1954, 1956) presents to illustrate that vorticity advection initiates cyclogenesis reveals that, in some of the cases, there was not appreciable vorticity advection over the incipient low at the time the initial development occurred; however, there was thundershower activity in the vicinity of the low center. It is hypothesized that, if numerical forecasts of these storms had been performed and the convective rainfall not predicted, the initiation of cyclogenesis would not have been properly forecast.

4c. Quantitative Reasonableness

In order to establish dynamically the magnitude of surface development consistent with the rainfall pattern observed in association with the onset of cyclogenesis, solutions were obtained to the diagnostic quasi-geostrophic omega equation for thermally induced motions (see, e.g., Danard, 1964),

$$\left( \nabla^2 + \frac{f_0^2}{\delta} \frac{\partial^2}{\partial p^2} \right) \omega = -\frac{R}{c_p p \delta} \nabla^2 Q, \quad (1)$$

and to the vorticity equation,

$$\frac{\partial f}{\partial t} = \frac{1}{f_0} \nabla^2 \frac{\partial \Phi}{\partial t} = f_0 \frac{\partial \omega}{\partial p} \quad (2)$$

where  $\Phi$  is the geopotential;  $\omega \equiv \frac{dp}{dt}$  represents the vertical motion;  $f$  is the geostrophic relative vorticity;  $f_0$  is a constant value of the coriolis parameter; the stability parameter  $\delta \equiv \left( \frac{\partial \theta}{\partial p} \right) \frac{\partial \ln \theta}{\partial p}$  is a function only of pressure; and  $Q$  is the diabatic heating.

It should be noted that the intent here is not to analyze the effect of individual showers, but rather to examine the collective influence of the latent heat released by convective activity in the vicinity of the low center on the deepening of the cyclone. More specifically, the question which is addressed is whether the latent heat release alone can account for the observed initial development.

The horizontal distribution of rainfall is modeled analytically as an ellipse in which the maximum precipitation rate,  $P_m$ , is at the center and values of  $P$  decrease exponentially therefrom. Thus,

$$P(x, y) = P_m e^{-\left[\frac{x^2}{A^2} + \frac{y^2}{B^2}\right]} \quad (3)$$

where  $A$  and  $B$  are scale factors which specify the minor and major axes ( $x$  and  $y$ , respectively) of the ellipse defined by  $P(x, y) = .1 P_m$ .

It can be assumed that the precipitation recorded at the ground is an adequate reflection of the vertically integrated heating. As has been noted by others (e. g., Charney and Eliassen, 1964), however, little is known about the vertical distribution of the latent heat released by cumulus convection. Therefore, detailed treatment of the vertical variation of heating and of other parameters is not justified. Thus, a model with the simplified vertical structure shown in Fig. 66 was adopted.

The omega equation was applied to levels 1 and 3. With the assumption that the latent heat release is confined to the layer between 900 mb and 200 mb, it can be shown that the heating at these levels is as follows<sup>12</sup>:

$$Q_1 = \frac{2g L P(x, y) P_{H_2O}}{.575 p_0 (1+\gamma)}$$

$$Q_3 = \frac{\gamma 2g L P(x, y) P_{H_2O}}{.575 p_0 (1+\gamma)}$$

(4)

Here,  $\gamma$  is an adjustable parameter which measures the ratio of the

---

<sup>12</sup> Stepwise integration of  $\frac{1}{g} \int_{900}^{200} Q(\tau) d\tau = L P P_{H_2O}$

upper to lower tropospheric heating (i. e.,  $\gamma = Q_3/Q_1$ ), and  $L$  is the latent heat of condensation.

When vertical derivatives are expressed in finite difference form, the omega equation at levels 1 and 3 becomes:

$$\begin{aligned} \nabla^2 \omega_1 + \frac{f_1^2 (\omega_3 - 3\omega_1)}{\delta_1 2 (\Delta p)^2} &= -\frac{R}{c_p p \delta_1} \nabla^2 Q_1 \\ \nabla^2 \omega_3 + \frac{f_3^2 (\omega_1 - 3\omega_3)}{\delta_3 2 (\Delta p)^2} &= -\frac{R}{c_p p \delta_3} \nabla^2 Q_3 \end{aligned} \quad (5)$$

The simultaneous solution of these equations for  $\omega_1$  and  $\omega_3$  at the center of the precipitation distribution was obtained via a Fourier transform technique which is outlined in Appendix B. A parabolic profile was then fit to the values of  $\omega_0$  ( $\omega_0 = 0$ ),  $\omega_1$ , and  $\omega_2$  ( $\omega_2 = \frac{\omega_1 + \omega_3}{2}$ ) in order to obtain  $\frac{\partial \omega}{\partial p}$  at the 1000 mb surface and thereby enable solution of Eq. (1) for the 1000 mb geopotential tendency, which may readily be translated to the deepening rate of the sea-level pressure system. The Fourier transform method of solving Eq. (1) also appears in Appendix B.

Observed one-hour precipitation amounts in the center of storms during the initial phase of development were typically between .5 and 1.0 in (see, for example, the rainfall histogram of Tulsa, Oklahoma, Fig. 11). The value of  $P_m$  used in the calculations, therefore, was .75 in  $\text{hr}^{-1}$ . On the basis of the characteristic dimensions of the precipitation areas, the values of  $A$  and  $B$  utilized in Eq. (3)

were such that the ellipse had major and minor axes of 750 and 250 km, respectively. Average values of  $\delta_1$  and  $\delta_2$  were ascertained from the values of  $\delta_1$  and  $\delta_2$  computed for each of the soundings available within a radius of 500 km from the low center of Cases I - VI during the initial stage of development. Numerically, the mean values of  $\delta_1$  and  $\delta_2$  were  $1.2 \times 10^{-2}$  and  $7.4 \times 10^{-2} \text{ m}^{-2} \text{ sec}^{-2} \text{ mb}^{-2}$ , respectively.

The computed deepening rates appear in Table 5. Values range from  $-.61 \text{ mb hr}^{-1}$  with  $\gamma = 3$  to  $-1.52 \text{ mb hr}^{-1}$  with  $\gamma = .5$ . As noted above, little is known about the vertical distribution of the latent heat released by cumulus convection. Theoretical treatments by various investigators (e.g., Kuo, 1965; Kasahara and Asai, 1967) predict substantially different vertical variations of the heating. There does appear, however, to be agreement that a larger portion of the heating occurs in the upper rather than the lower troposphere with a ratio of the upper to lower tropospheric heating having a maximum value of about 3. Thus, the most reasonable computed values of the deepening rate are between  $.6$  and  $1.2 \text{ mb hr}^{-1}$ . Typical values of the deepening rate observed during the onset of cyclogenesis were about the same.

At this point, a few comments are in order concerning the suitability of the geostrophic equations in this study. The magnitude of the assumed precipitation rate was considerably greater than the 2 cm or less per day consistent with the geostrophic assumption (Phillips, 1957). Undoubtedly, if numerical integrations were to be

performed with such a large value of the precipitation rate, serious errors in the forecasts would result after a number of time steps. The quantitative reliability of the instantaneous (i. e., diagnostic) relationship between the precipitation rate and computed quantities is not known.

Thus, although the computed deepening rates are comparable with those observed, doubt concerning the quantitative reliability of the geostrophic equations, as well as the relative crudeness of the modeling approximations, must temper any conclusions to be drawn. Nevertheless, the results of the computations are indeed consistent with the notion that the release of latent heat can account for the observed initial development. In other words, it is quantitatively reasonable that cumulus convection through the release of latent heat plays an important role in the initiation of cyclogenesis.



CHAPTER V

ARGUMENT IV: ALTERNATIVE SOURCES OF THE  
SYSTEMATIC ERROR

This chapter presents a discussion of Argument IV: there appears to be no defensible alternative explanation for the observed systematic error.

The numerical prognoses utilized in this investigation, with or without proper consideration of cumulus convection, are not perfect representations of the real atmosphere. Errors in the predictions can be introduced by any one or a combination of various physical, dynamical, or computational limitations, such as lack of horizontal and vertical resolution, insufficient initial data, initializing procedures, artificial boundary conditions, etc. The possibility must therefore be considered that the failure to forecast properly the onset (or continuation) of development was for reasons other than the failure to predict convective precipitation.

A priori, the most likely alternative explanation is the characteristic tendency for forecast 500 mb troughs to lag behind their observed positions, while the associated surface features move correctly to the east or northeast. Fig. 67 illustrates this type of error. In this 24-hour NMC-PE forecast, the surface low shows only a small error in position, but the 500 mb trough is slow in its translation eastward. The net effect is that the slope between the

500 mb trough axis and the surface low is greater than that actually observed<sup>13</sup>. In the forecast, therefore, the surface low is further ahead of the region of maximum positive vorticity advection that lies in advance of the upper-level trough. Consequently, the failure to properly forecast the onset of development of some storms could conceivably be attributed to failure to predict enough vorticity advection over the incipient low center.

However, prediction of too great a slope between the 500 mb and surface systems is generally observed to be greatest in the 36-hour forecasts and least pronounced, often nonexistent (especially in the LFM forecasts), in the 12-hour forecasts; and in most cases, the adequacy in predicting the initial development was evaluated on the basis of the 12-hour forecasts. Moreover, difference between the observed and forecast vorticity advection over the incipient low centers, assessed qualitatively, was not systematically related to whether the onset of development was properly predicted. The greater slope between the forecast 500 mb troughs

---

<sup>13</sup> The nature of this type of error, with reference to the NMC-PE, has been discussed by Fawcett (1969). The slowness in translation of the 500 mb trough can reasonably be ascribed to truncation error. The correct motion of the surface system, Fawcett asserts, can be shown experimentally to be due to latent heat feedback. The precipitation predicted in advance of a low tends to accelerate it towards the center of heaviest rainfall; however, it is the experience of this author that, although latent heat may accentuate the effect, the relative slowness of predicted 500 mb troughs with respect to the surface lows occurs also when no precipitation is forecast. Furthermore, Fawcett (1967) indicates that this type of error was a feature of the NMC-PE before precipitation was incorporated into the model. Additionally, it is noted that this error is somewhat greater in the FNWC-PE than in the NMC-PE and less in the LFM.

and surface features likely contributed to the magnitude of the error between the observed and predicted initial development, but it was not crucial to prediction of the initiation of cyclogenesis.

Principal other alternative explanations for the failure to predict the onset of development are: i) inability to resolve all relevant energy-producing systems, and ii) initialization procedures. The models can resolve motions only on a scale greater than twice the grid interval, so that any processes occurring on a smaller scale, which could be of importance, are eliminated. The smoothing inherent in preparation of initial data for use in primitive equation models could eliminate from the initial state detail that in the real atmosphere was crucial to the onset of cyclogenesis. Although these, and perhaps other alternative explanations as well, could indeed result in failure to predict the initial development (or continued development) in any given situation<sup>14</sup>, there does not appear to be any reason for the systematic error that was observed. That is, no explanation can be given as to why the models consistently failed to predict the initiation of cyclogenesis only when the actual initial development coincided with an outbreak of convective showers and the convective rainfall was not forecast.

---

<sup>14</sup> It is recalled that in only one case did a model fail to predict the continuation of development for reasons other than the occurrence of convective showers (NMC-PE forecast from 00Z Feb. 13 - Case V).

CHAPTER VI

SUMMARY AND CONCLUSIONS

The goal of this thesis has been to determine whether cumulus convection plays a role in the development of extratropical cyclones, and if it does, to determine the nature of that role. The basic approach adopted in investigating this question was to determine whether there is a systematic relationship between the extent and degree of convection within cyclones and the departure of the actual storm evolution from that predicted by operational forecast models.

On the basis of detailed analysis of the two storms initially chosen for study, the following hypothesis was formulated, and the balance of the investigation directed primarily towards ascertaining its validity:

In some instances of extratropical cyclogenesis, cumulus convection plays a crucial role in the initiation of development through the release of latent heat in the vicinity of the cyclone center. In such cases, dynamical models which do not adequately simulate convective precipitation, especially as it might occur in an environment that is unsaturated, will fail to properly forecast the onset of development.

Evidence either to support or refute the hypothesis was derived from detailed analysis of seven additional storms, cursory examination of twelve others, and both qualitative and quantitative

consideration of the physical mechanisms involved. Although the evidence may not be conclusive proof of the hypothesis, it does provide sufficient support to elevate its stature from a statement of provisional conjecture, which it was originally, to an assertion that may be accepted as highly probable.

The case in support of the hypothesis was summarized in terms of four arguments:

- I. In some storms, there was a coincidence in time between the initial development and the occurrence of convective showers in the vicinity of the low center. Almost invariably, the environment in which the convection occurred was unsaturated.
- II. In those cases in which the initial development was accompanied by convective showers in the vicinity of the low center and the environment in which the convection occurred was unsaturated, the dynamic prognoses systematically failed to properly forecast the onset of development, apparently because of the models' failure to predict the convective rainfall.
- III. The importance of the latent heat release by cumulus convection to the initiation of development of some extratropical cyclones, which is implied by the apparent source of the systematic error, is physically plausible and quantitatively reasonable.
- IV. There appears to be no defensible alternative explanation for the observed systematic error.

It was noted that significant shower activity occurred in the center of storms generally only during the early phases of their

life history. The characteristic distribution of the convection during the initial stage of development was a line of thunderstorms which extended south of the low and which was imbedded in a more general area of scattered to broken showers and thunderstorms that extended and broadened somewhat to the north of the low (for example, see Fig. 2). In terms of the net amounts of convective rainfall that were being produced, the degree of convection was greatest in the center of the storm. Following an initial period of development, which lasted anywhere from 6 to 36 hours, significant shower activity became dissociated from the low center.

In those storms in which the initial development was accompanied by an outbreak of convective showers and the precipitation was not forecast, the models generally did forecast cyclogenesis, but the predictions lagged behind the real atmosphere in the onset of development. It would appear, therefore, that the release of latent heat by cumulus convection can initiate development prior to when it would occur if large-scale motions and processes alone were operative.

Convective activity which was not in the immediate vicinity of the storm center did not appear to be crucial either to the initiation of development or to the trend of continued development following the onset of cyclogenesis. This observation was based upon the fact that only when the convection occurred in the center of the storm was there a consistent contemporary relationship between it and the actual storm evolution or was there a systematic error in the forecasts of the initiation or continuation of development. However,

the possibility cannot be ruled out that convective activity on the periphery of the storm, through the release of latent heat or otherwise, plays some role in the detail and magnitude of the storm evolution, since the approach employed in this investigation may not have been adequate to deduce such a role.

Each of the storms analyzed for this investigation developed over the eastern two thirds of the United States or western Atlantic. In approximately half the cases, the initial development was accompanied by an outbreak of convective showers in the vicinity of the low center. On the basis of synoptic experience and the fact that the storms selected for analysis were chosen without prior specific knowledge of the extent of convective activity accompanying their development, the sample is considered representative of the intense cyclones occurring east of the Rocky Mountains. It should be noted, however, that because of this region's close proximity to a source of warm moist air, in the Gulf of Mexico and Caribbean Sea, it is an area particularly susceptible to the generation of the convective instability necessary for the occurrence of the shower activity (Fawbush, et al., 1951). Some other geographical areas are not so favored. For example, convective instability is less likely over northern Europe because of the relatively cold waters adjoining this region. The extent of convective activity is therefore not as great in northern European cyclones as in storms occurring over the eastern two thirds of the United States (Palmen and Newton, 1969). An additional point is that while significant shower activity,

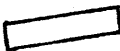
if any, is generally confined close to the center of a cyclone over land (though not necessarily in the center itself), showers in oceanic cyclones occur in the cold air to the west of the low center (Palmen and Newton, 1969). Thus, one can speculate that the release of latent heat by cumulus convection is an important factor in the initial development of a smaller fraction of storms occurring over northern Europe (or other regions not especially conducive to the generation of convective instability) than in storms east of the Rockies, and is an important factor in storms developing over land more often than in oceanic cyclones. A study such as presented in this thesis is recommended to confirm this speculation.

Finally, it is noted that even in those cases in which the initiation or trend of continued development was forecast, the magnitude of the predicted development was generally less than observed. Whether this reflects lack of incorporation or inadequate formulation of some relevant physical process, computational limitations of the models, or a combination thereof, is not known. Future research should be directed towards answering this question because of its importance both to numerical forecasting and to an improved understanding of the complex phenomenon of cyclogenesis. The most direct and possibly most productive approach to the problem would be to perform several reruns of the prediction of selected cases of cyclogenesis with various modifications of potentially relevant parameters and processes. Presumably, those modifications



which consistently yield the best forecasts will reflect the relative importance of the various parameters and processes considered. Particular emphasis should be placed on assessing further, through improvement of parameterization schemes, the role of cumulus convection, or more generally, the role of sub-synoptic-scale motions and processes in extratropical cyclogenesis.

Table 1. Symbols utilized in radar charts.\*

<u>Character of Echoes</u>		
<u>Symbol</u>	<u>Echo System</u>	<u>Definition</u>
⊖	Widely scattered area	Related or similar echoes covering 1/10 of the reported area.
⊗	Broken area	Related or similar echoes in a pattern that covers 6/10 or more of the reported area but contains breaks or corridors.
⊕	Solid area	Contiguous echoes covering, usually, more than 9/10 of the reported area.
	Line of echoes (scattered, broken, or solid)	Related echoes in an extended pattern.

Note: HHH indicates position of individual cells imbedded in echo system. HHH is height of echo top in hundreds of feet.

Characteristic Type of Precipitation

<u>Symbol</u>	<u>Precipitation</u>
R	Rain
S	Snow
RW, SW	Showers
TRW	Thundershowers
Z	Freezing Precipitation

Echo Intensity

<u>Symbol</u>	<u>Estimated Precipitation Rate (in hr<sup>-1</sup>)</u>
--	Very light (< .01)
-	Light (.01 - 0.1)
	Moderate (0.1 - 1.0)
+	Heavy (1.0 - 5.0)
++	Very heavy (> 5.0)

\* Symbols and meanings as described in Weather Radar Manual (WBAN), Part A, U. S. Dept. of Commerce, National Oceanic and Atmospheric Administration, Washington, D. C.

Table 2. Models considered for the initial times relevant to the nine detailed case studies.

<u>Case</u>	<u>Initial Time</u>	<u>NMC-PE</u>	<u>FNWC-PE</u>	<u>LFM</u>
I	12Z 4 Feb. 1971*	X	X	
	00Z 5 Feb. 1971*	X	X	
II	12Z 1 April 1970	X		
	00Z 2 April 1970	X		
III	00Z 11 Nov. 1968	X		
	12Z 11 Nov. 1968	X		
	00Z 12 Nov. 1968	X		
IV	12Z 2 March 1971*	X		
	00Z 3 March 1971	X	X	
	12Z 3 March 1971	X	X	
	00Z 4 March 1971	X	X	
V	00Z 12 Feb. 1971*	X		
	12Z 12 Feb. 1971	X	X	X
	00Z 13 Feb. 1971*	X	X	
VI	00Z 23 March 1969	X		
	12Z 23 March 1969	X		
VII	00Z 26 Feb. 1971*	X	X	
	12Z 26 Feb. 1971*	X	X	
VIII	12Z 25 Dec. 1970	X	X	X
	00Z 26 Dec. 1970*	X	X	
IX	12Z 25 Jan. 1971*	X	X	
	00Z 26 Jan. 1971*	X	X	

\* Objective analysis of the initial field of sea-level pressure not available (see Section 2f and/or Appendix A).

Table 3. Characterization of the initial development of the nine detailed case studies.

<u>Case</u>	<u>Convective Precipitation in Storm Center?</u>	<u>Environment of Low Saturated?</u>	<u>Convective Precipitation Predicted?</u>	<u>Adequate Forecast of the Onset of Development?</u>
I	Y	N	N	N
II	Y	N	N	N
III	Y	N	N	N
IV	Y	N	N	N
V	Y	N	N	N
VI	Y	Y	Y	Y
VII	N	N	-	Y
VIII	N	N	-	Y
IX	N	N	-	Y

Y = Yes

N = No

Table 4. Characterization of the initial development of the twelve storms for which a cursory examination was made.

<u>Case</u>	<u>Convective Precipitation in Storm Center?</u>	<u>Environment of Low Saturated?</u>	<u>Convective Precipitation Predicted?</u>	<u>Adequate Forecast of the Onset of Development?</u>
6-7 March 1971*	Y	N	N	N
5-7 April 1971*	Y	N	N	N
14-16 December 1971	Y	N	N	N
9-10 December 1971	Y	N	N	N
3-4 February 1972	Y	N	N	N
25-26 March 1971*	Y	Y	Y	Y
18-19 February 1971*	N	N	-	Y
23-24 March 1971*	N	N	-	Y
30-31 October 1971	N	N	-	Y
1-3 November 1971	N	N	-	Y
18-19 November 1971	N	N	-	Y
2-4 January 1972	N	N	-	Y

Y = Yes

N = No

Note: NMC-PE forecasts were considered in all cases. LFM forecasts were available for those cases indicated by an asterisk (\*).

Table 5. Computed deepening rates.

<u><math>V = Q_3/Q_1</math></u>	<u>Surface Deepening Rate (mb hr<sup>-1</sup>)</u>
3.0	- .61
2.5	- .69
2.0	- .79
1.5	- .99
1.0	-1.15
.67	-1.42
.50	-1.52

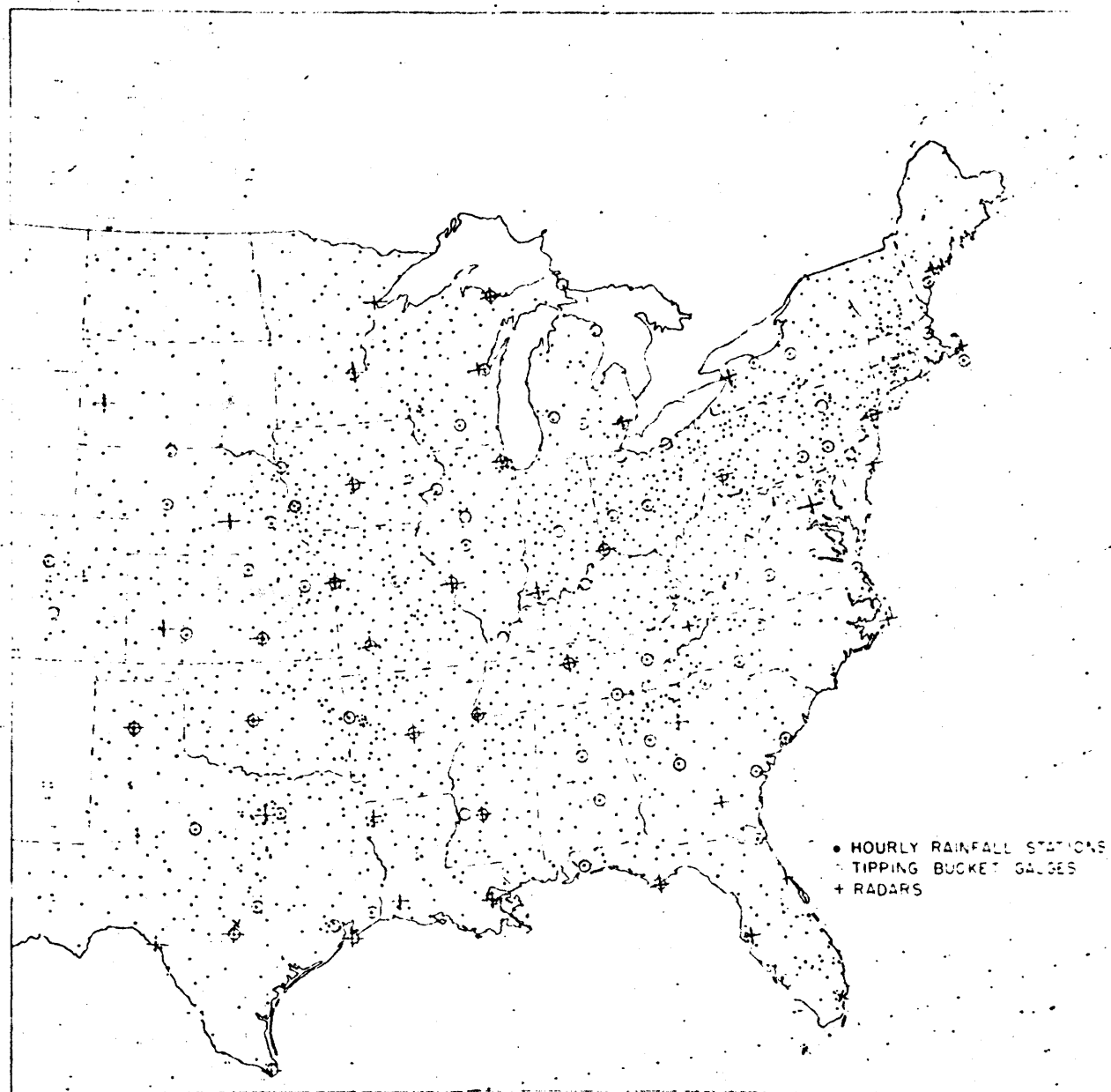


Fig. 1. Location of hourly rainfall stations, tipping-bucket gauges, and weather radars. (The general operating range of radars is 250 naut. mi. The effective range for detecting precipitation, however, is somewhat less owing to earth curvature effects and beam spreading.)

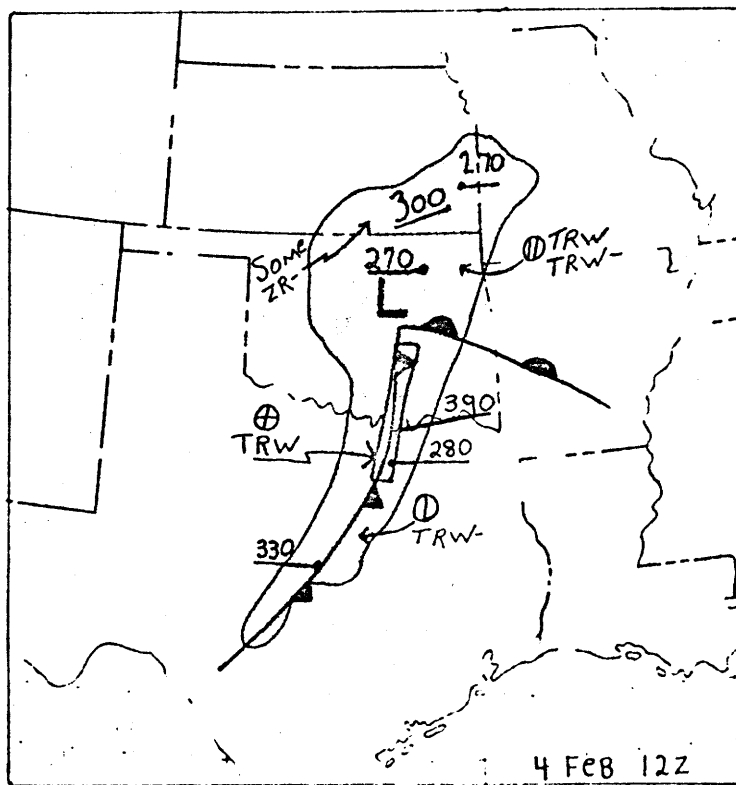
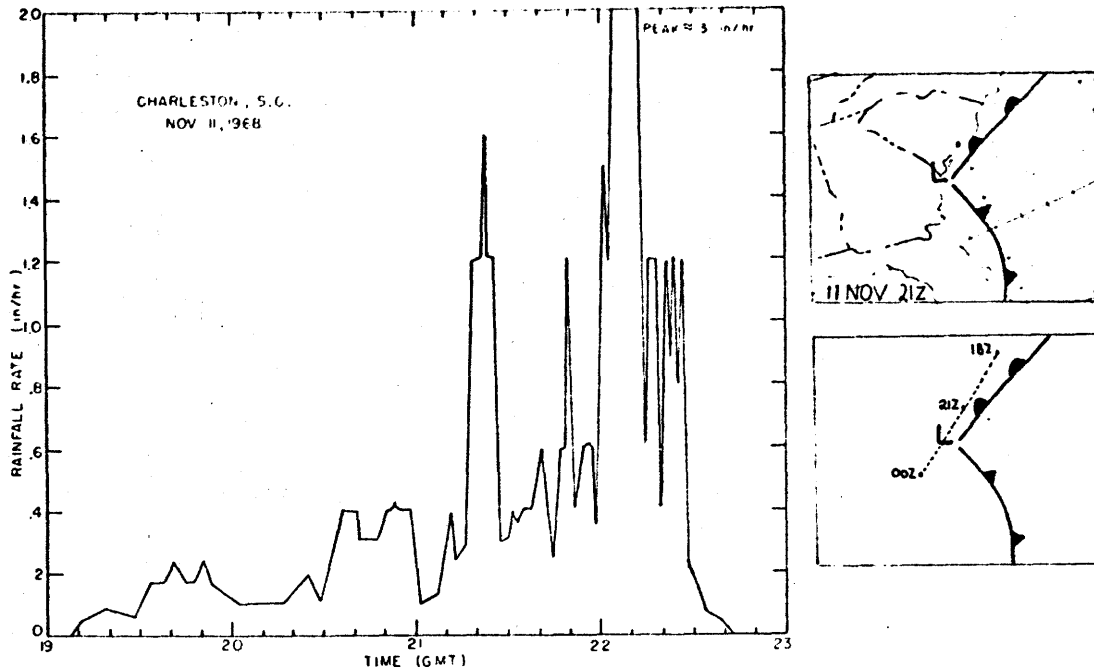
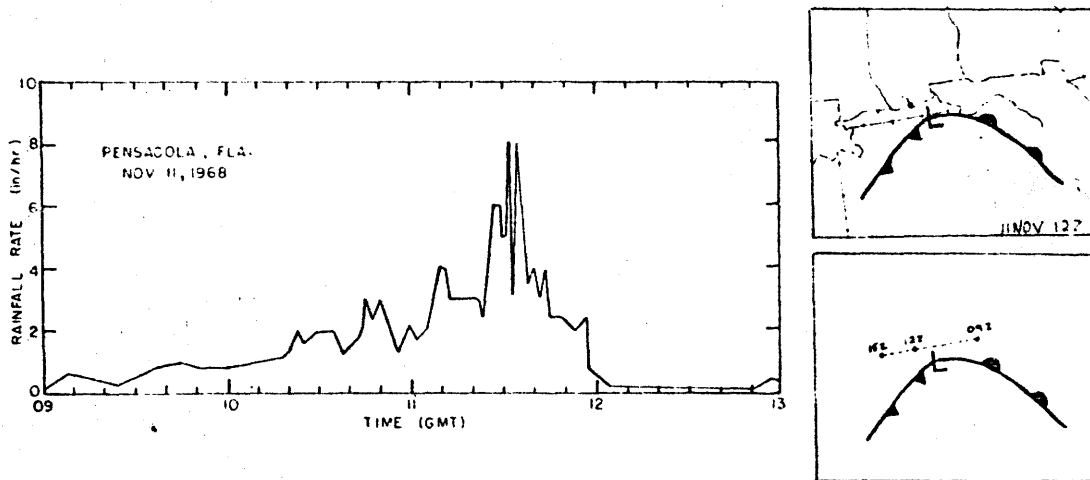


Fig. 2. Surface-radar chart. Stippling indicates areal echo coverage. Shading indicates area of squall line. For the meanings of symbols, see Table 1.





(a)



(b)

Fig. 3. Tipping-bucket recording rain-gauge traces with schematics showing line segments along which precipitation cross sections apply. Top figure of schematics indicates geographical location of station at specified time, while the bottom figure shows successive positions of station with respect to the moving surface system.

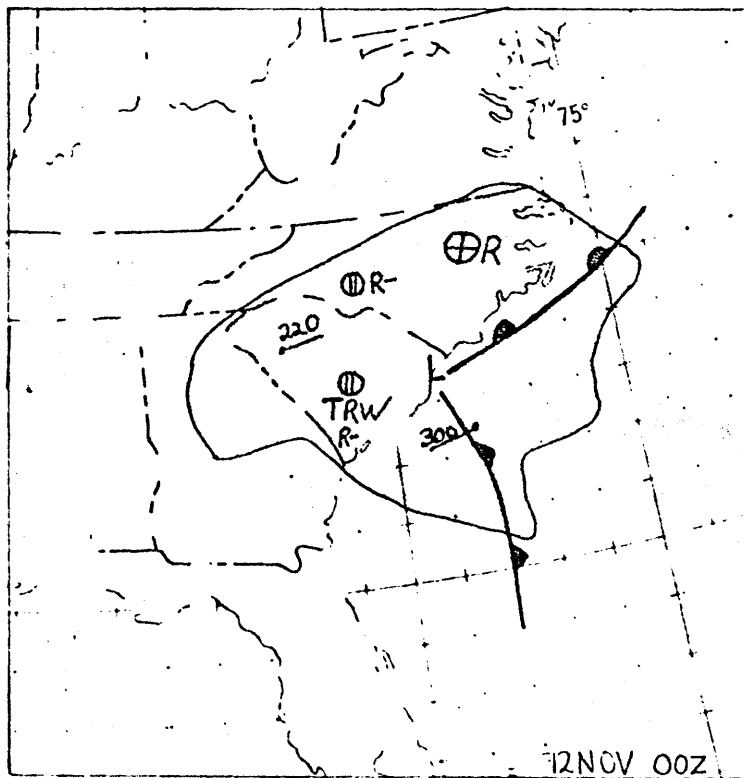
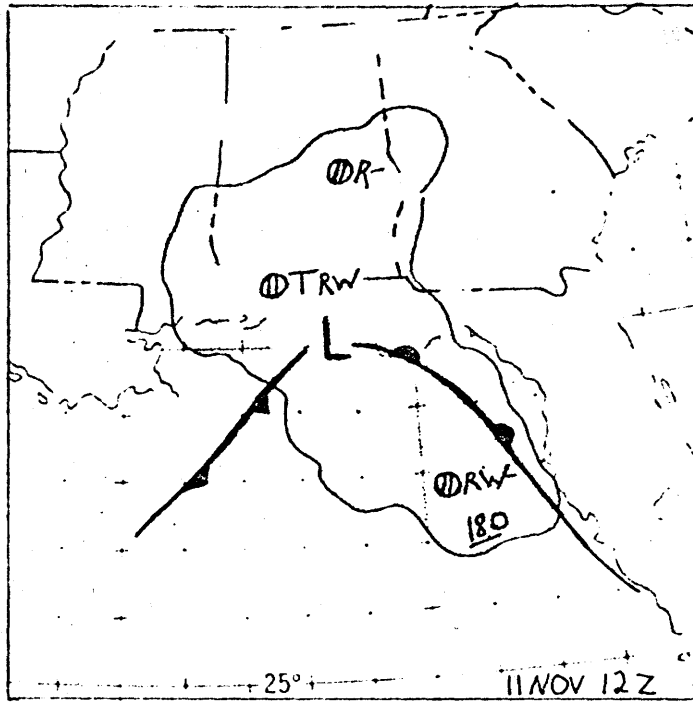
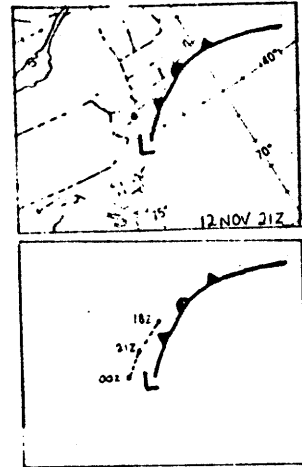
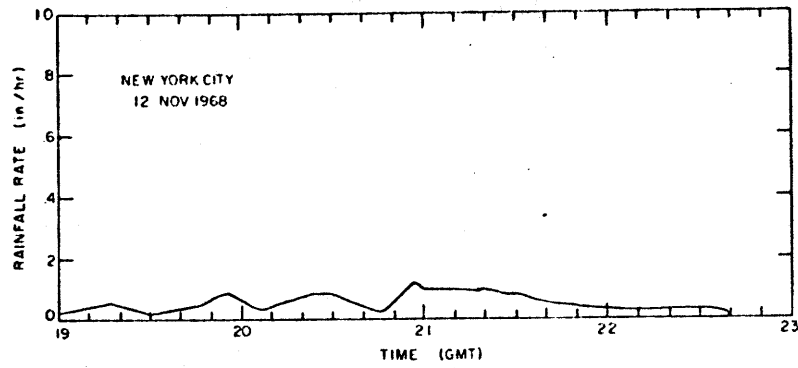
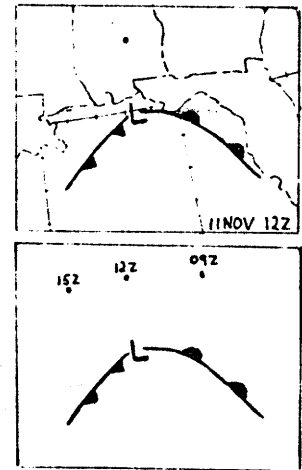
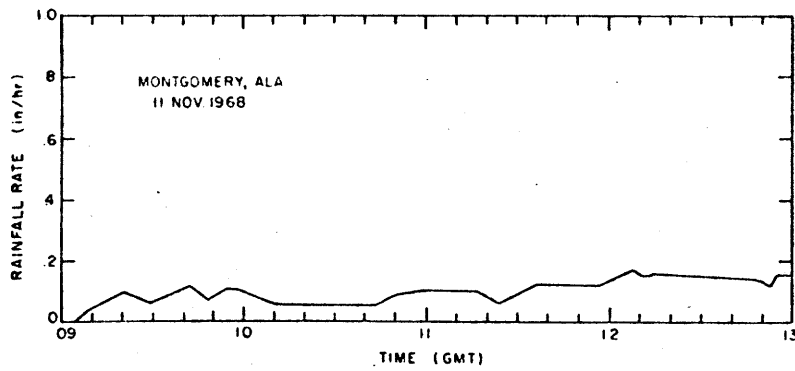


Fig. 4. Surface-radar charts. Same as Fig. 2, except for times indicated.

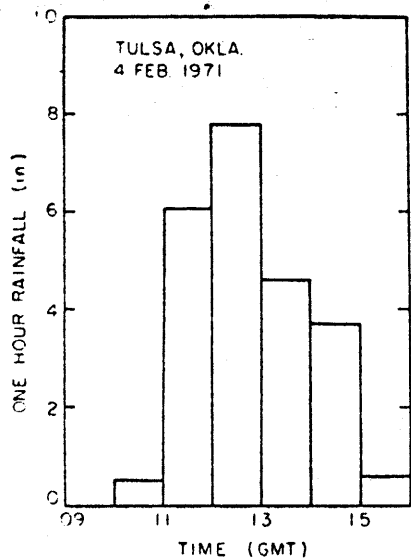


(a)

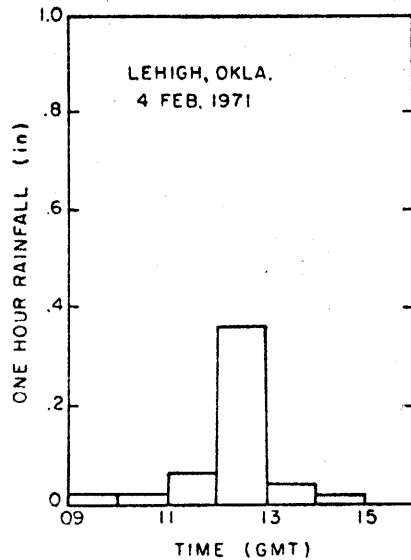


(b)

Fig. 5. Precipitation cross sections.  
Same as Fig. 3, except for New York and Montgomery.



(a)



(b)

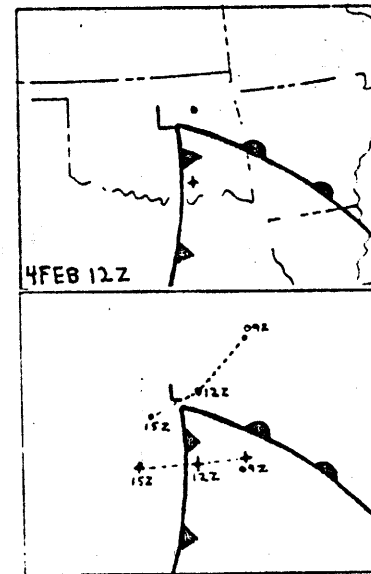
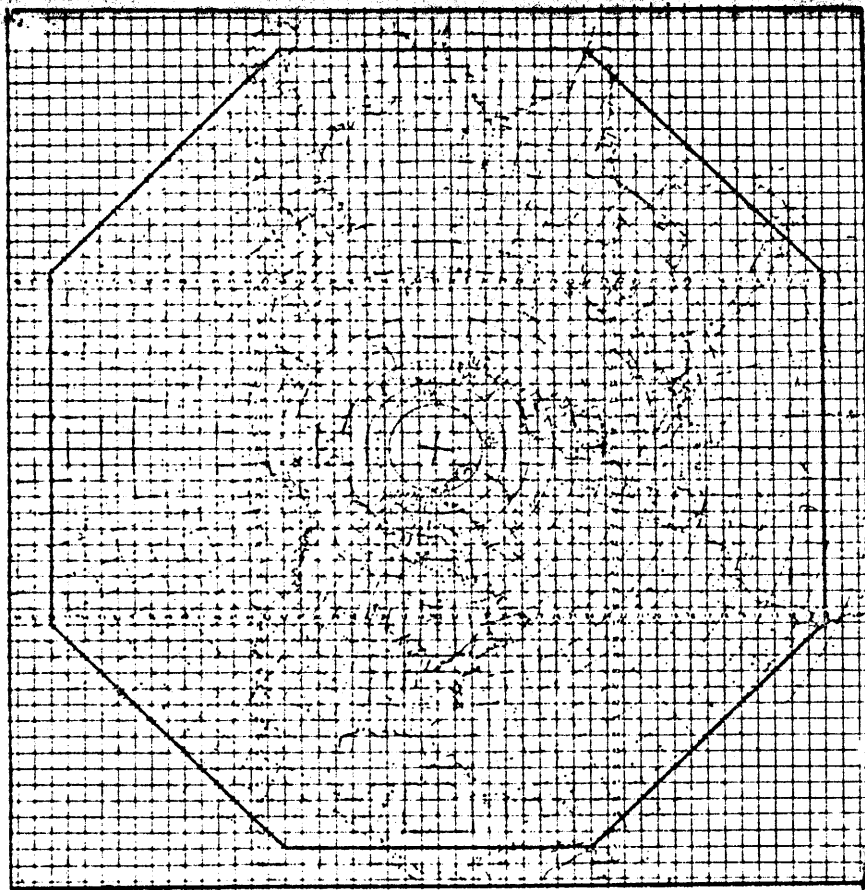
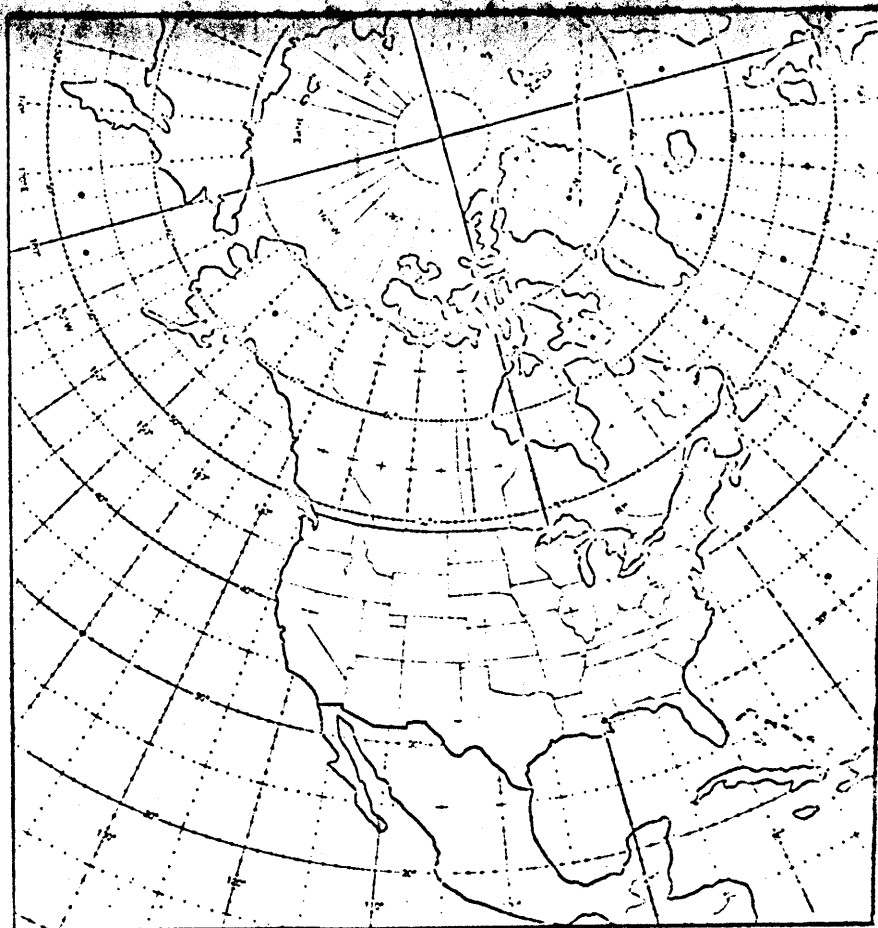


Fig. 6. Rainfall histograms with schematic showing line segments along which cross sections apply. Top figure of schematic indicates geographical location of stations, while the bottom figure shows successive positions of stations with respect to the moving surface system. • Tulsa; † Lehigh.

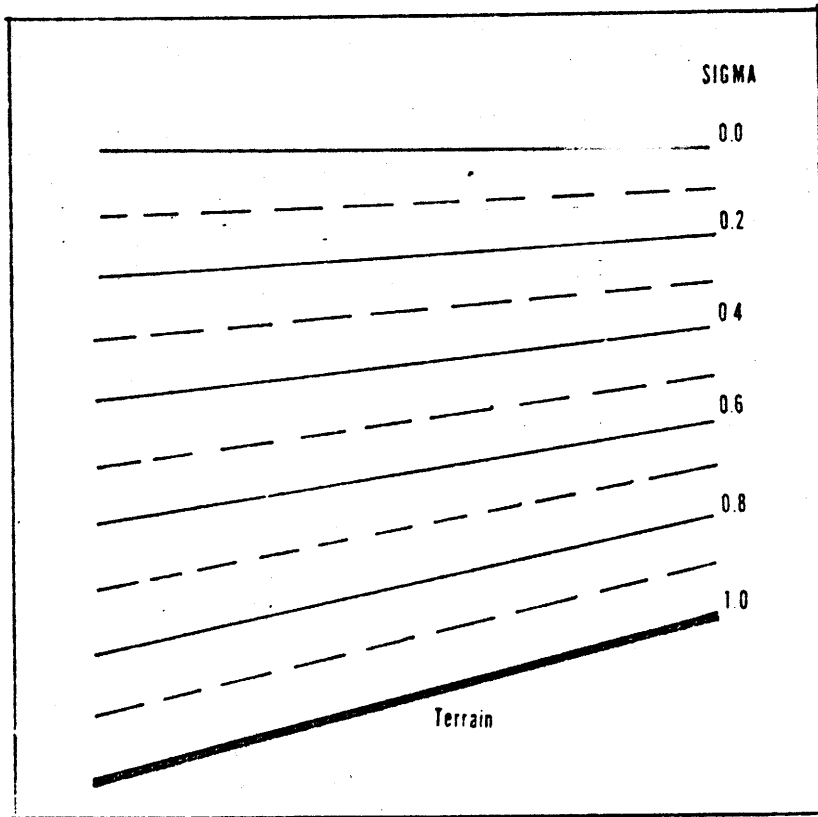


(a)

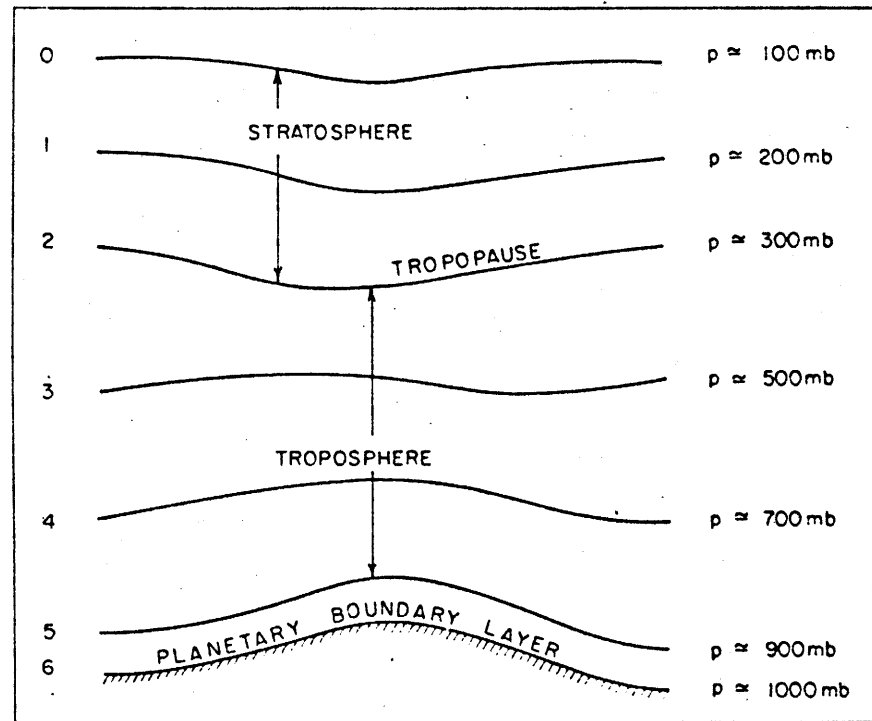


(b)

Fig. 7. - (a) Horizontal domain of integration of NMC-PE [after Shuman and Hovermale (1968)]. NMC-PE domain is a subset of the FNWC-PE domain in which the equator is an inscribed circle; (b) Horizontal domain of LFM [after Howcroft (1970)].



(c)



(d)

Fig. 7. - (c) Vertical structure of FNWC-PE [after Kesel (1970)]; (d) Vertical structure of NMC-PE and LFM [after Shuman and Hovermale (1968)].

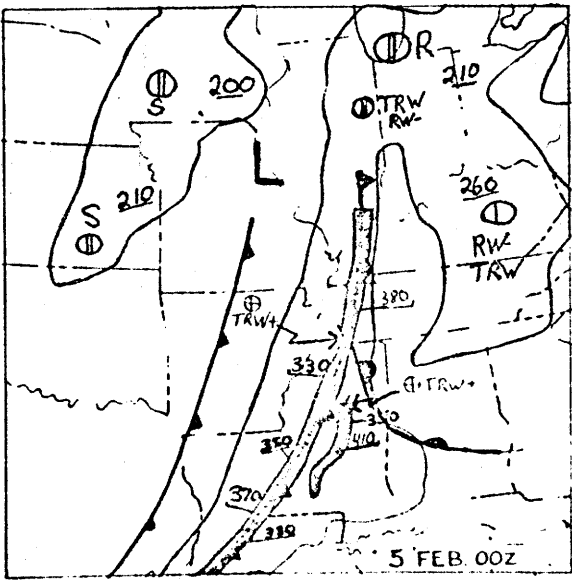
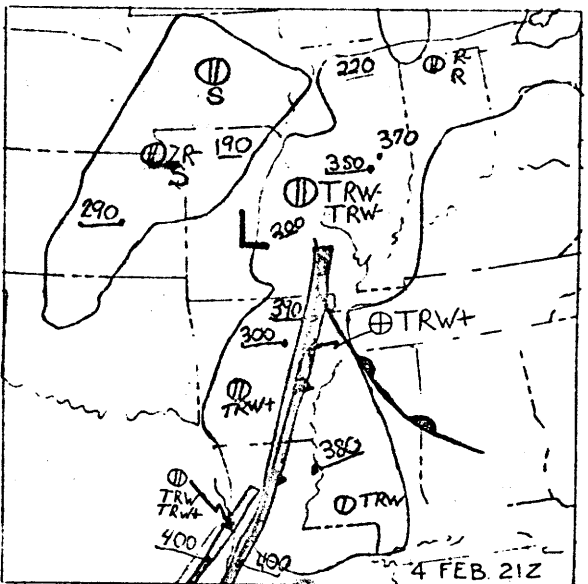
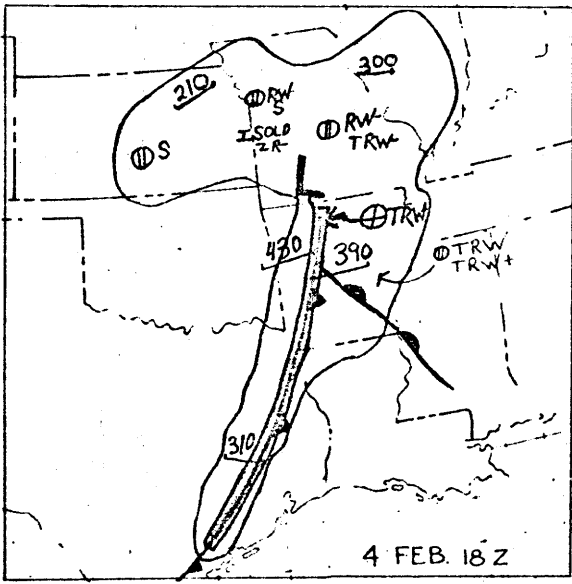
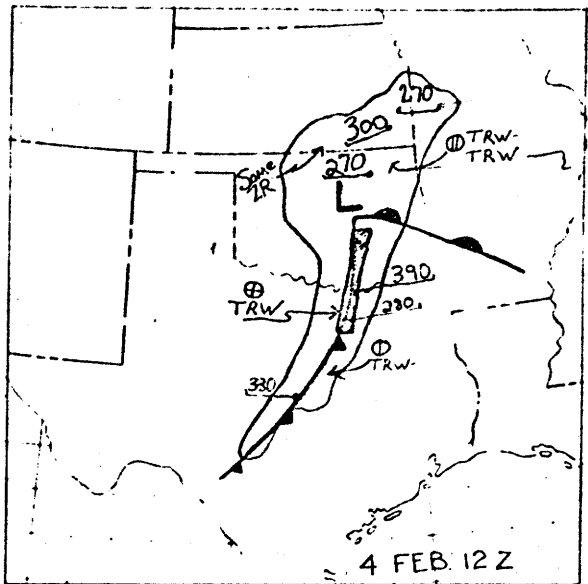
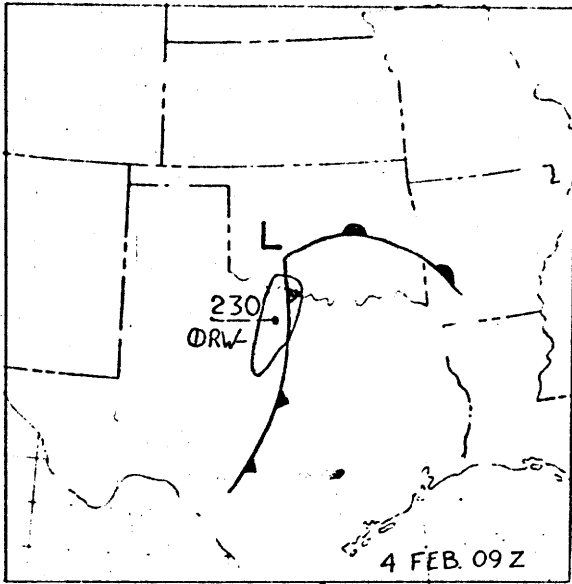


Fig. 8. Surface-radar charts. Same as Fig. 2, except for times indicated.

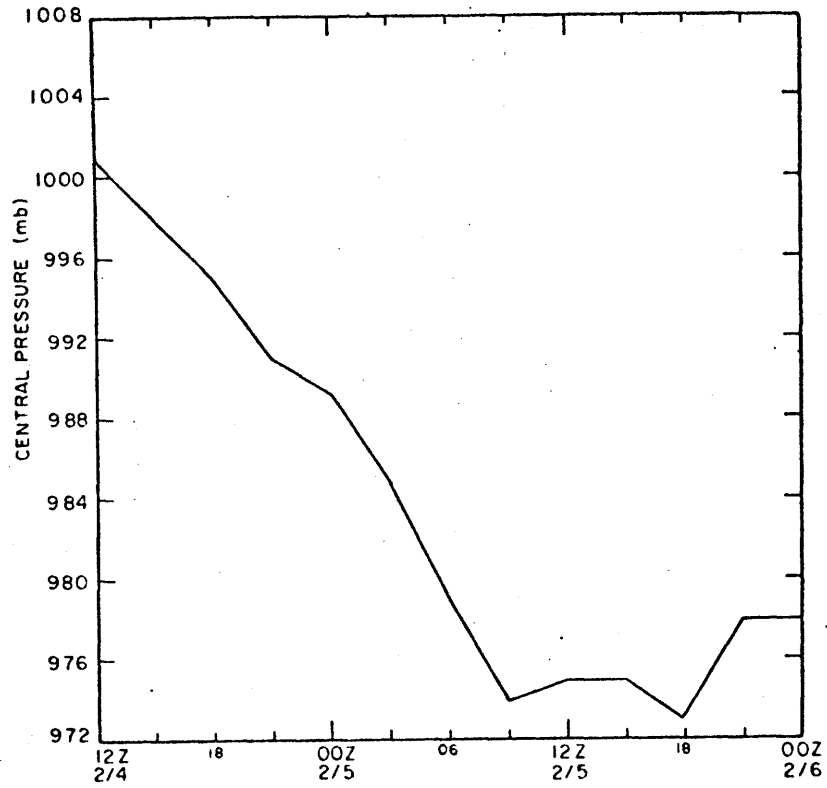


Fig. 9. Observed central pressure vs. time (plotted generally at 3-hour intervals).

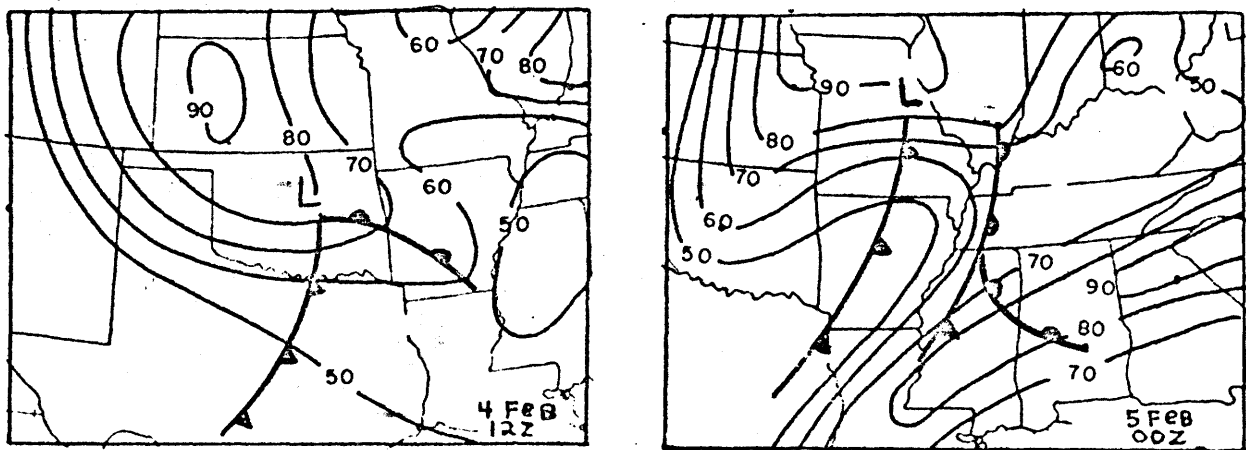


Fig. 10. Surface-mean relative humidity charts (per cent).



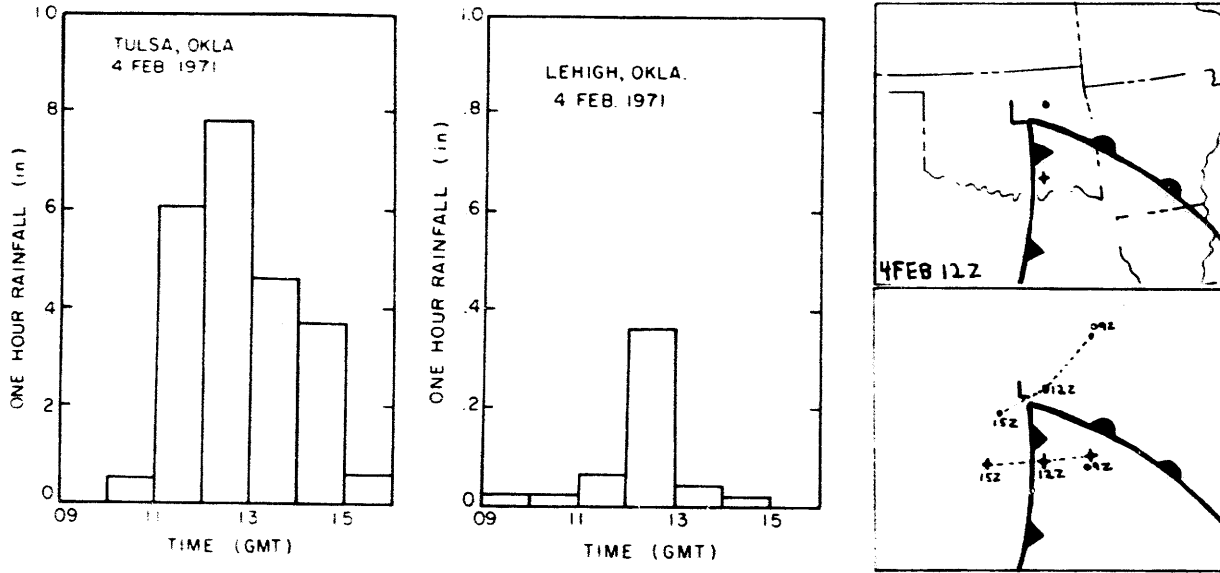


Fig. 11. Precipitation cross section. Same as Fig. 6.

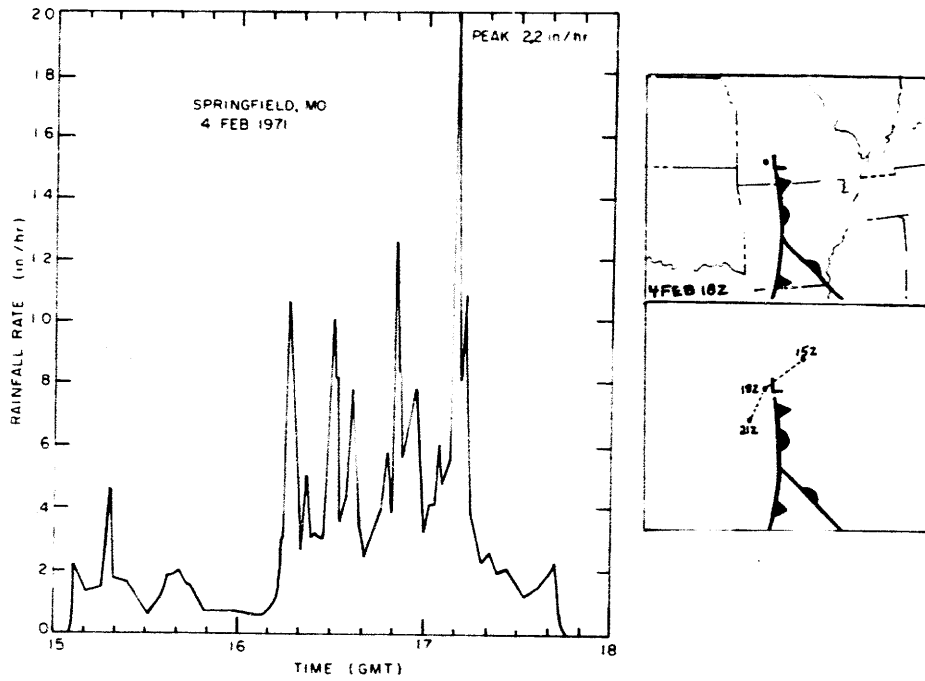


Fig. 12. Precipitation cross section. Same as Fig. 3, except for Springfield, Mo.

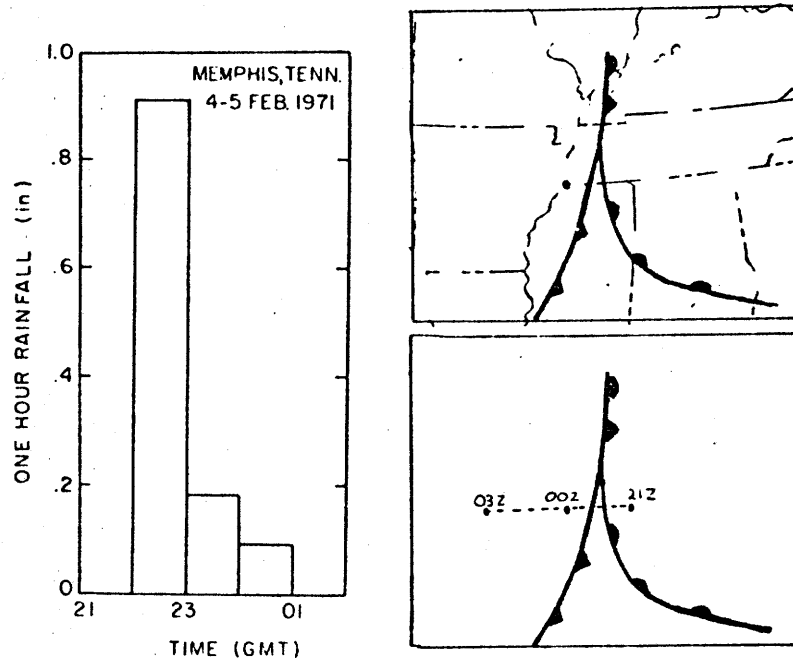


Fig. 13. Precipitation cross section. Same as Fig. 6, except for Memphis, Tennessee.

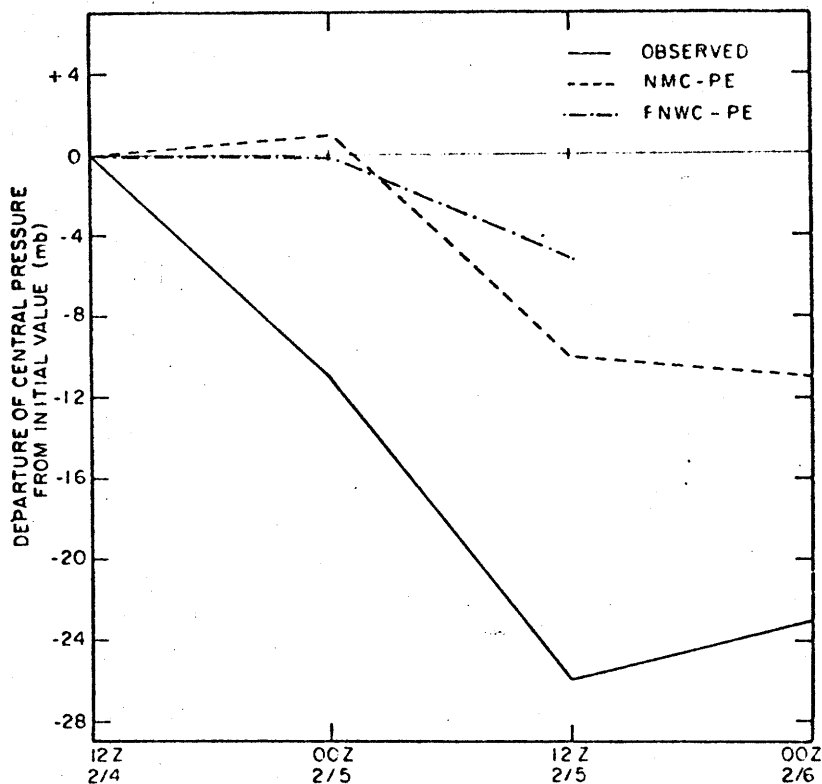


Fig. 14. Observed and forecast central pressure vs. time in terms of departure from initial value at 12Z 4 Feb. 1971 (values plotted at 12-hour intervals).

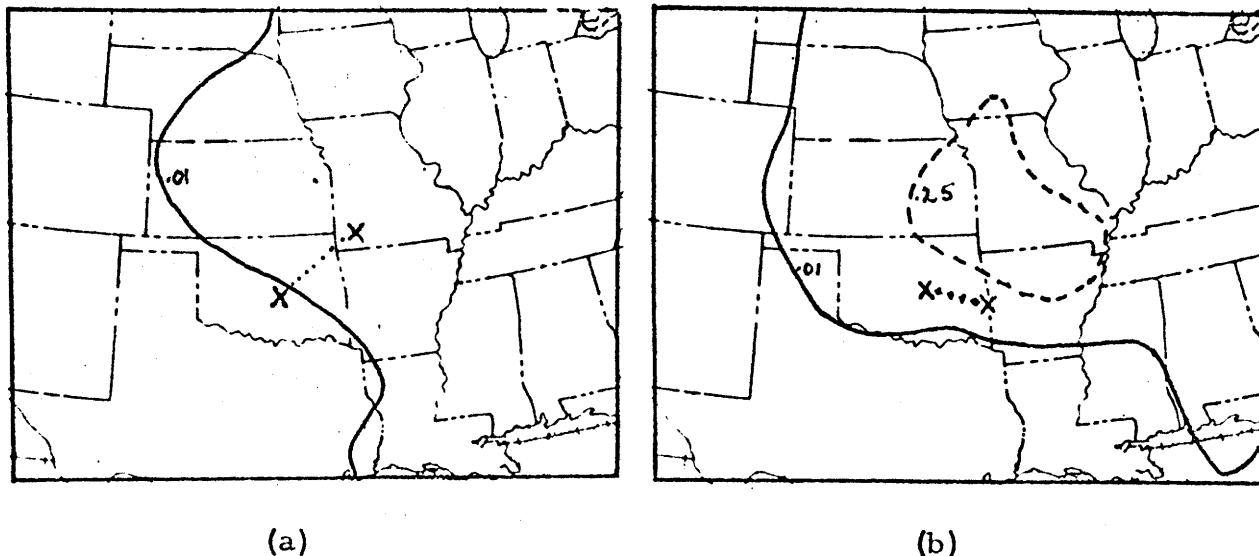


Fig. 15. FNWC-PE (a) and NMC-PE (b) 12-hour precipitation forecasted from 12Z 4 Feb. 1971. Solid line (—) contours .01, .50, 1.0, etc. Dashed line (---) intermediate contours at .25 in intervals. Track of forecast low center (X · · · · X) superimposed.

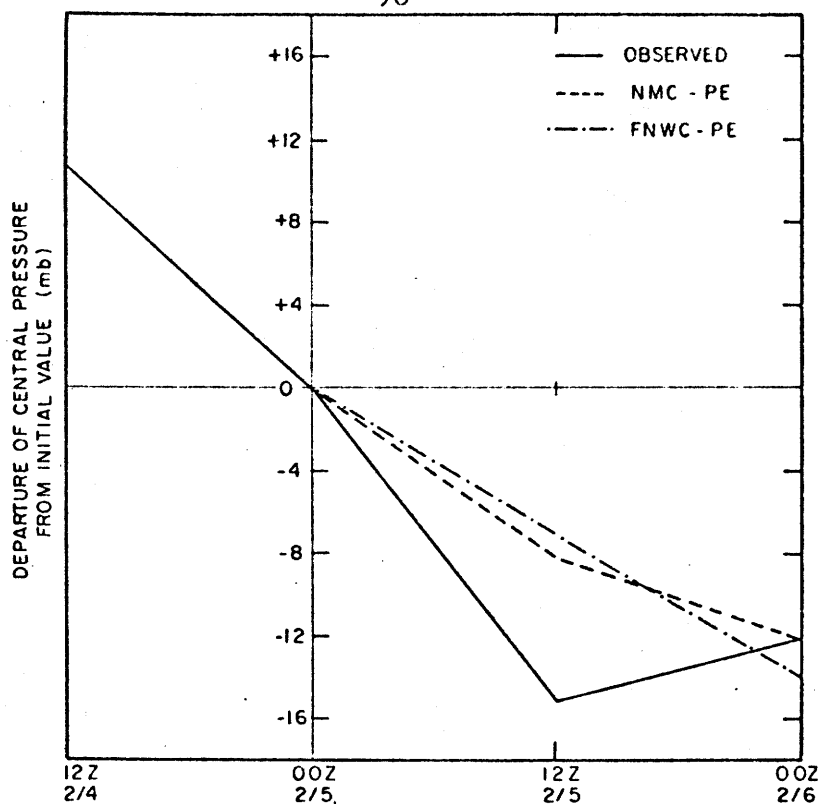


Fig. 16. Observed and forecast central pressure vs. time in terms of departure from initial value at 00Z 5 Feb. 1971 (values plotted at 12-hour intervals).

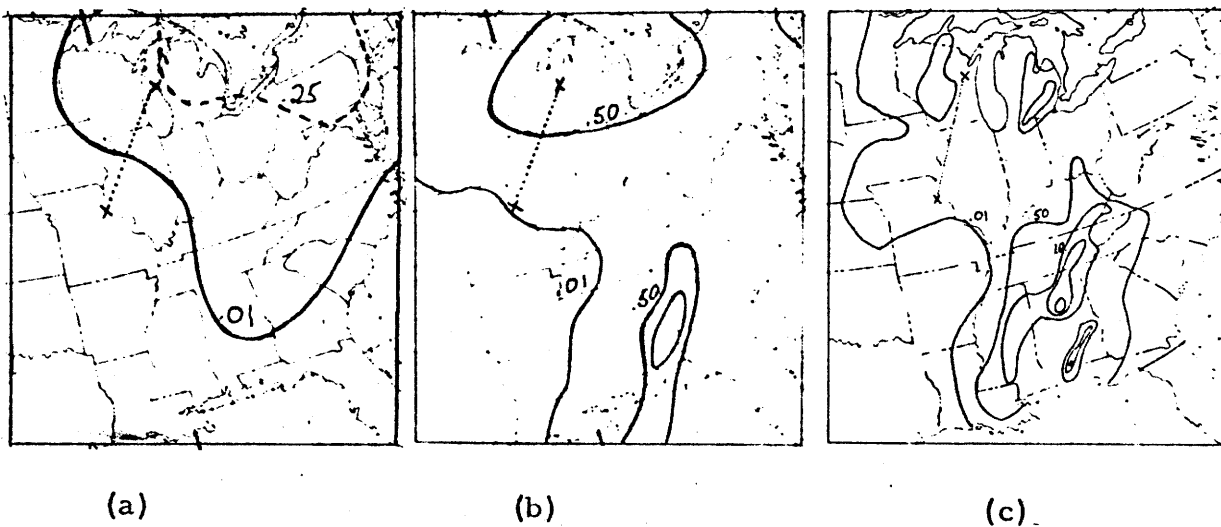


Fig. 17. NMC-PE (a), FNWC-PE (b) 12-hour precipitation forecasted from 00Z 4 Feb. 1971, and 12-hour observed precipitation, 00Z-12Z 5 Feb. 1971(c). Contour intervals as in Fig. 15. Track of forecast and observed low center (X . . . . X) superimposed.

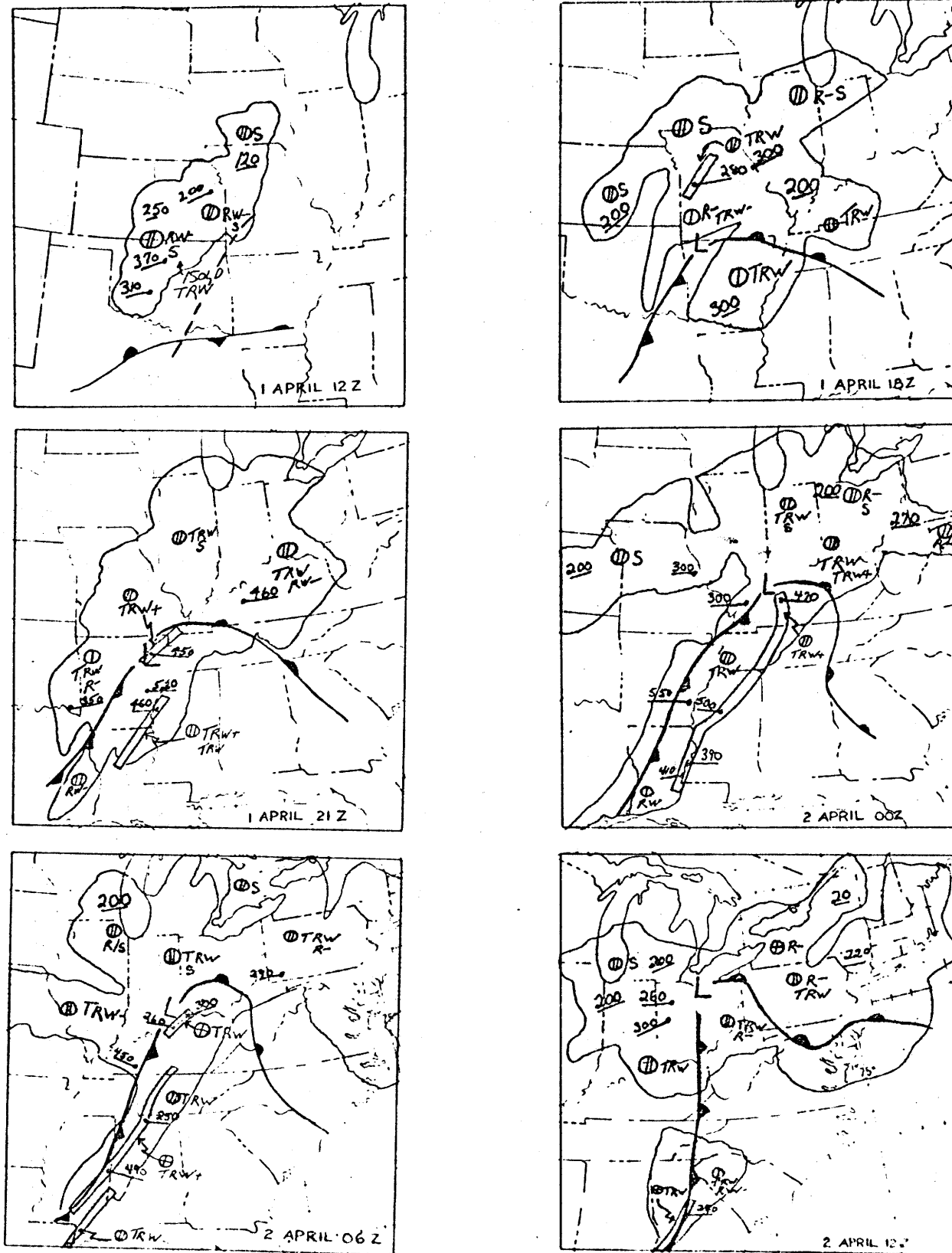


Fig. 18. Surface-radar charts. Same as Fig. 2, except for times indicated. Dashed line (---) in 1 April chart indicates trough axis.

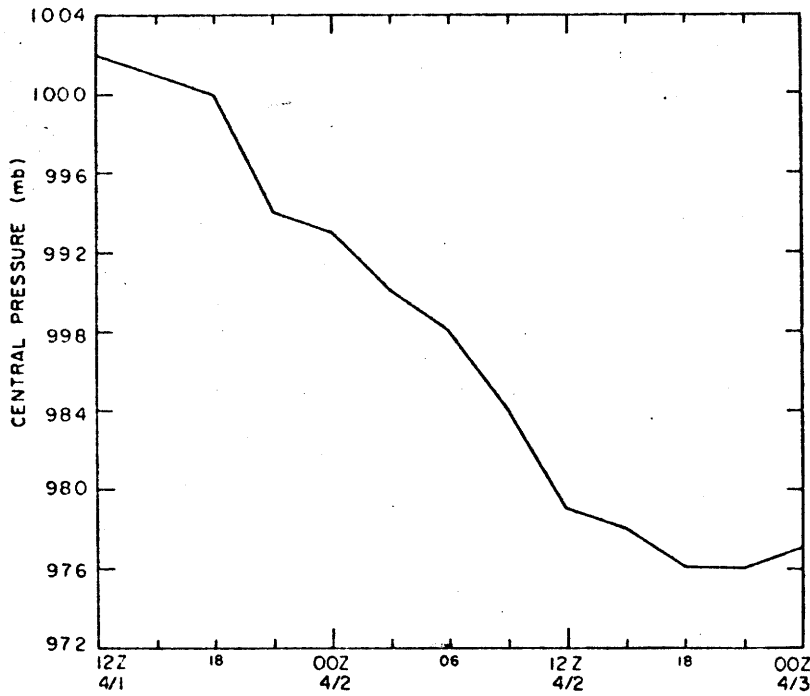


Fig. 19. Observed central pressure vs. time (plotted generally at 3-hour intervals).

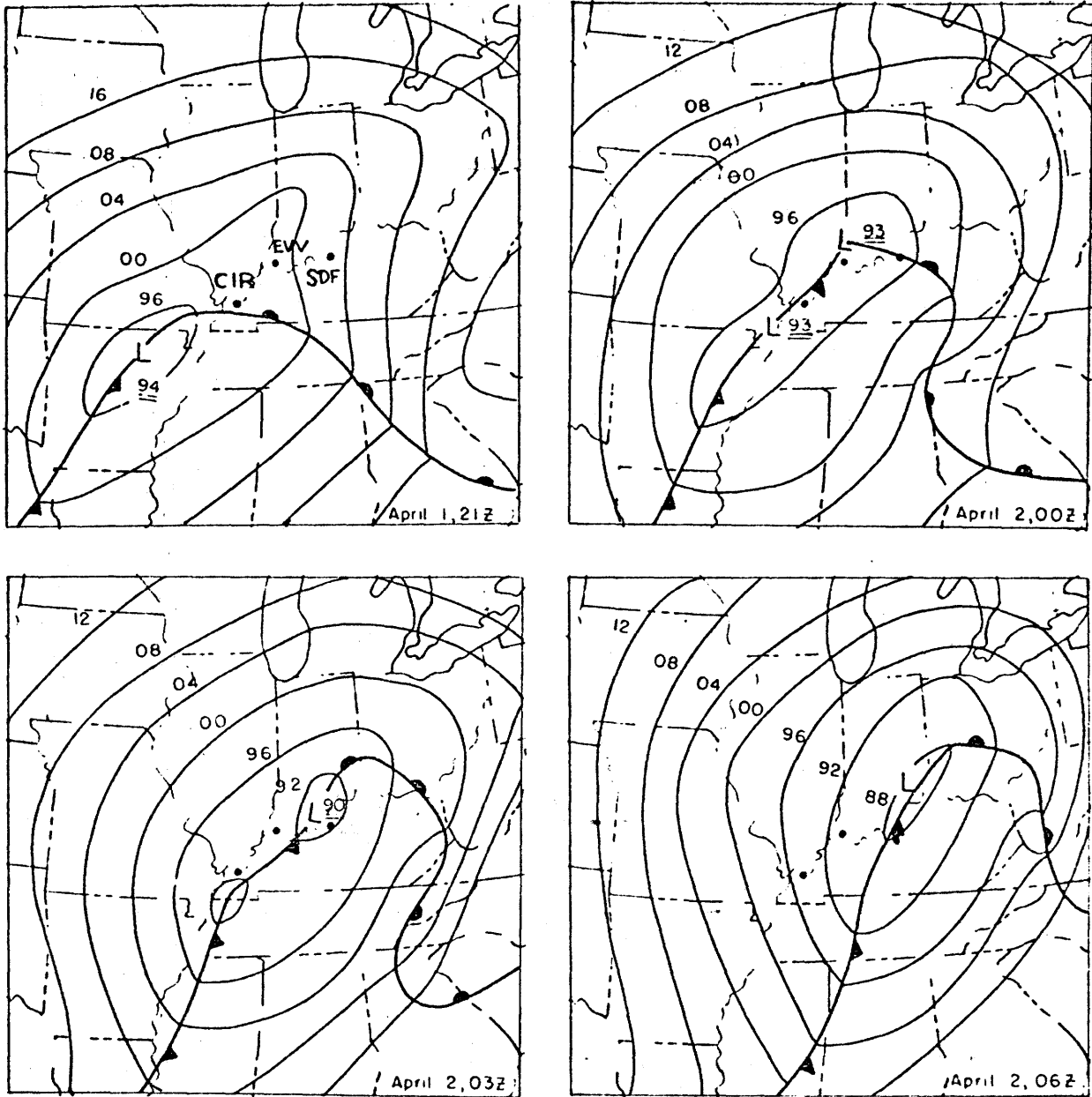


Fig. 20. Surface analyses, 1-2 April 1970. Locations of Cairo, Ill. (CIR); Evansville, Ind. (EVV); and Louisville, Ky. (SDF) as indicated.

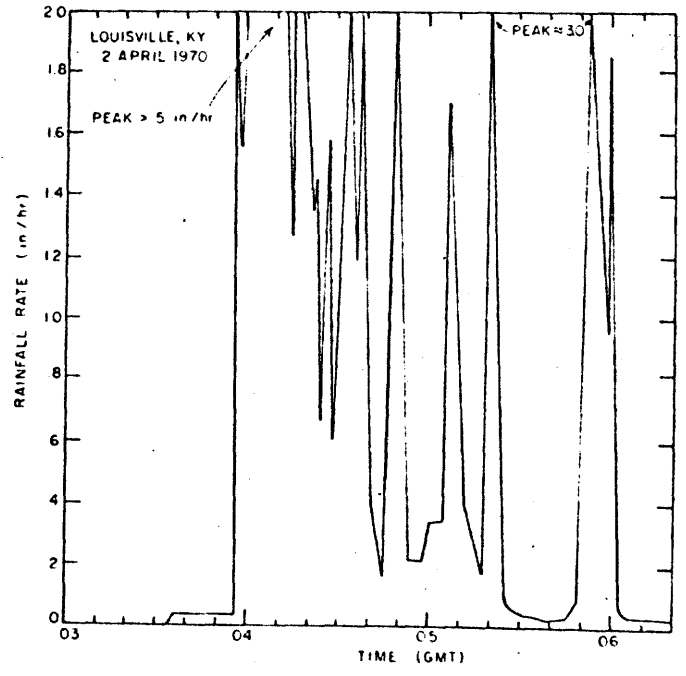
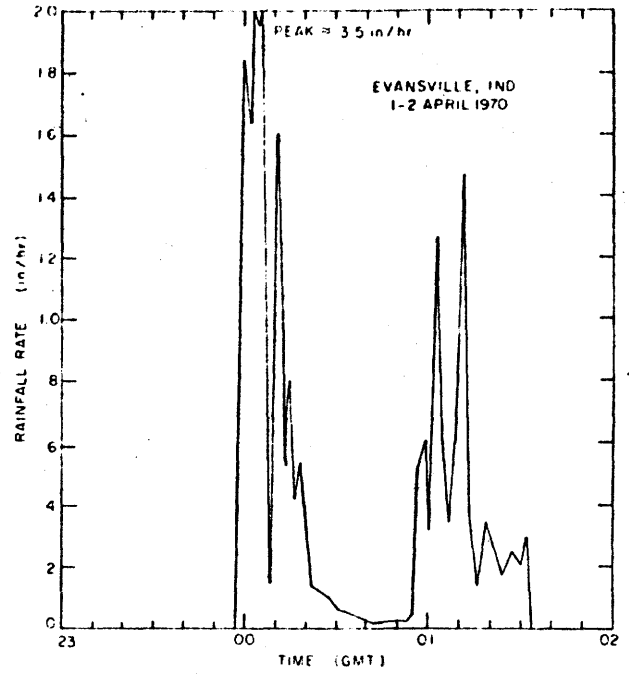
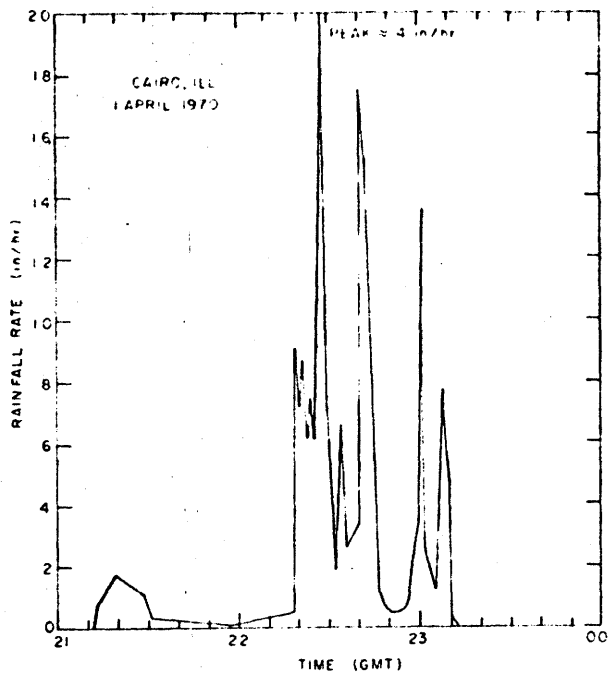


Fig. 21. Tipping-bucket traces.



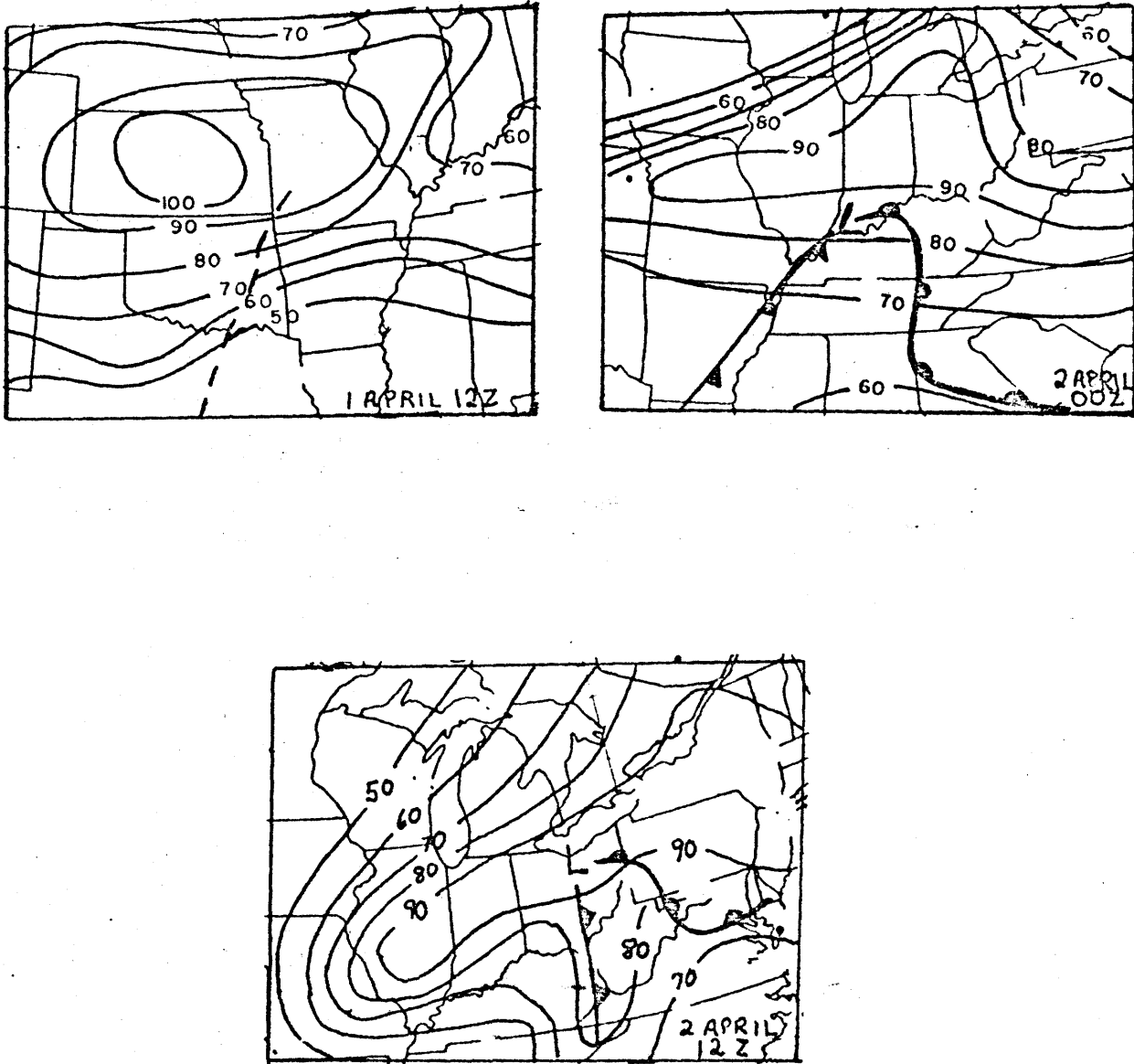
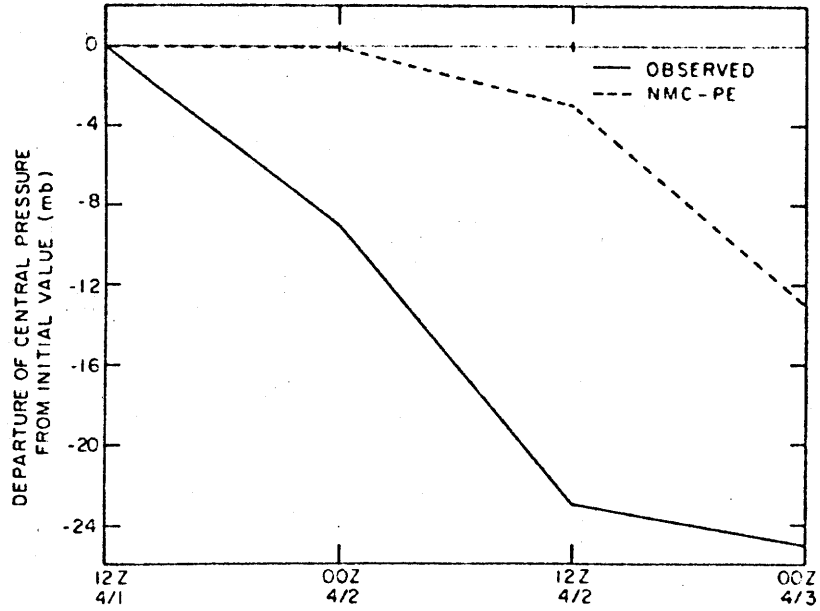
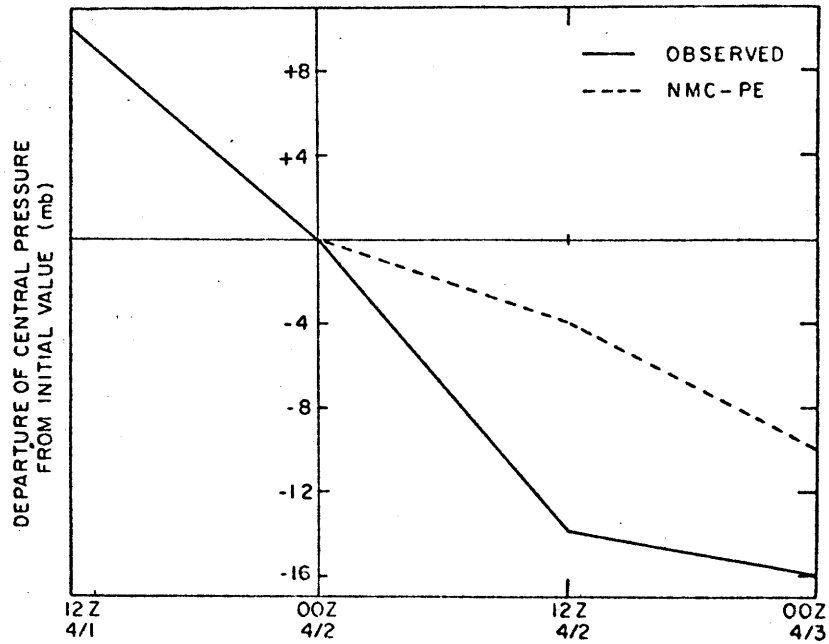


Fig. 22. Surface-mean relative humidity charts (per cent).  
Dashed line (---) on 1 April 12Z chart for trough axis.



(a)



(b)

Fig. 23. Observed and forecast central pressure vs. time in terms of departure from initial values at 12Z 1 April 1970 (a) and 00Z 2 April 1970 (b).

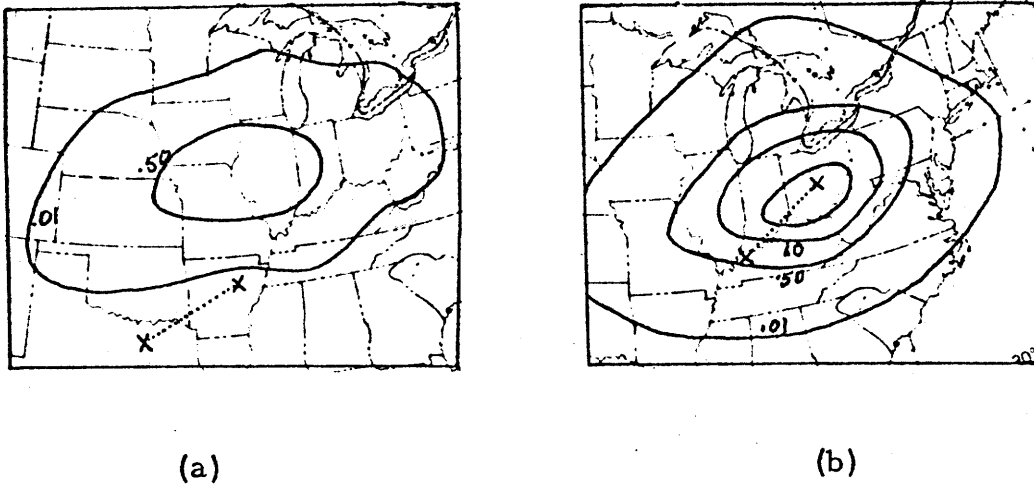


Fig. 24. NMC-PE 12-hour precipitation forecasted from 12Z 1 April 1970 (a) and 00Z 2 April (b). Contour intervals as in Fig. 15. Track of forecast low center (X . . . . X) superimposed.

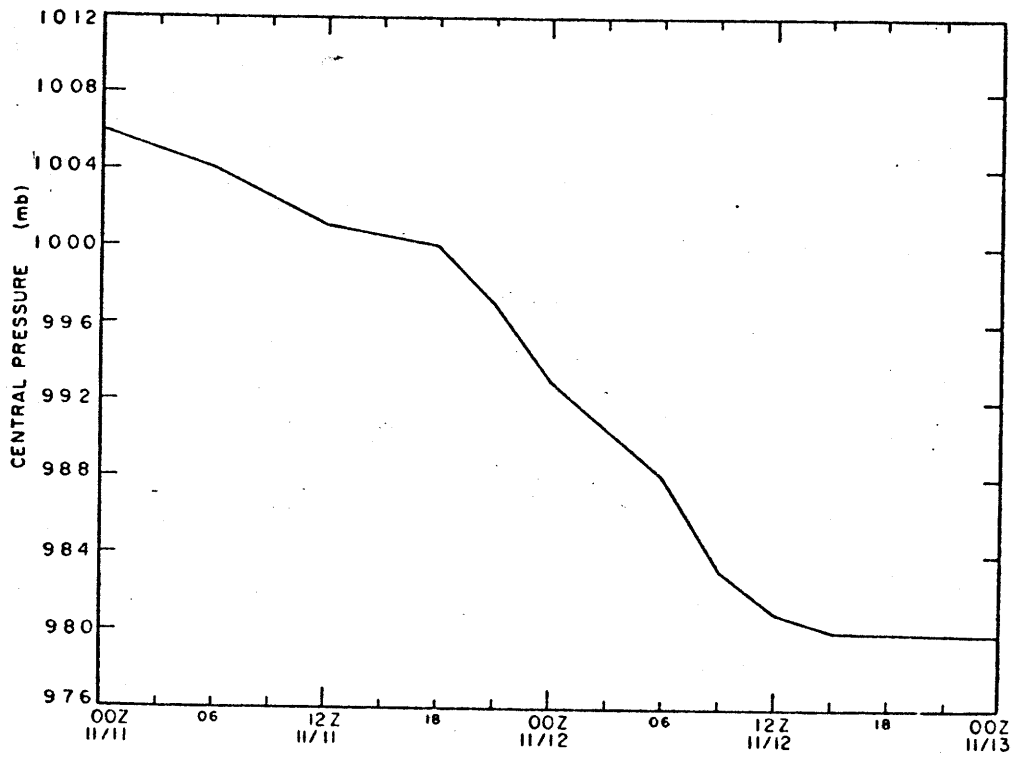


Fig. 25. Observed central pressure vs. time (plotted generally at 3-hour intervals).

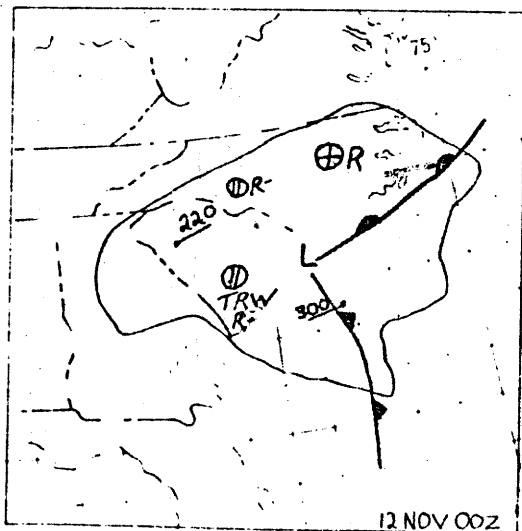
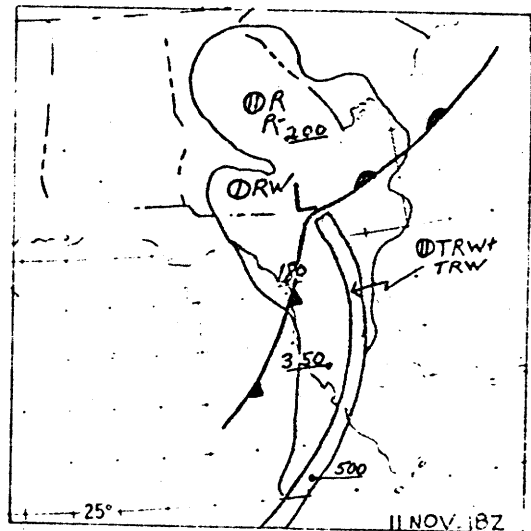
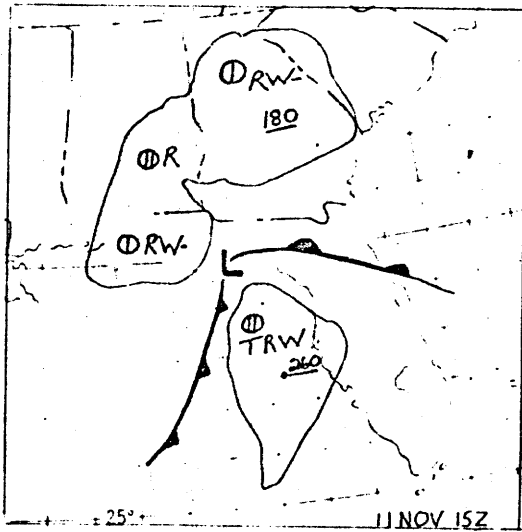
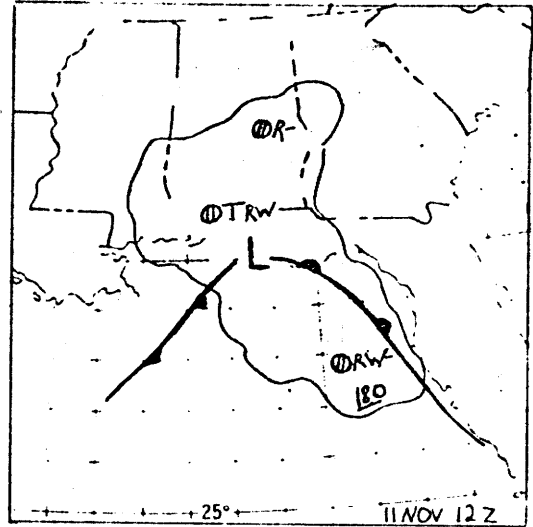
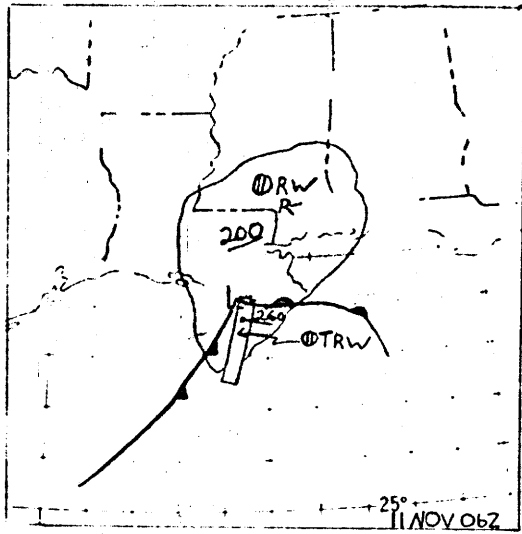


Fig. 26. Surface-radar charts. Same as Fig. 2, except for times indicated.

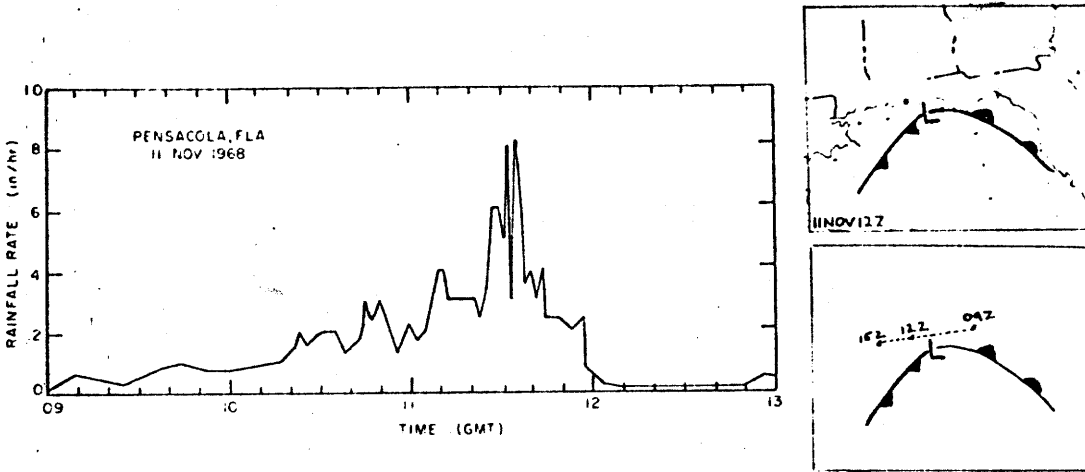


Fig. 27. Precipitation cross section. Same as Fig. 3, except for Pensacola, Fla.

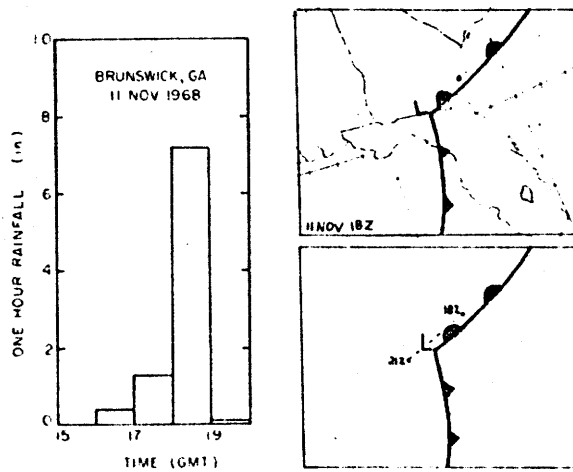


Fig. 28. Precipitation cross section. Same as Fig. 6, except for Brunswick, Ga.

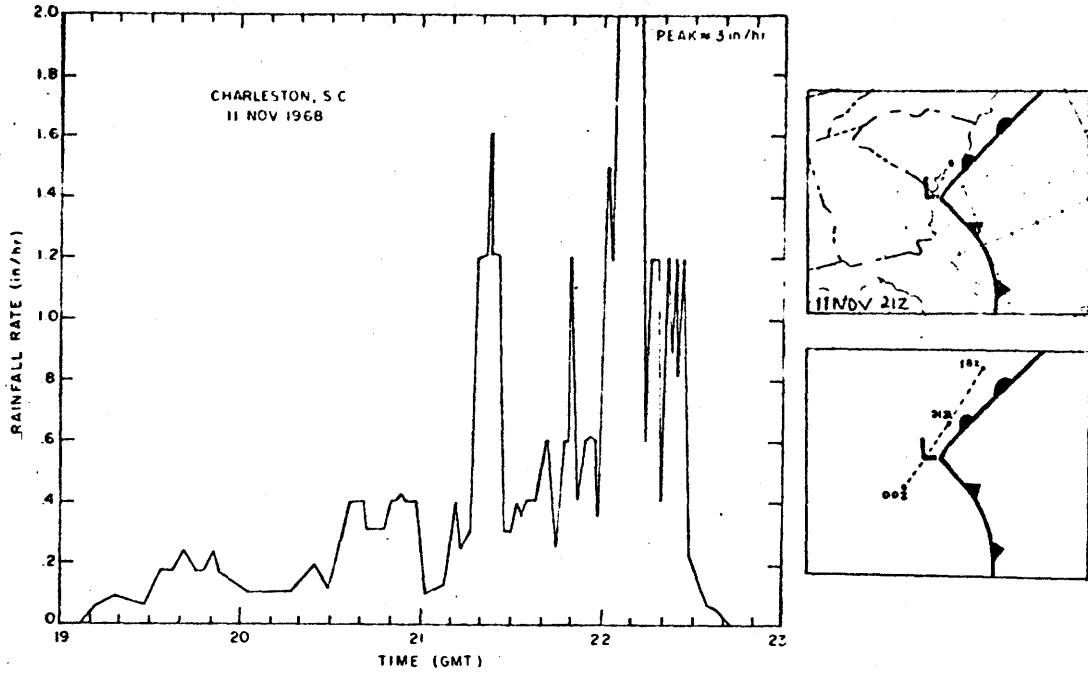


Fig. 29. Precipitation cross section. Same as Fig. 3, except for Charleston, S. C.

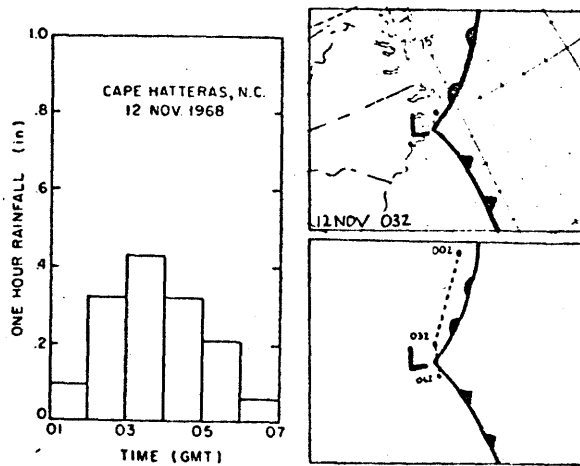


Fig. 30. Precipitation cross section. Same as Fig. 6, except for Cape Hatteras, N. C.

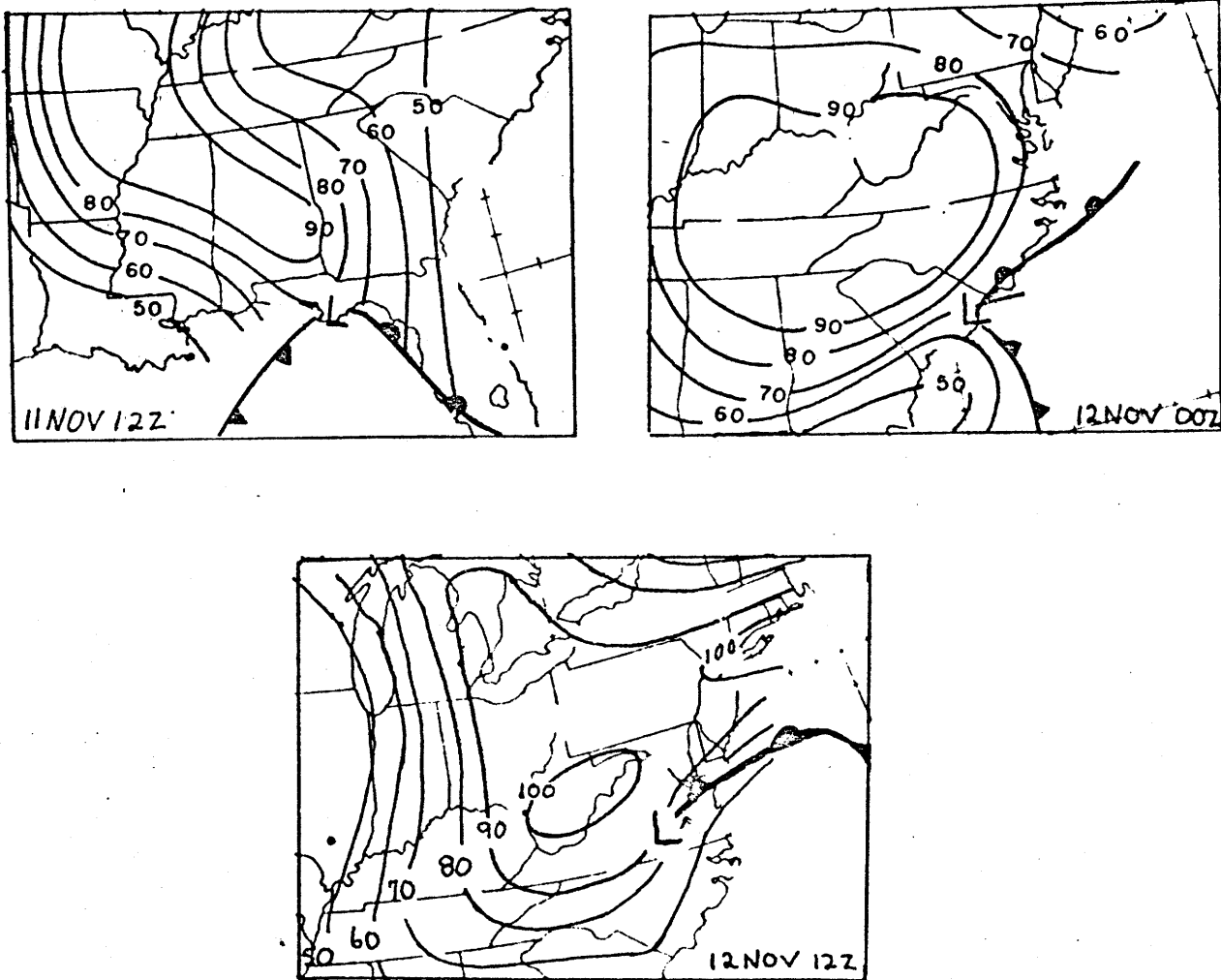
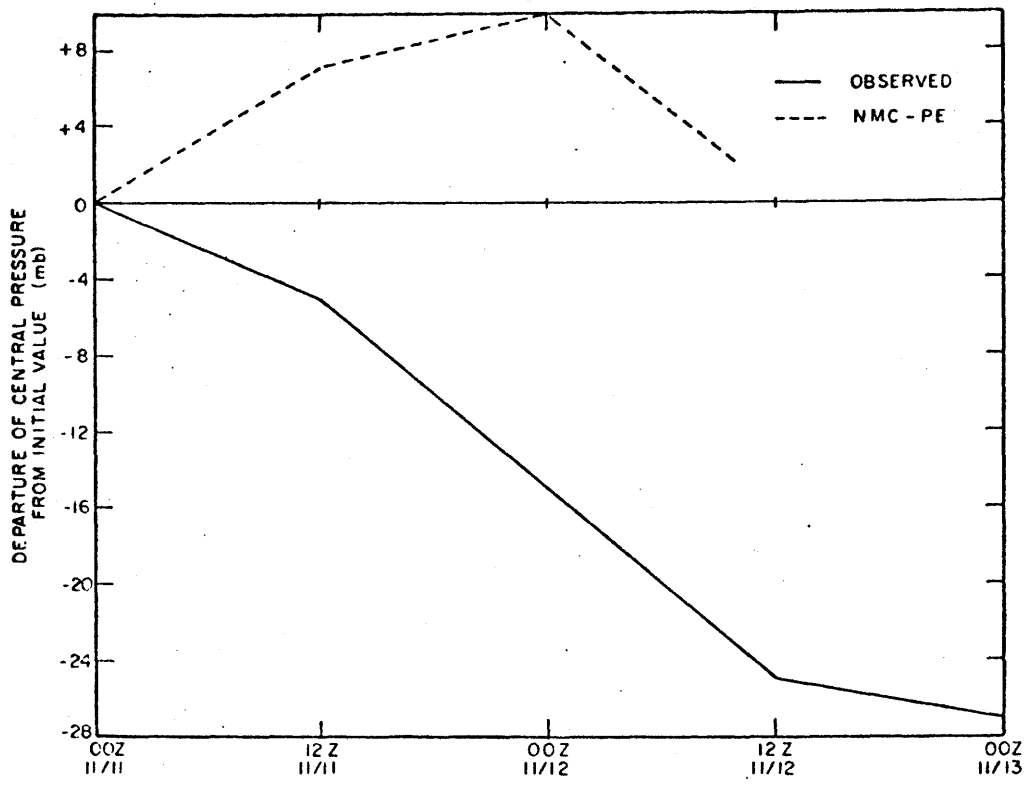
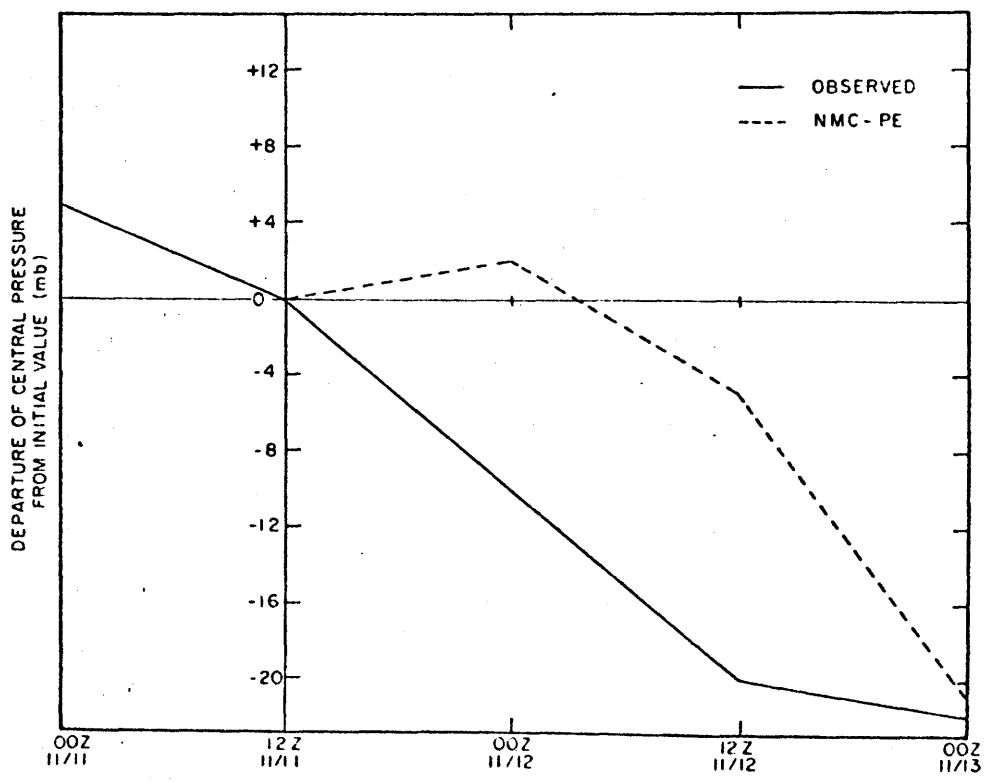


Fig. 31. Surface-mean relative humidity charts (per cent).



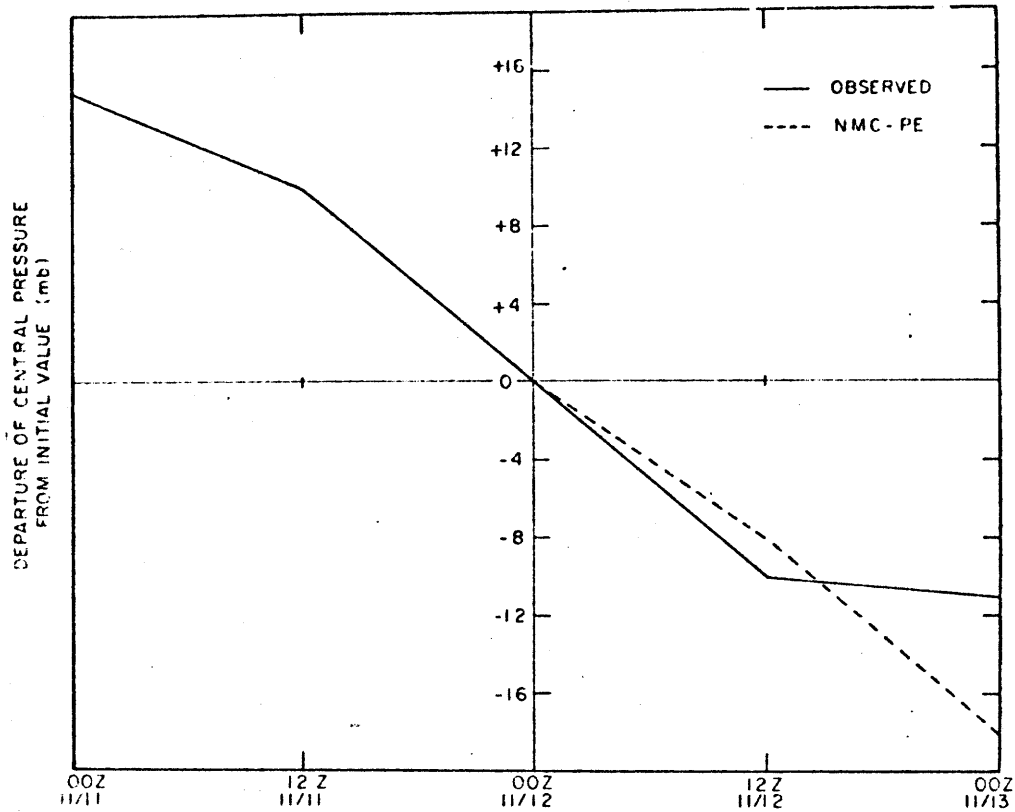


(a)



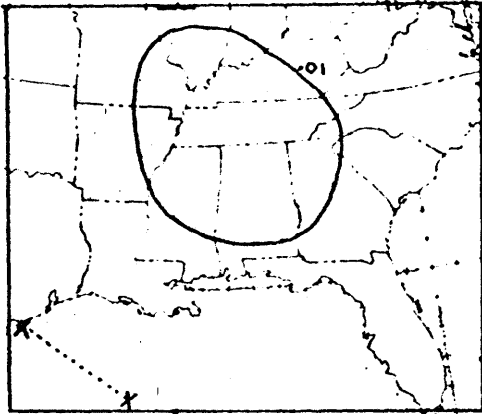
(b)

Fig. 32. (See next page).

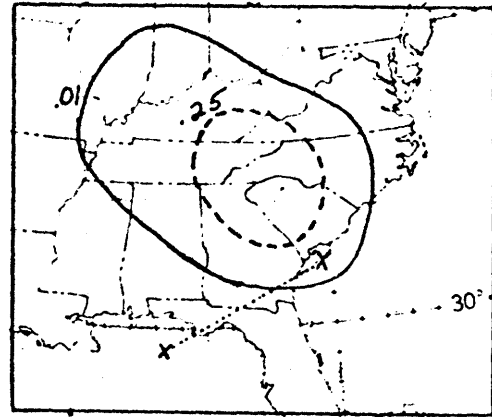


(c)

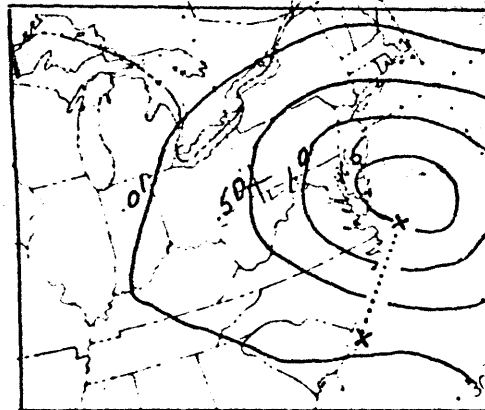
Fig. 32. Observed and forecast central pressure vs. time in terms of departure from initial value at 00Z 11 Nov. 1968 (a), 12Z 11 Nov. 1968 (b), and 00Z 12 Nov. 1968 (c) (values plotted at 12-hour intervals).



(a)



(b)



(c)

Fig. 33. NMC-PE 12-hour precipitation forecasted from 00Z 11 Nov. 1968 (a), 12Z 11 Nov. 1968 (b), and 00Z 12 Nov. 1968 (c). Track of forecast low center (X . . . X) superimposed. Contour intervals as in Fig. 15.

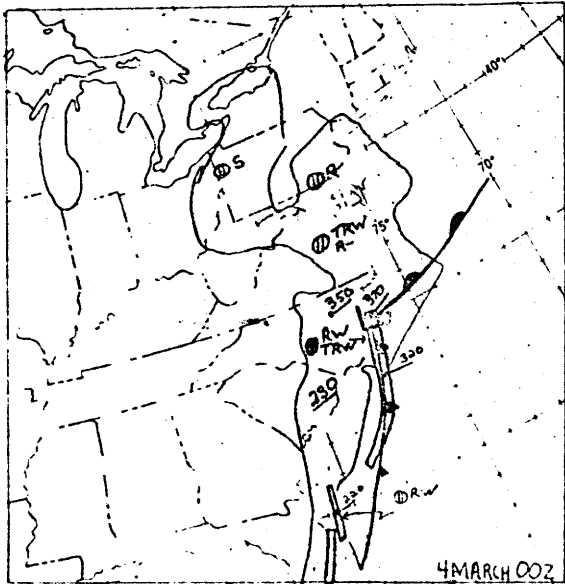
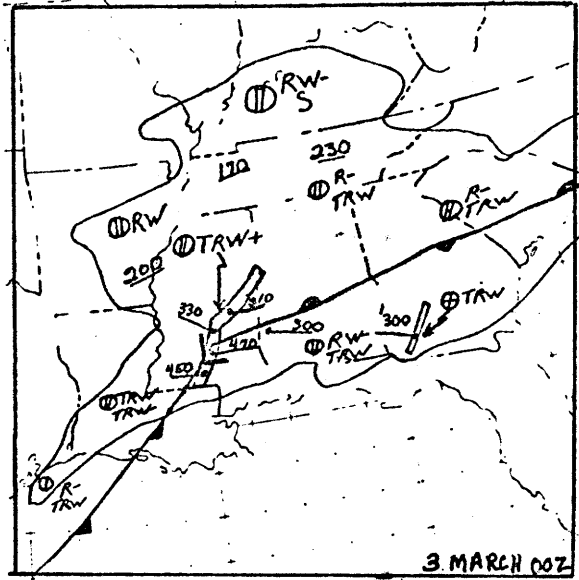
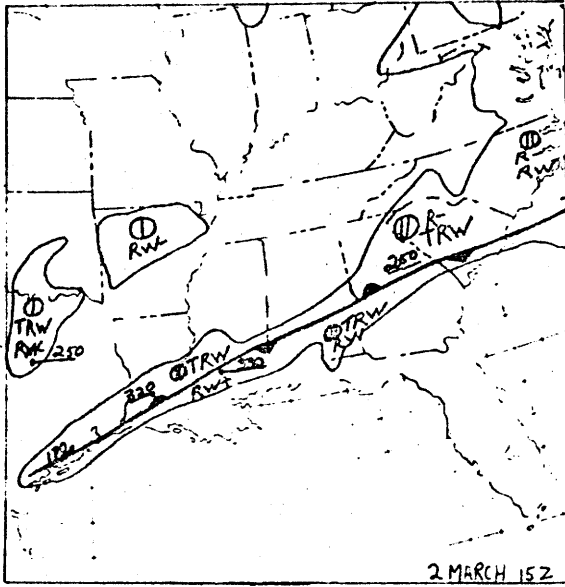


Fig. 34. Surface-radar charts. Same as Fig. 2, except for times indicated.

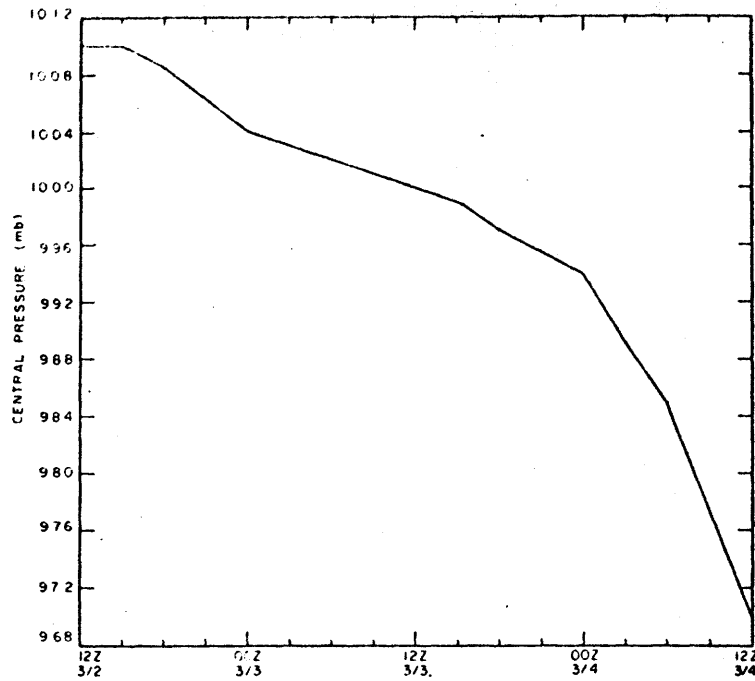


Fig. 35. Observed central pressure vs. time (plotted generally at 3-hour intervals).

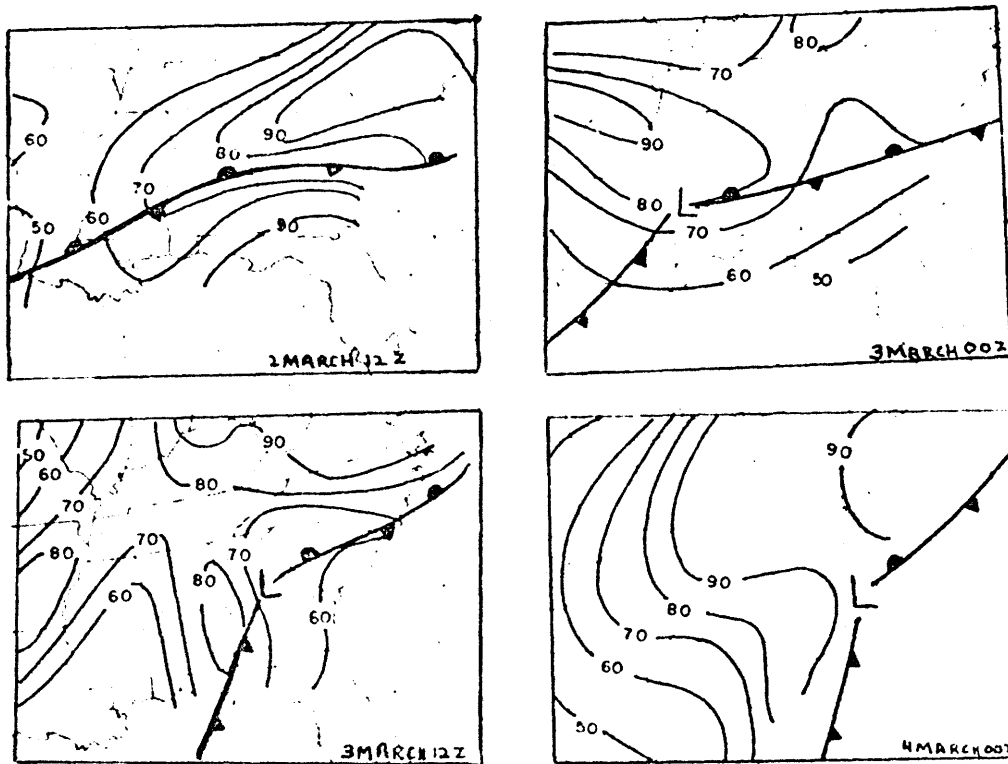


Fig. 36. Surface-mean relative humidity charts (per cent).

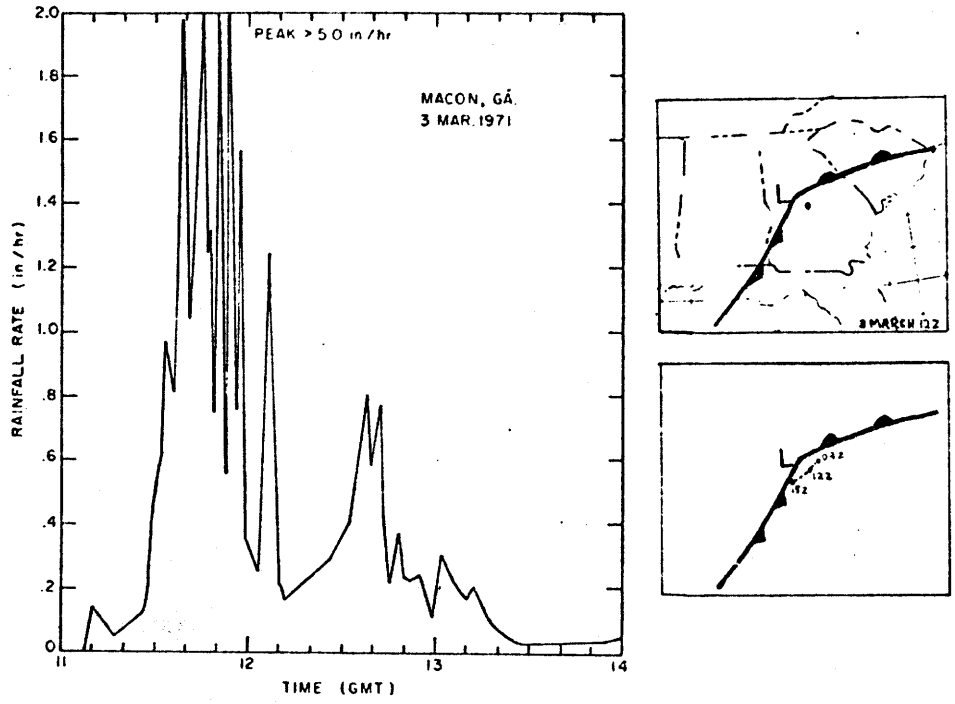
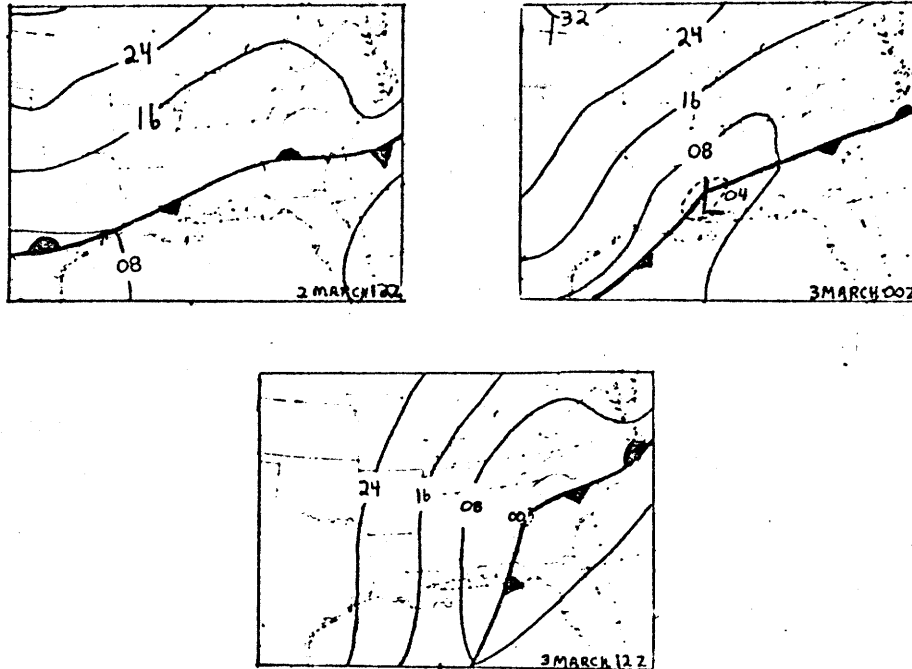
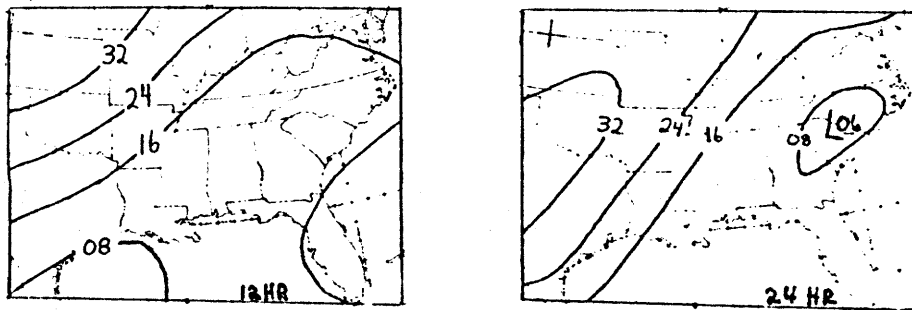


Fig. 37. Precipitation cross section.  
Same as Fig. 3, except for Macon, Ga.

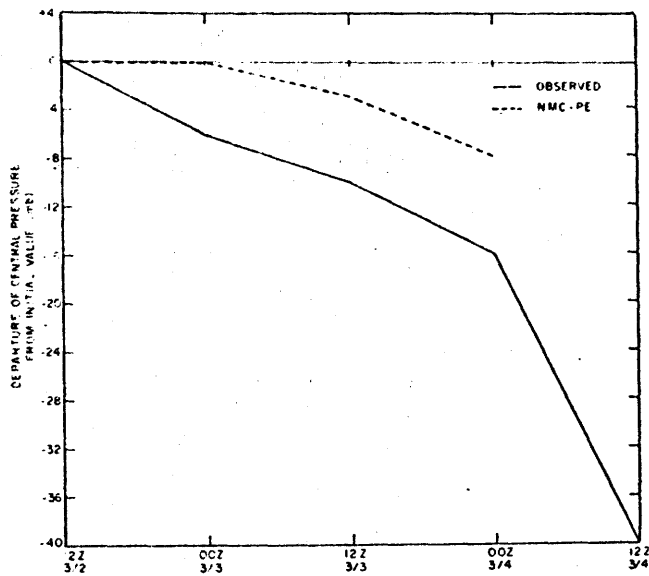


(a)

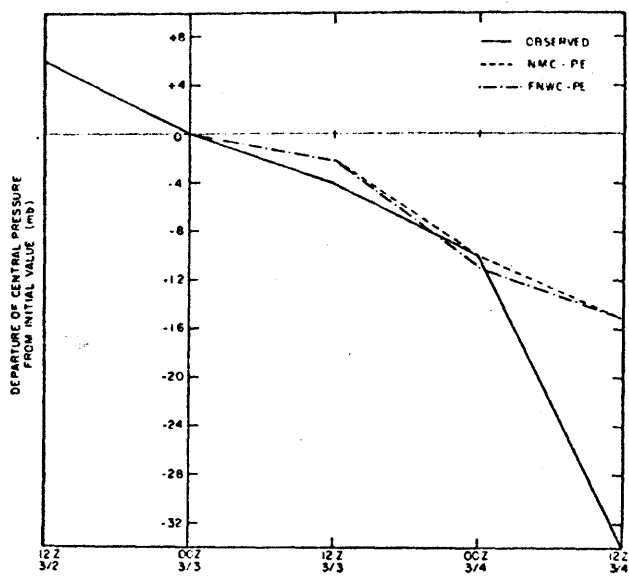


(b)

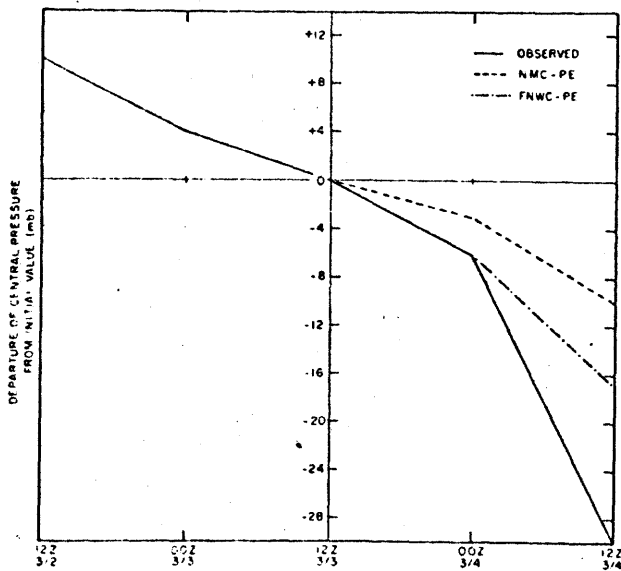
Fig. 38. NMC-PE 12- and 24-hour sea-level pressure charts generated from 12Z 2 March 1970 (b), verifying at 00Z and 12Z 3 March 1970 (a), respectively.



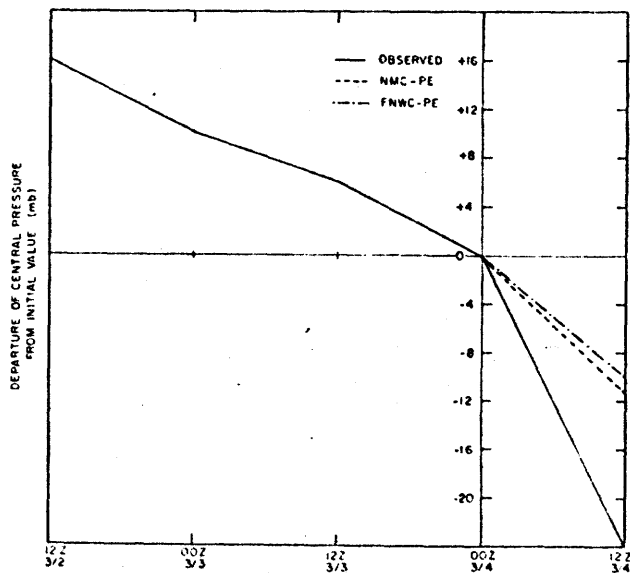
(a)



(b)



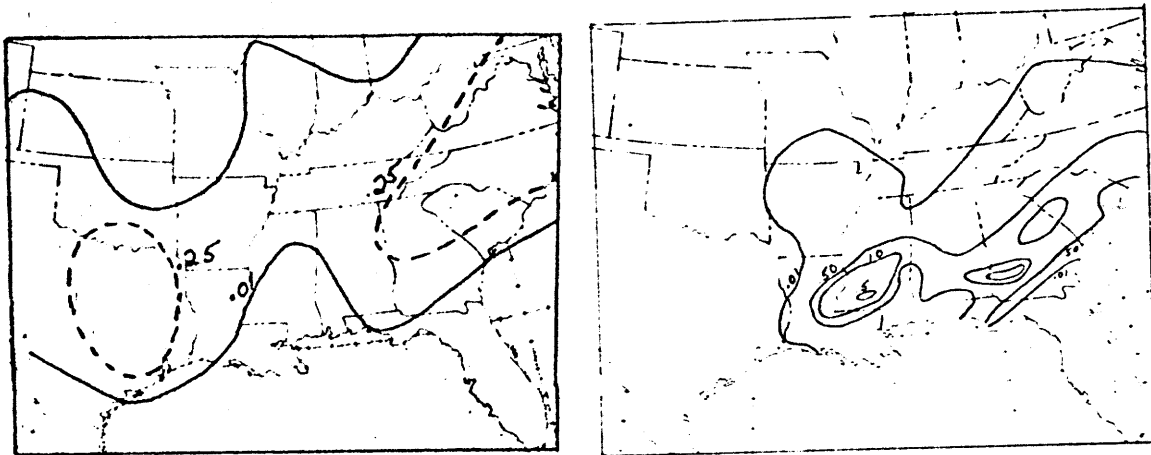
(c)



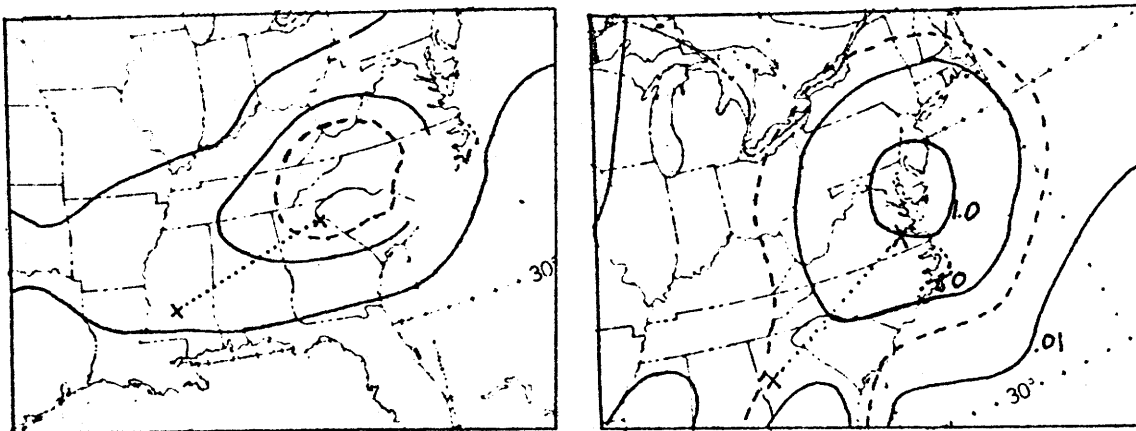
(d)

Fig. 39. Observed and forecast central pressure vs. time in terms of departure from initial values at 12Z 2 March 1971 (a), 00Z 3 March 1971 (b), 12Z 3 March 1971 (c), and 00Z 4 March 1971 (d).





(a)



(b)

(c)

Fig. 40. - (a) NMC-PE 12-hour precipitation forecasted from 12Z 2 March 1971 and observed precipitation for the verifying 12-hour period, 12Z 2 March to 00Z 3 March 1971; (b) NMC-PE 12-hour precipitation forecasted from 00Z 3 March 1971; and (c) NMC-PE 12-hour precipitation forecasted from 12Z 3 March 1971.

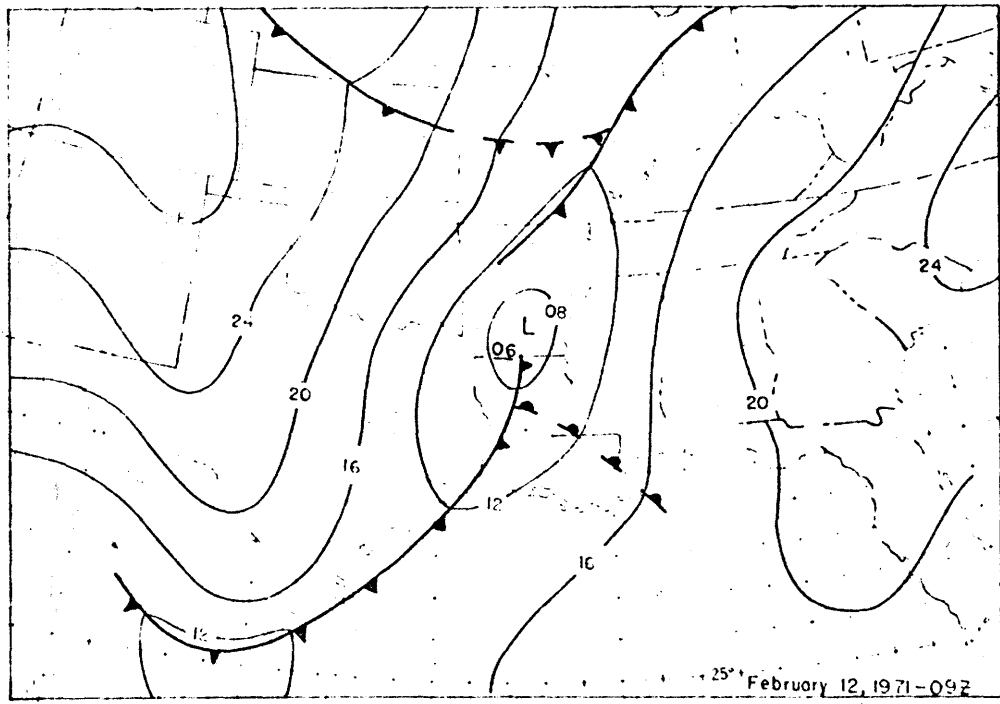
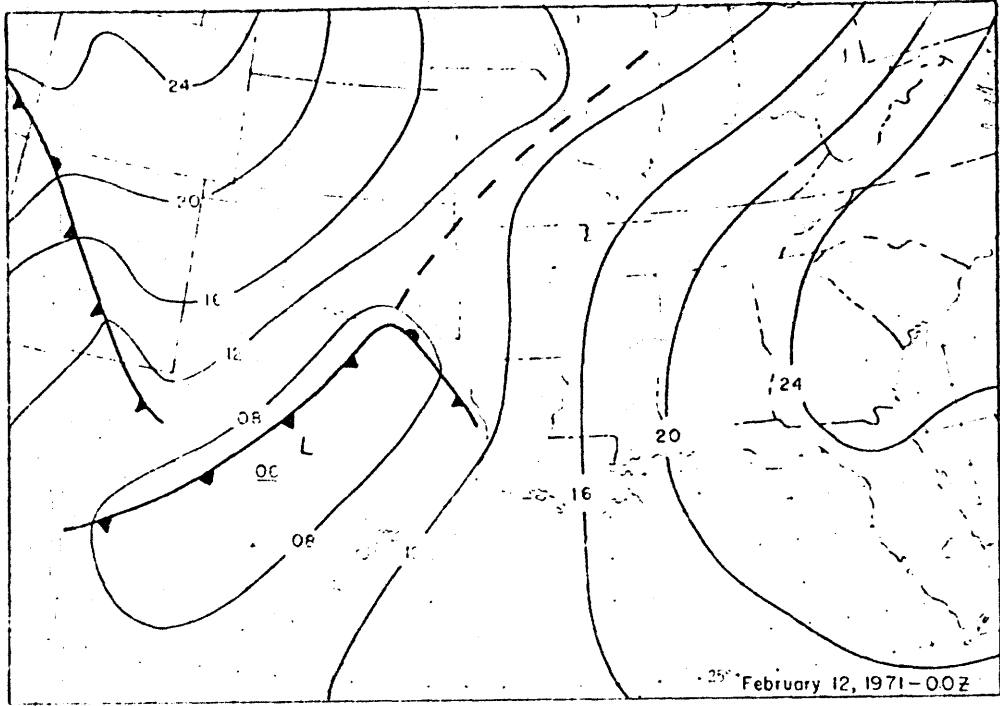


Fig. 41. Surface analyses, 12 Feb. 1971

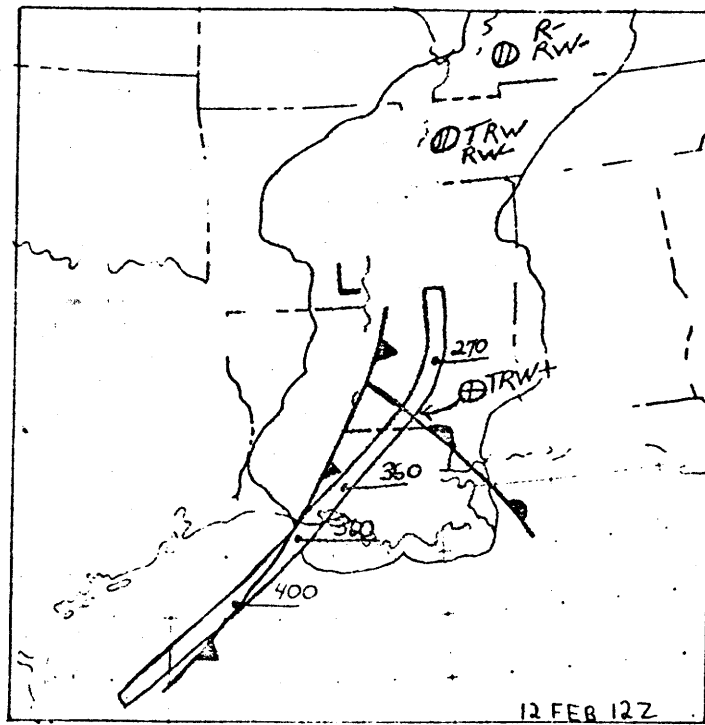
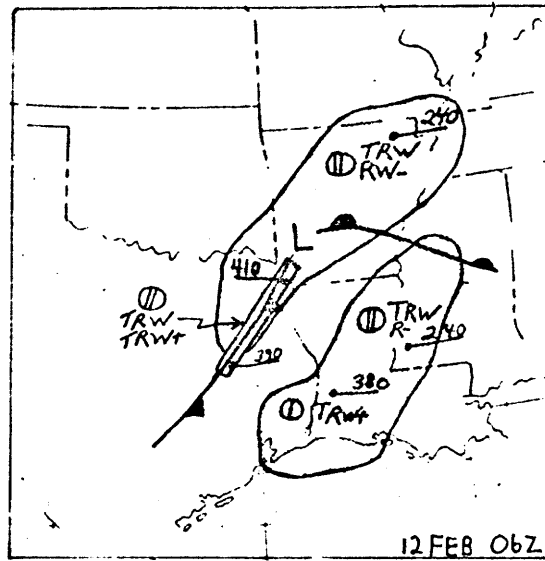


Fig. 42. Surface radar charts. Same as Fig. 2, except for times indicated.

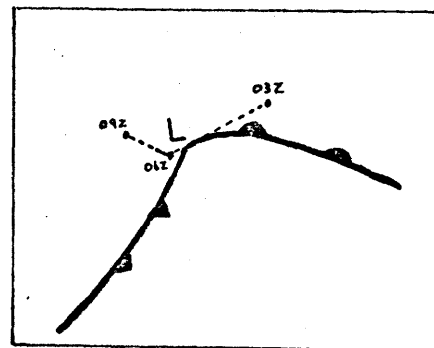
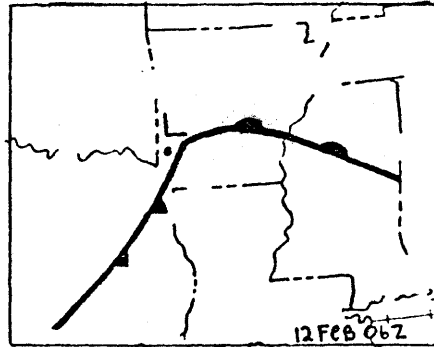
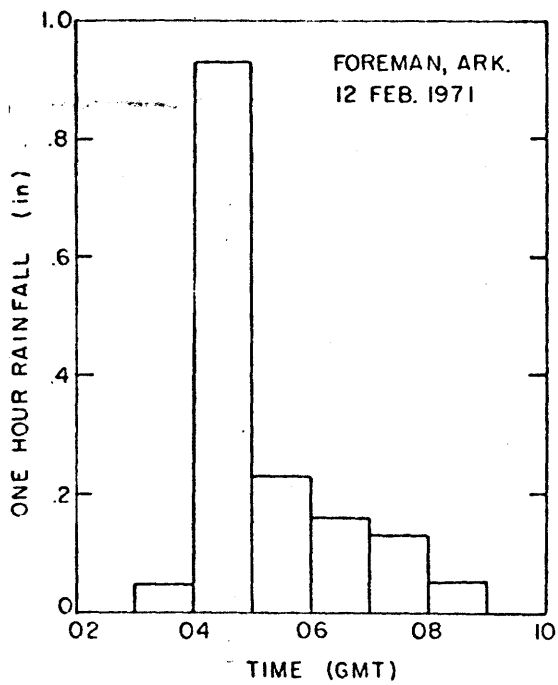


Fig. 43. Precipitation cross section. Same as Fig. 6, except for Foreman, Arkansas.

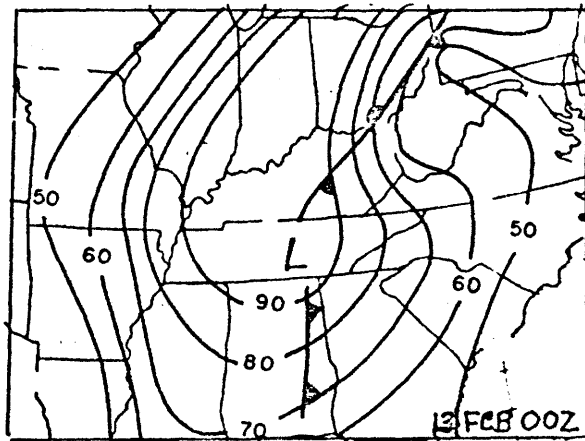
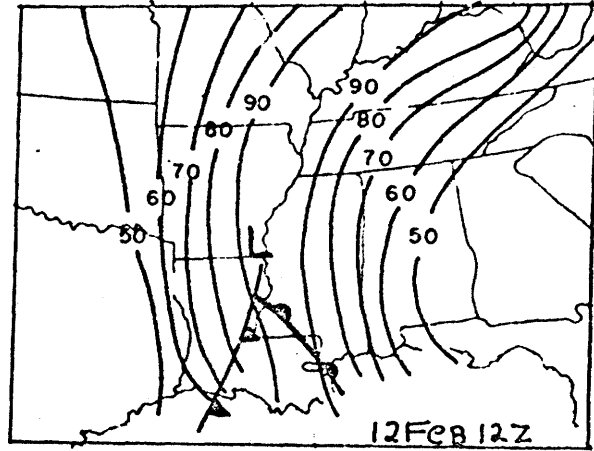
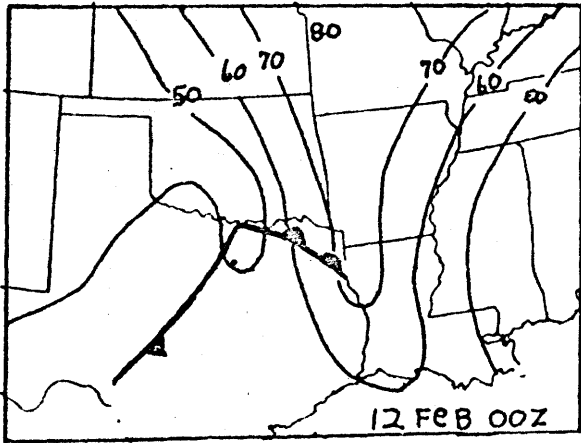


Fig. 44. Surface-mean relative humidity charts (per cent).

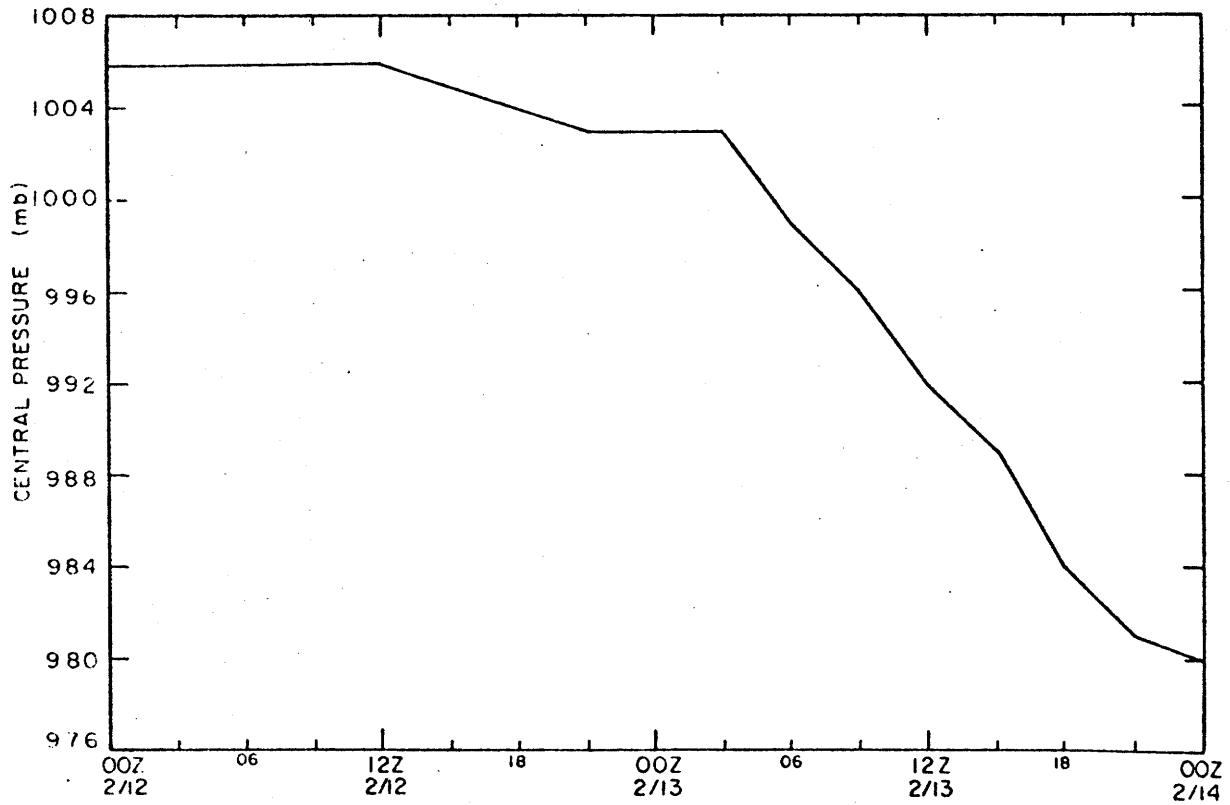
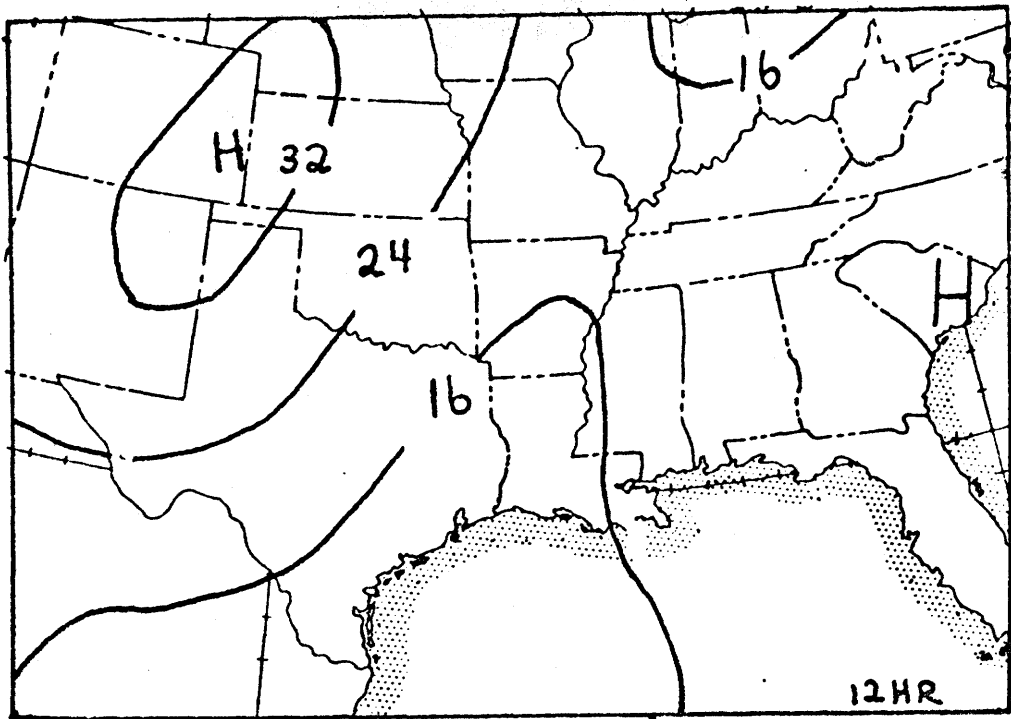
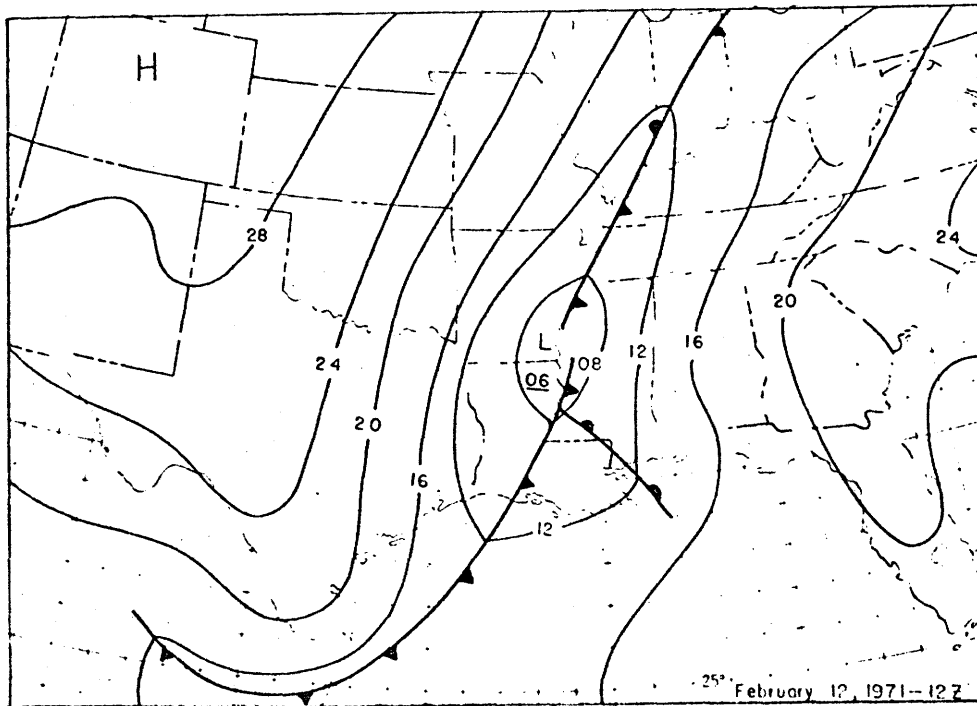


Fig. 45. Observed central pressure vs. time (plotted generally at 3-hour intervals).



(a)



(b)

Fig. 46. - (a) 12-hour NMC-PE sea-level pressure chart from 00Z 12 Feb.; and (b) verifying surface analysis.

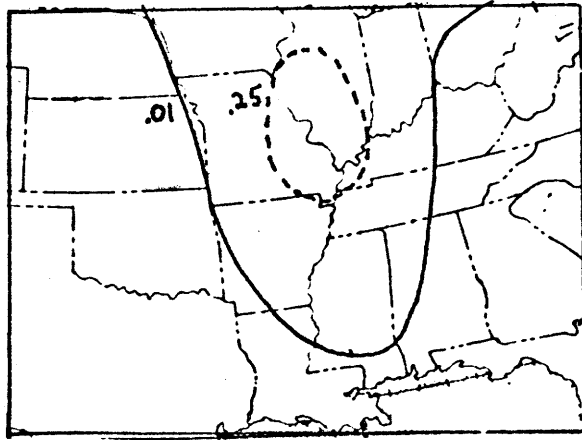
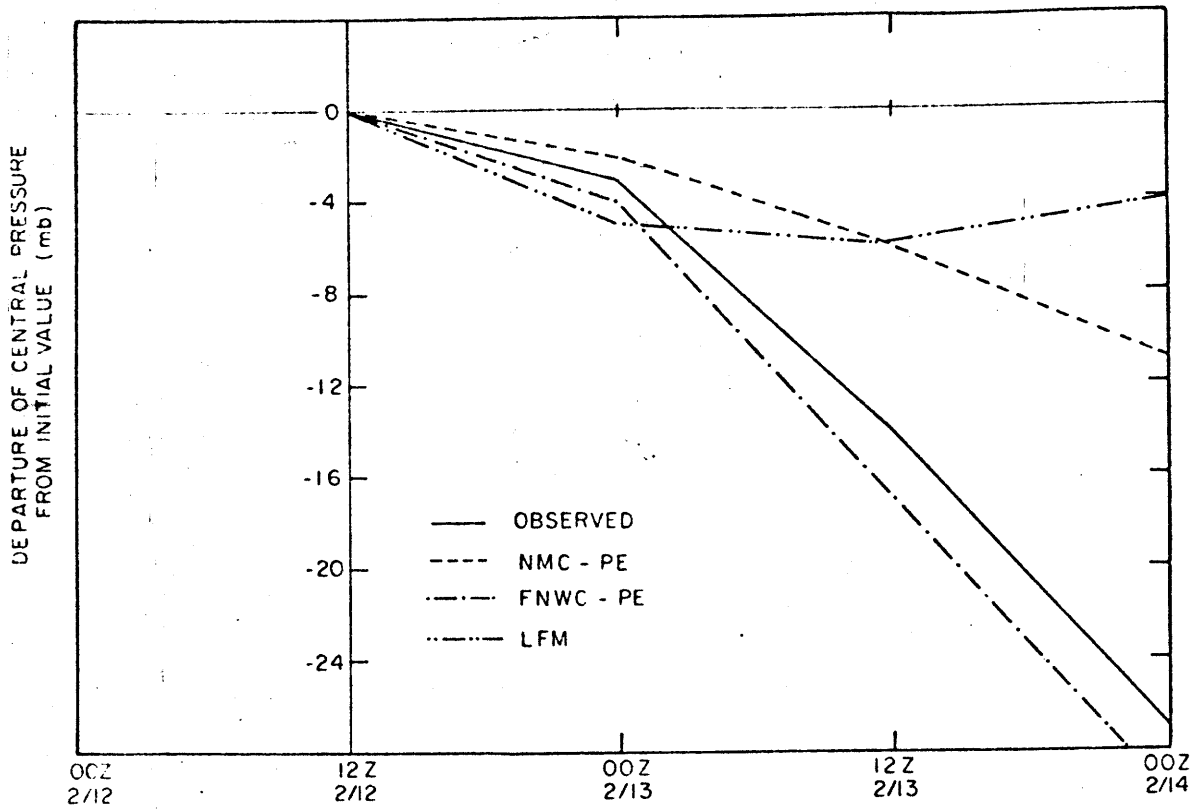
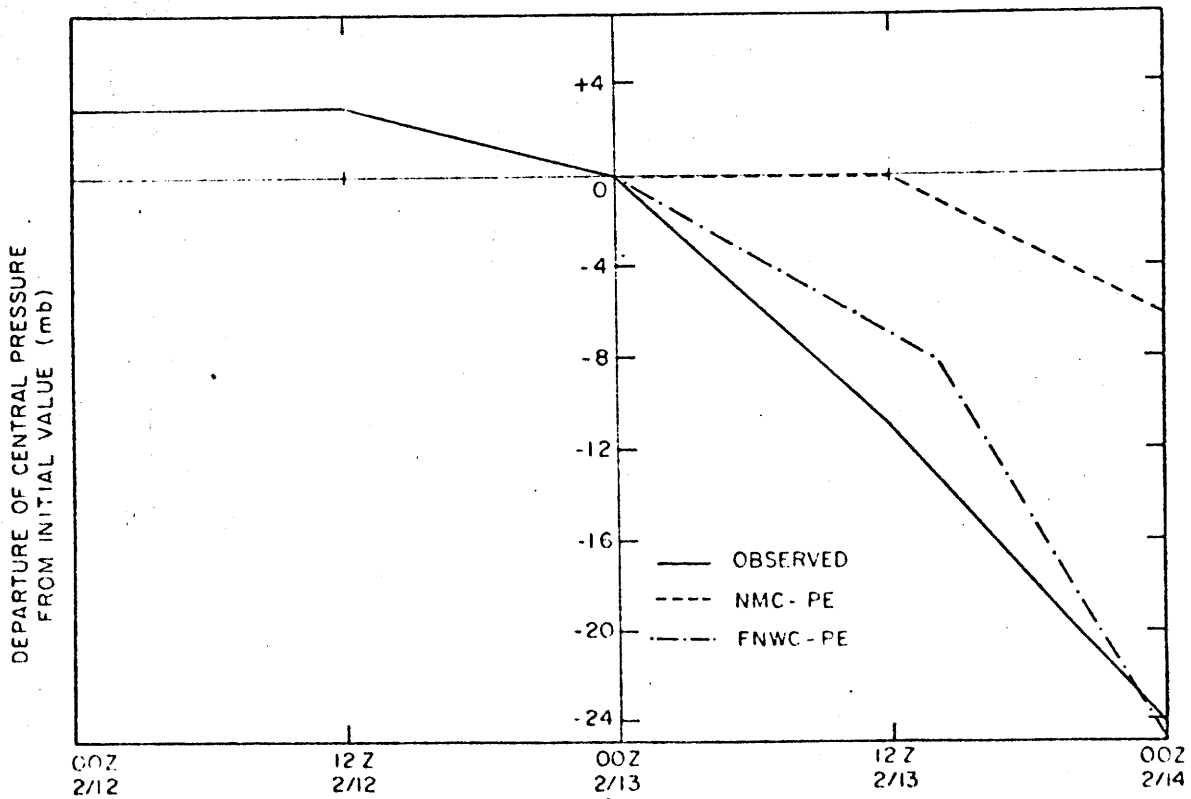


Fig. 47. NMC-PE 12-hour precipitation forecasted from 00Z 12 Feb. 1971.





(a)



(b)

Fig. 48. Observed and forecast central pressure vs. time in terms of departure from initial values at 12Z 12 Feb. 1971 (a), and 00Z 13 Feb. 1971 (b) (values plotted at 12-hour intervals).

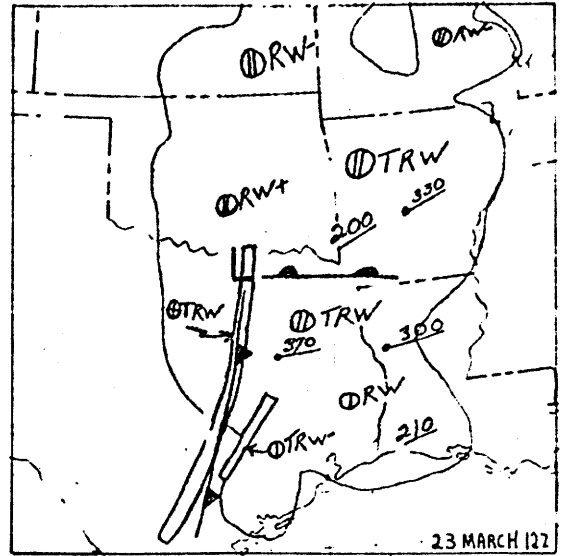
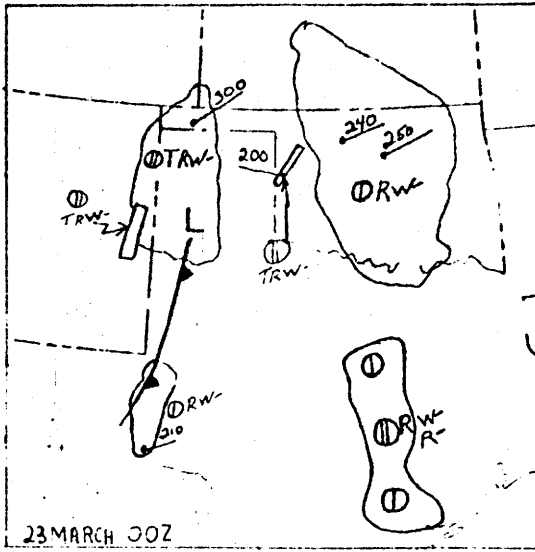


Fig. 49. Surface-radar charts. Same as Fig. 2, except for times indicated.

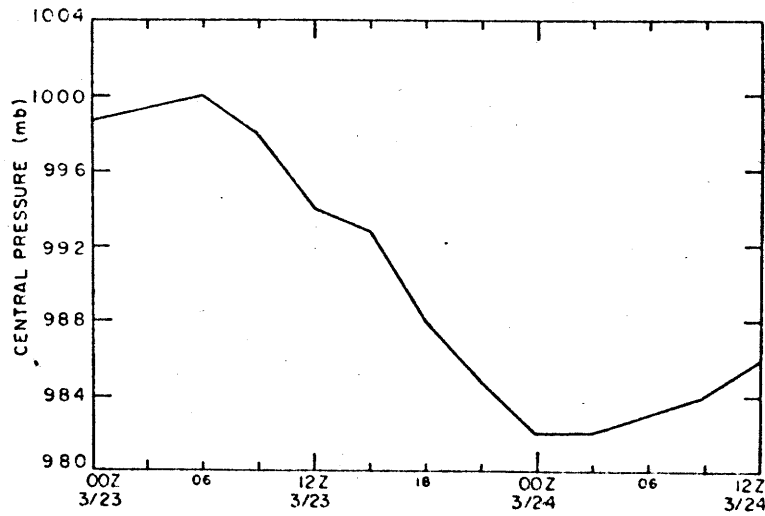


Fig. 50. Observed central pressure vs. time (plotted generally at 3-hour intervals).

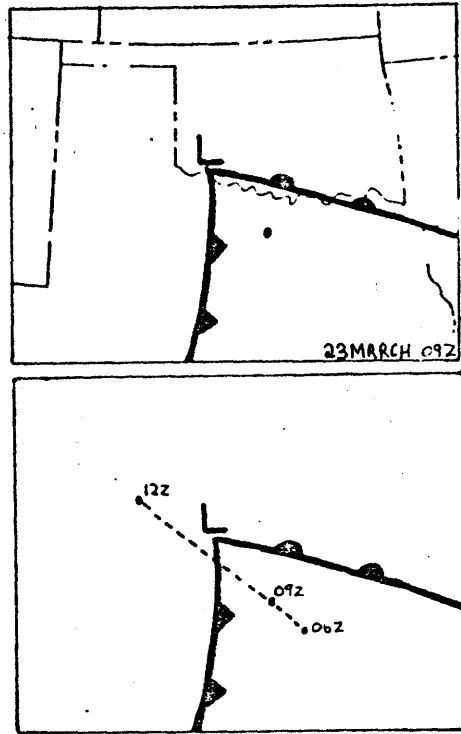
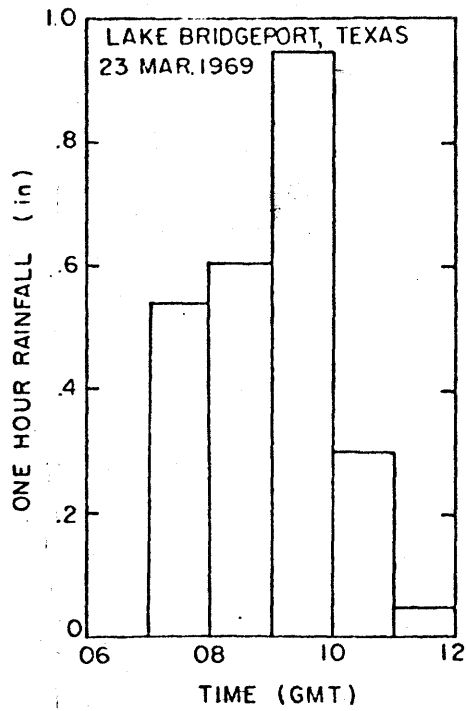


Fig. 51. Precipitation cross section. Same as Fig. 6, except for Lake Bridgeport, Texas.

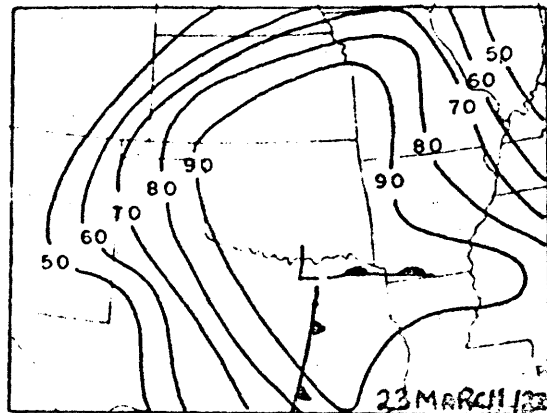
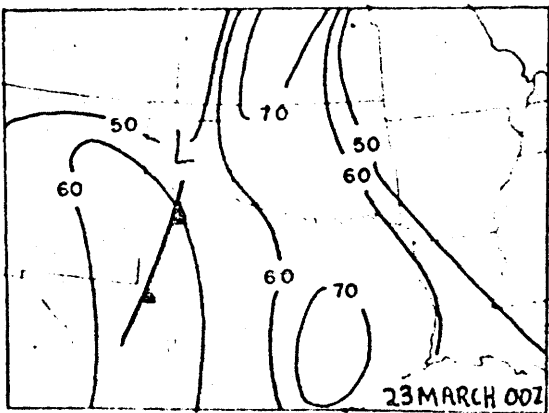
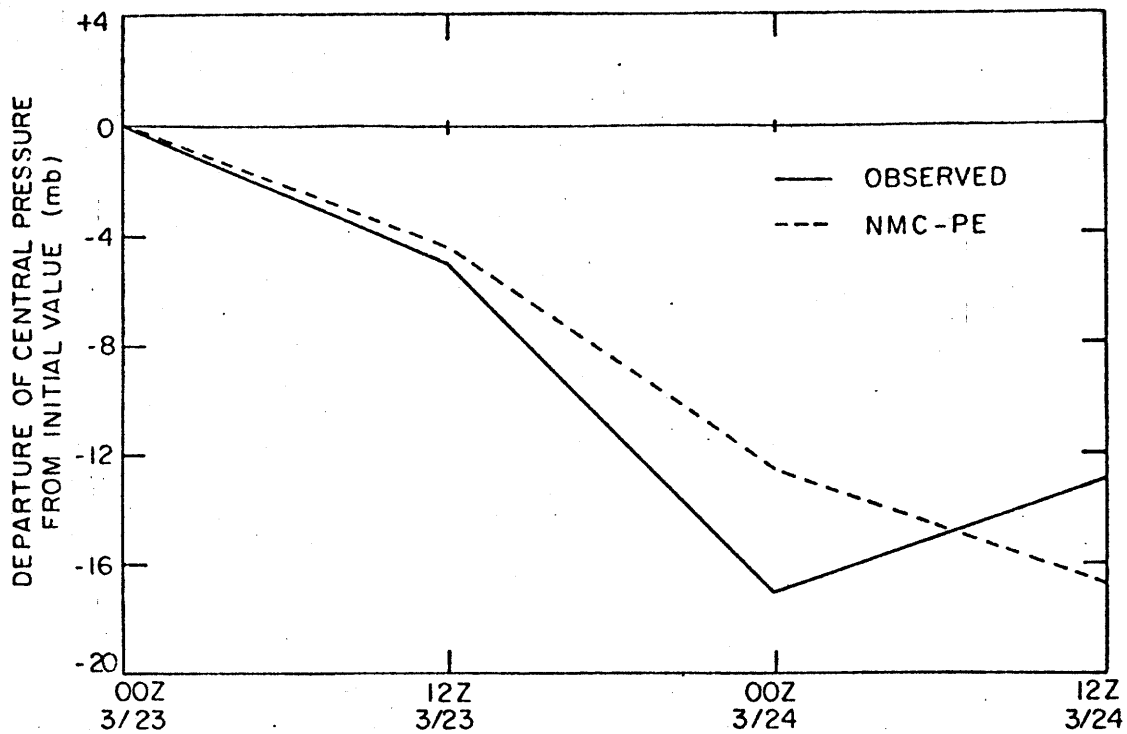
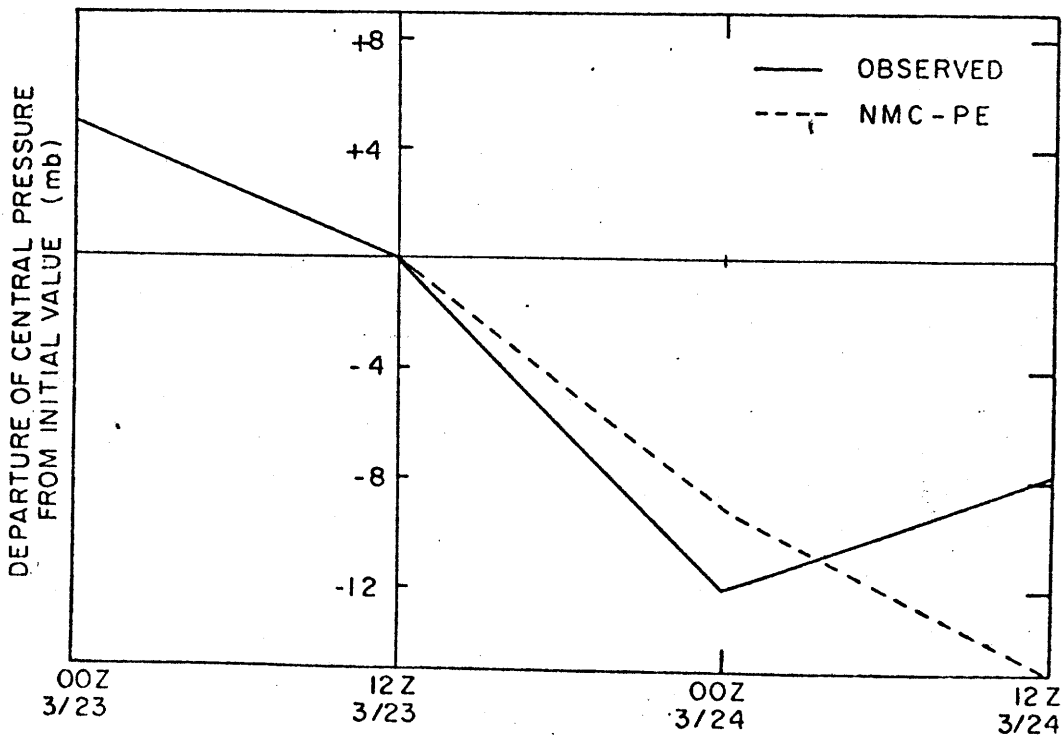


Fig. 52. Surface-mean relative humidity charts (per cent).



(a)



(b)

Fig. 53. Observed and forecast central pressure vs. time in terms of departure from initial values at 00Z 23 March 1969 (a) and 12Z 23 March 69 (b) (values plotted at 12-hour intervals).

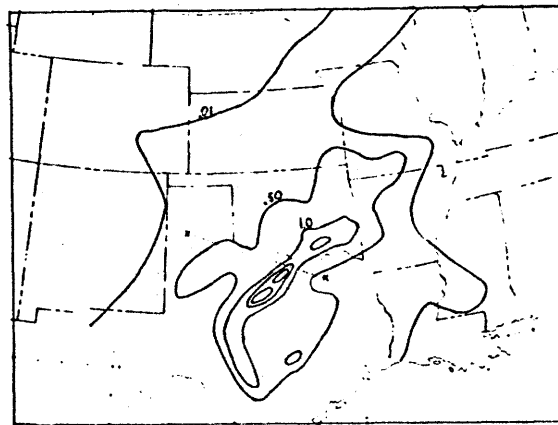
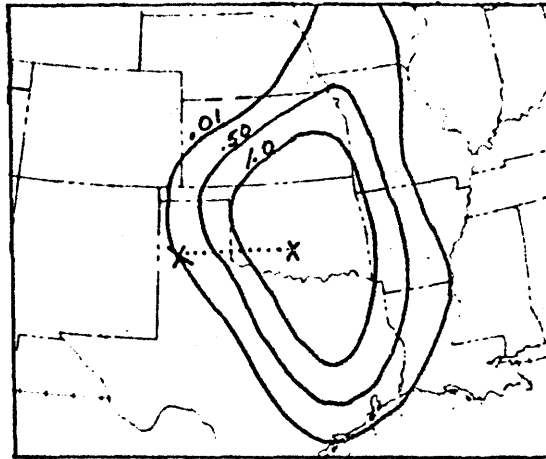


Fig. 54. NMC-PE 12-hour precipitation forecasted from 00Z 23 March 1969 (a) and 12-hour observed precipitation, 00Z to 12Z 23 March 1969 (b). Contour intervals as in Fig. 15. Track of respective forecast and observed low centers superimposed.

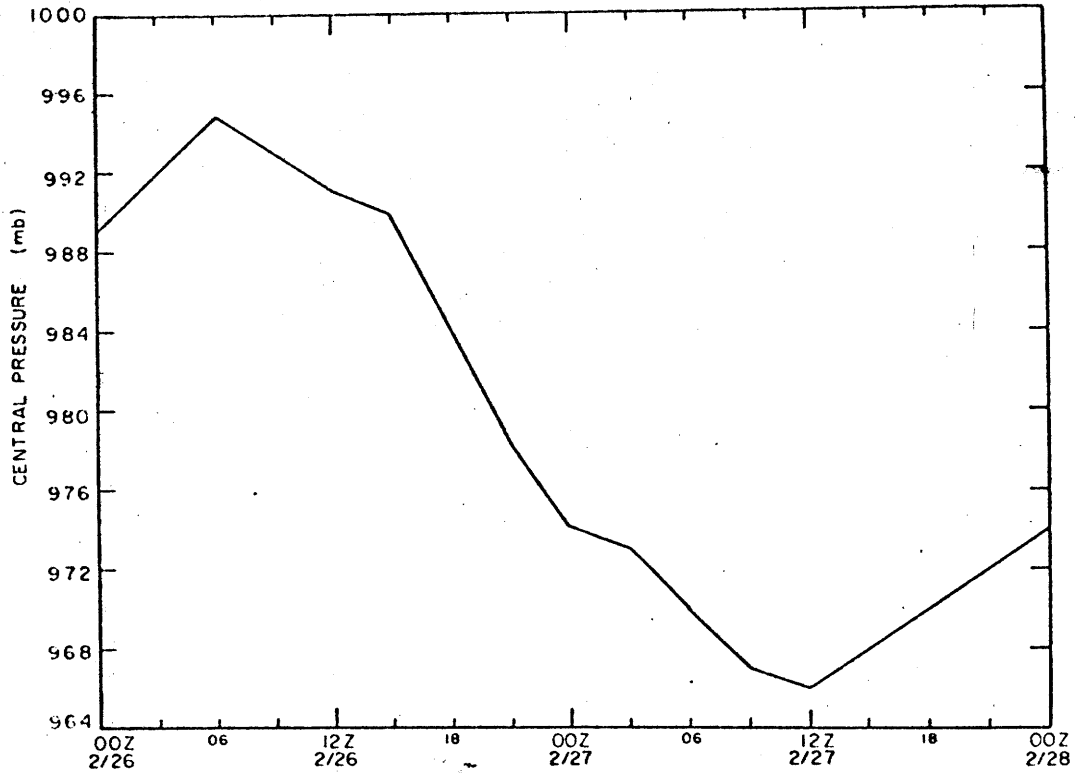


Fig. 55. Observed central pressure vs. time (plotted generally at 3-hour intervals).

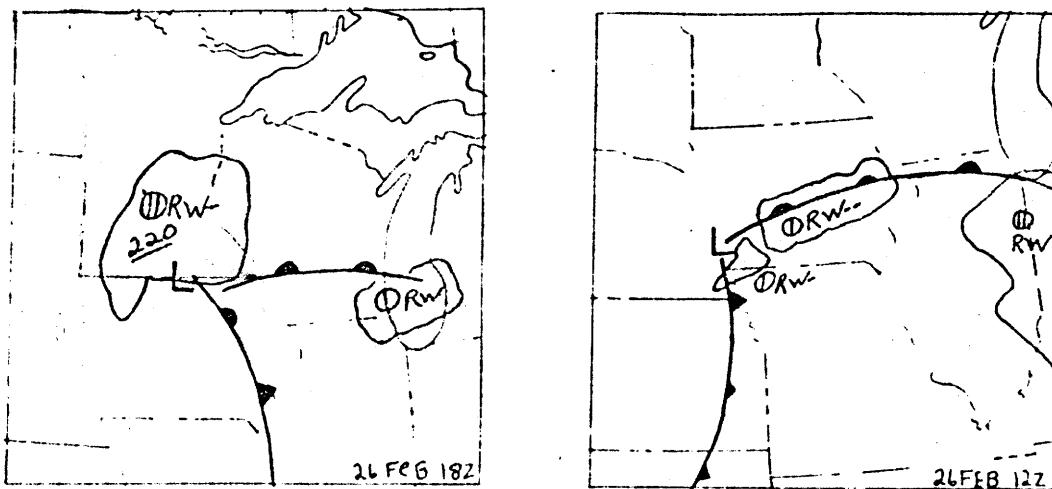


Fig. 56. Surface-radar charts. Same as Fig. 2, except for times indicated.

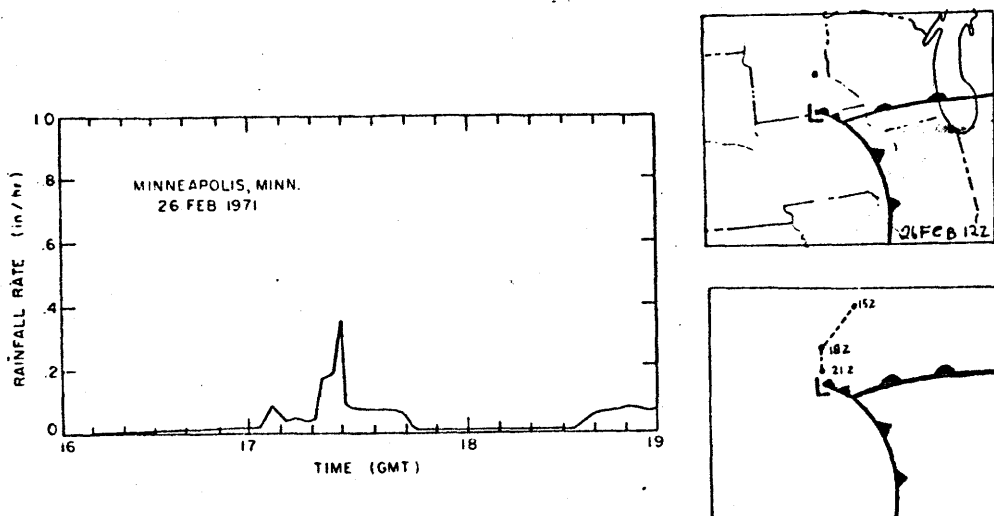
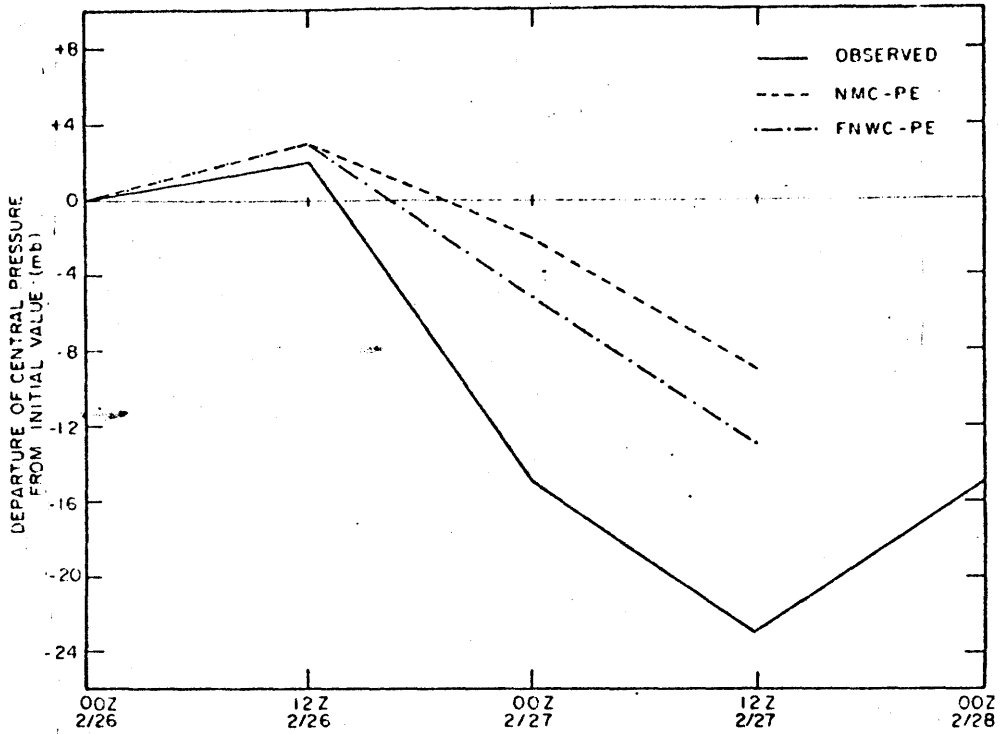
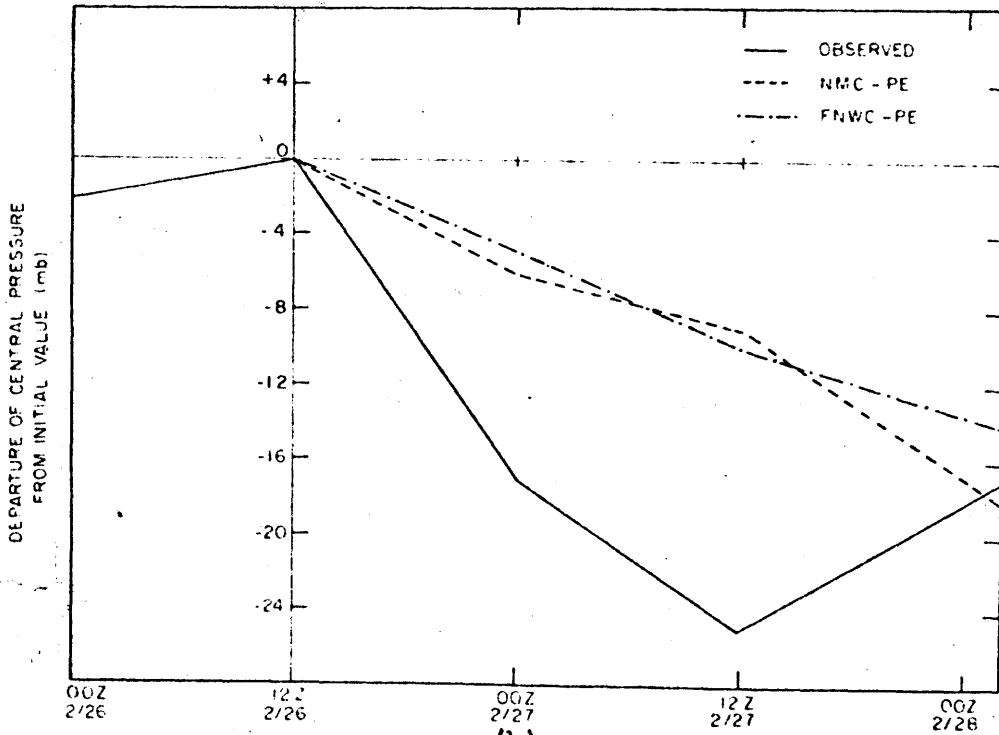


Fig. 57. Precipitation cross section. Same as Fig. 3, except for Minneapolis, Minn.



(a)



(b)

Fig. 58. Observed and forecast central pressure vs. time in terms of departure from initial values at 00Z 26 Feb. 1971 (a) and 12Z 26 Feb. 1971 (b) (values plotted at 12-hour intervals).



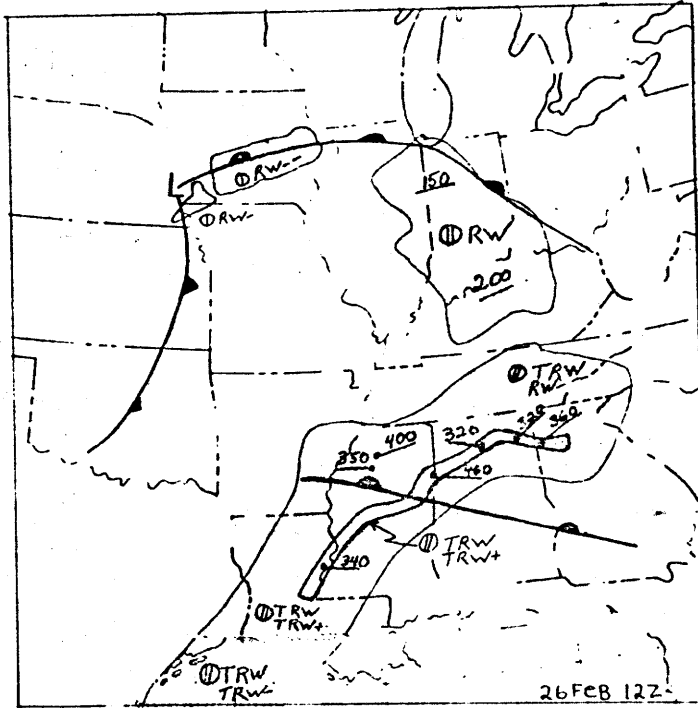


Fig. 59. Surface-radar chart. Same as Fig. 2, except for times indicated.

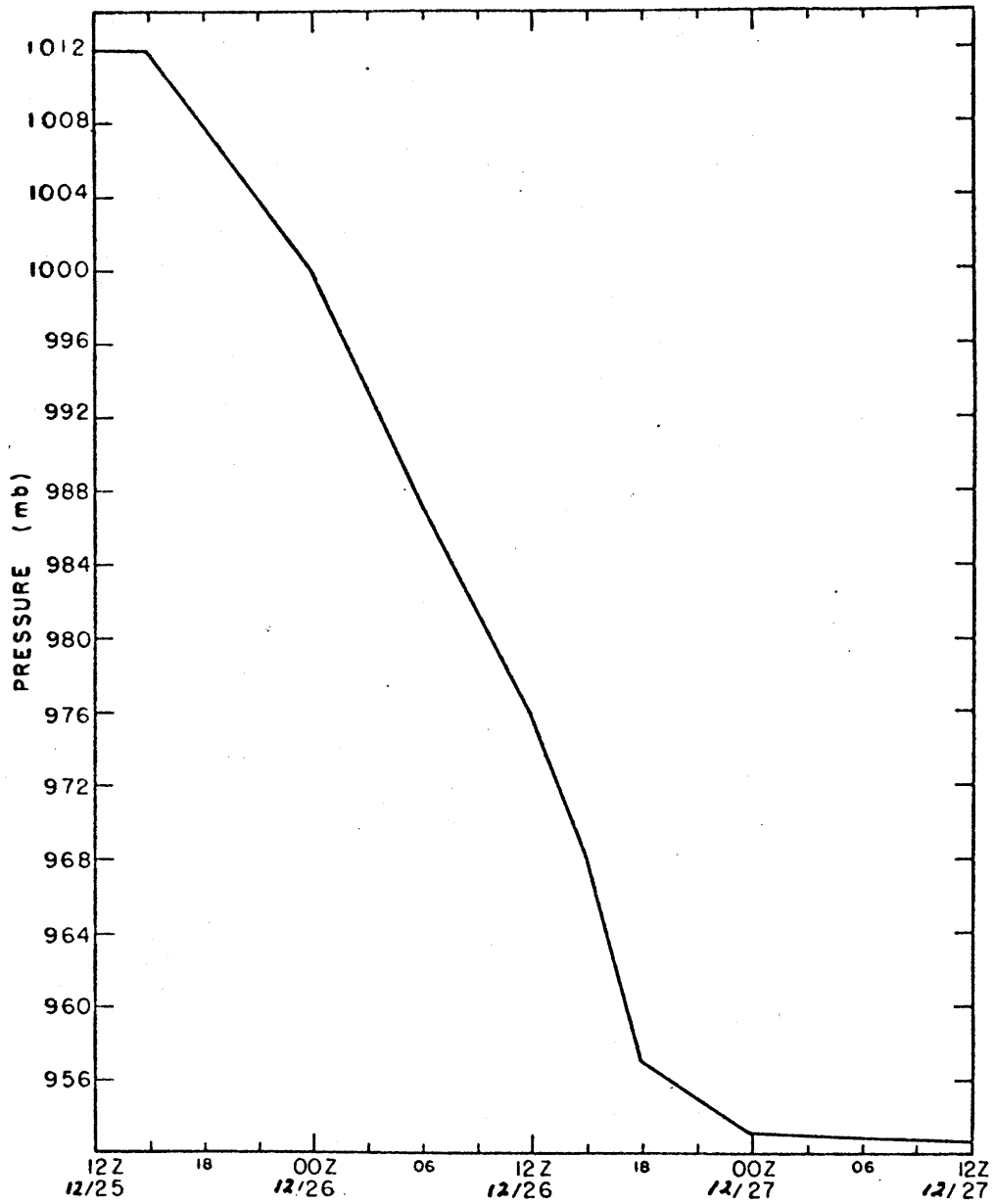
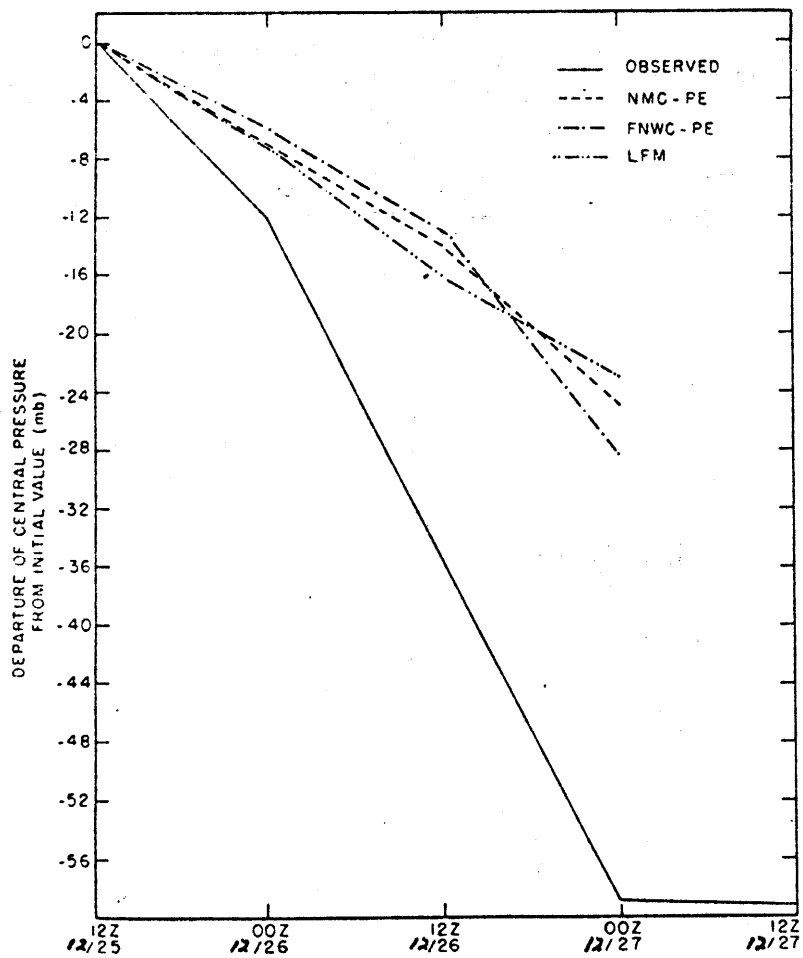
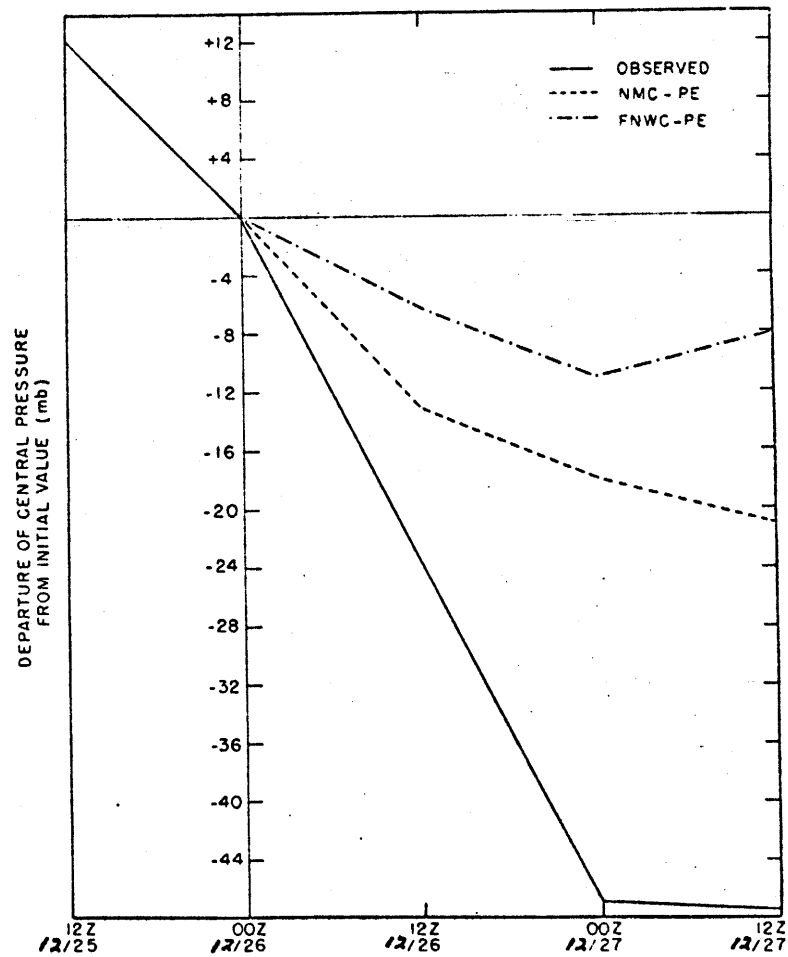


Fig. 60. Observed central pressure vs. time (plotted generally at 3-hour intervals).



(a)



(b)

Fig. 61. Observed and forecast central pressure vs. time in terms of departure from initial values at 12Z 25 Dec. 1970 (a) and 00Z 26 Dec. 1970 (b).

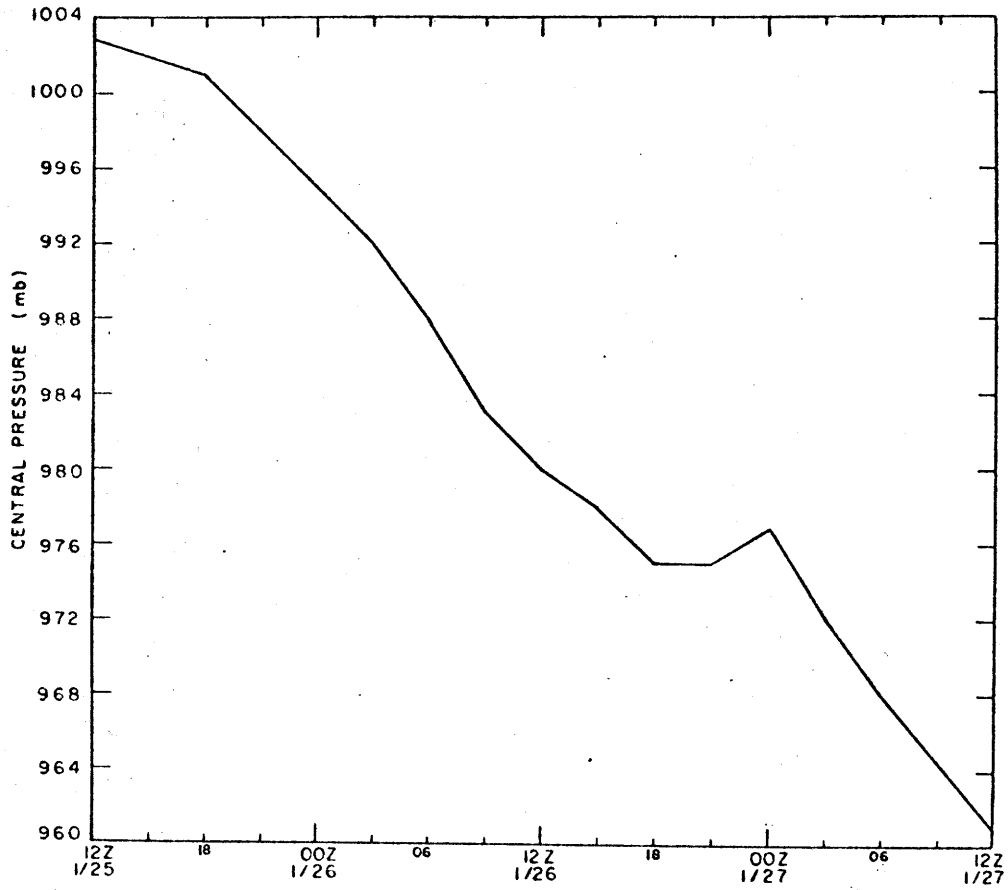
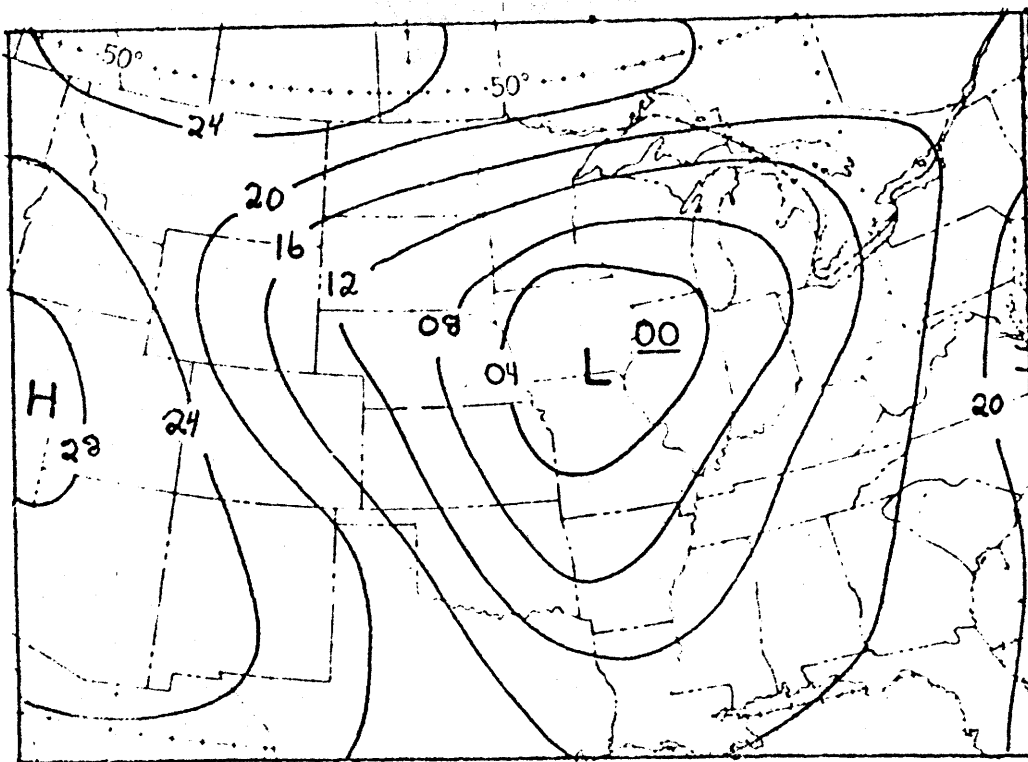
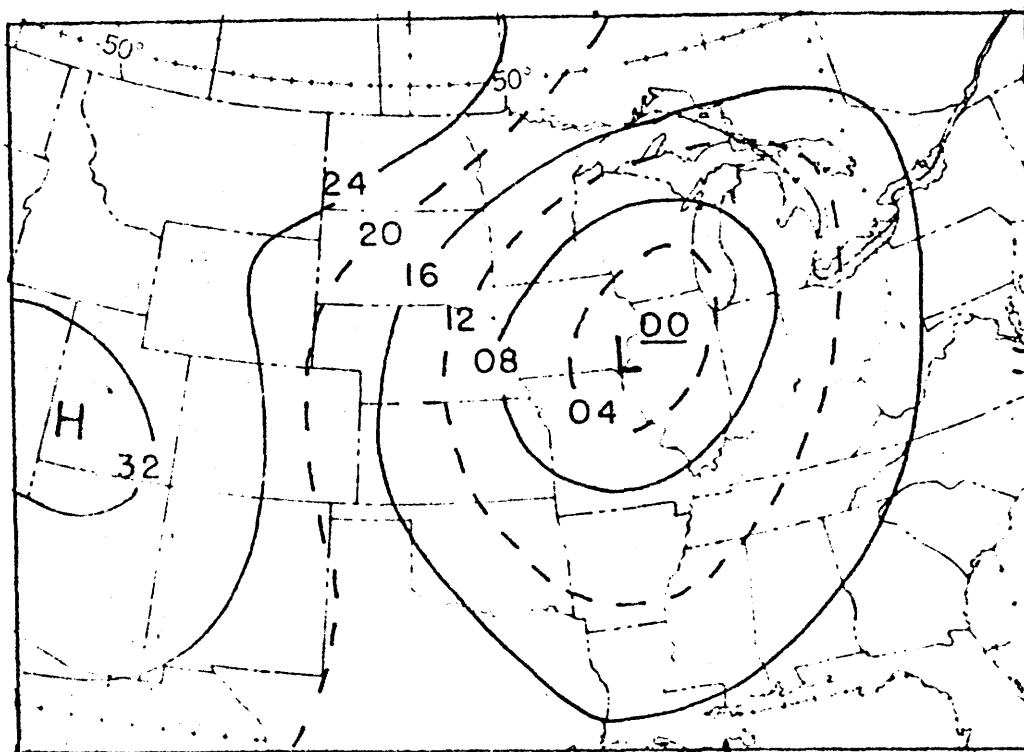


Fig. 62. Observed central pressure vs. time (plotted generally at 3-hour intervals).

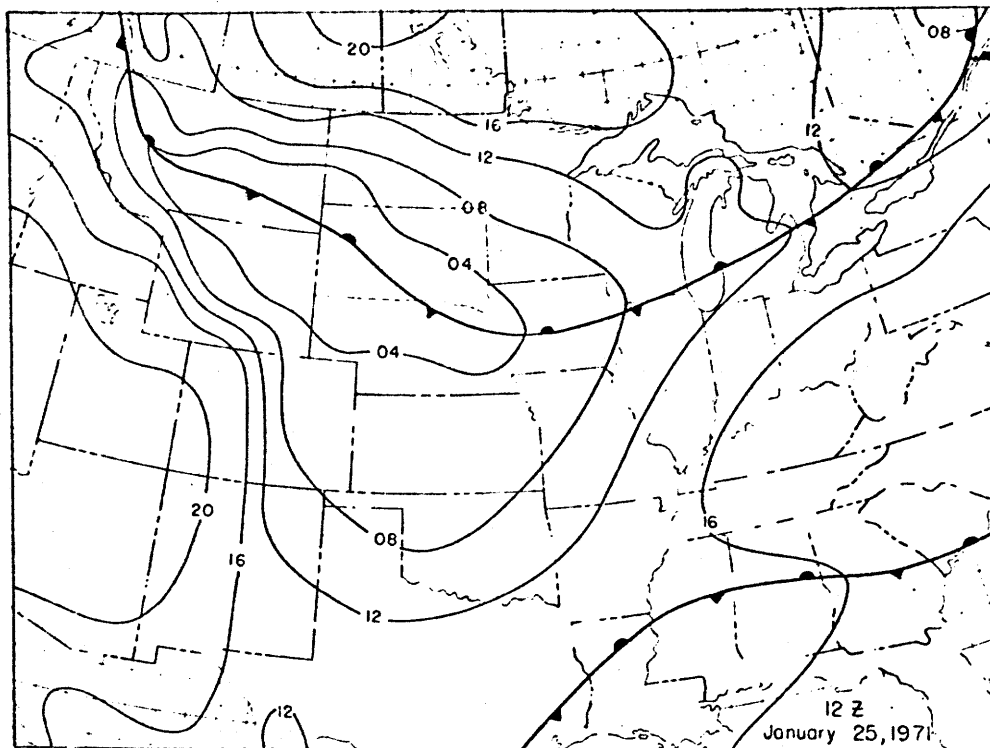


(a)

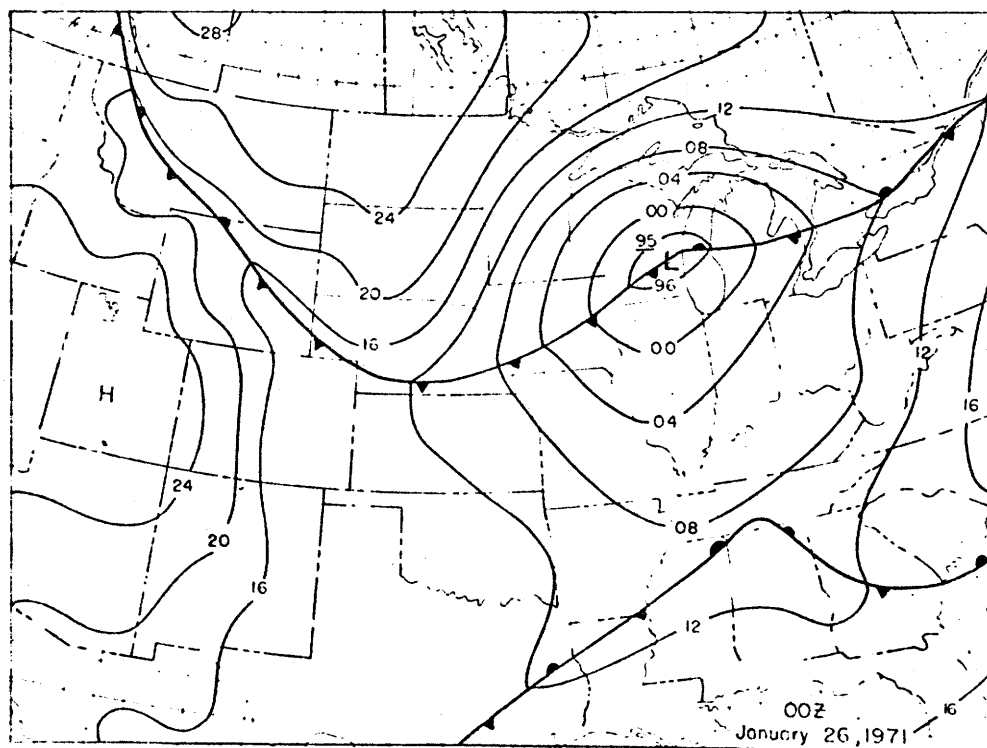


(b)

Fig. 63. See next page.

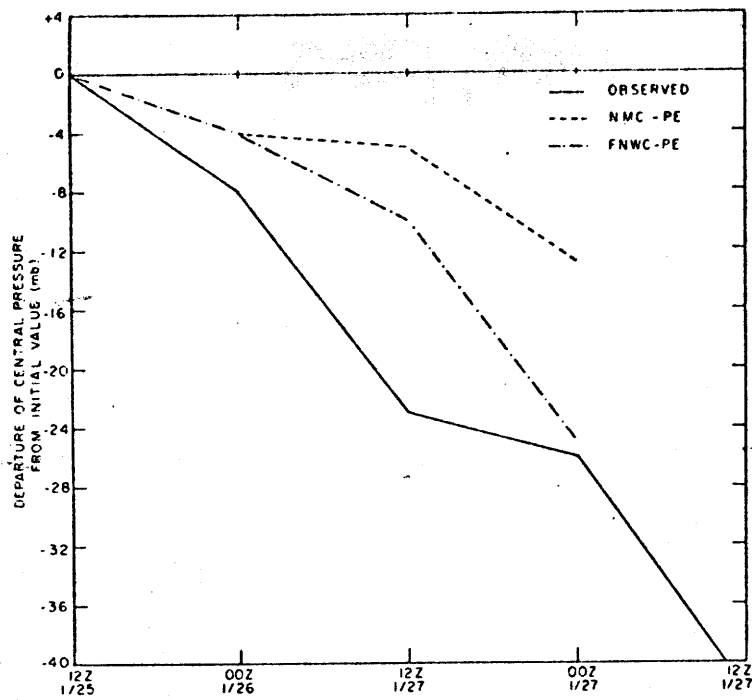


(c)

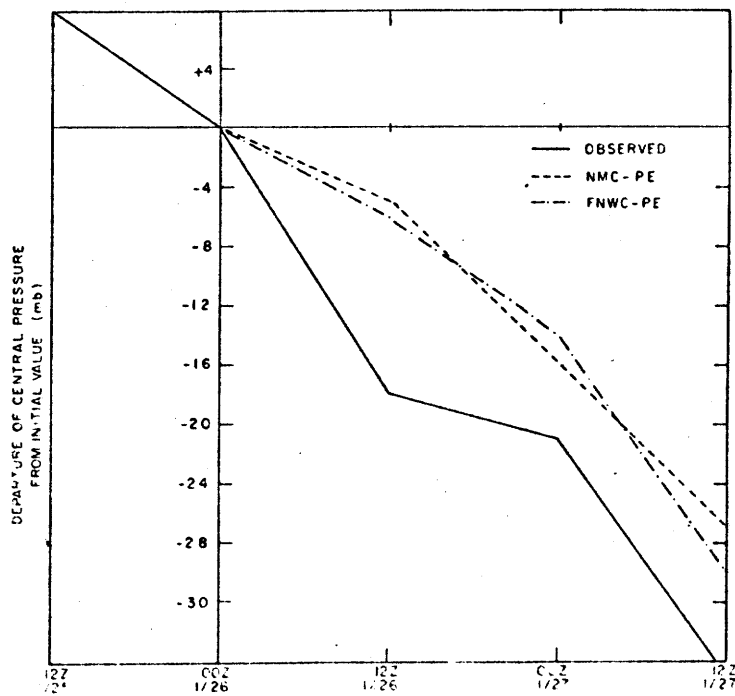


(d)

Fig. 63. FNWC-PE (a) and NMC-PE (b) 12-hour sea-level pressure forecasts from 12Z 25 Jan. 1971 (c) verifying at 00Z 26 Jan. (d).

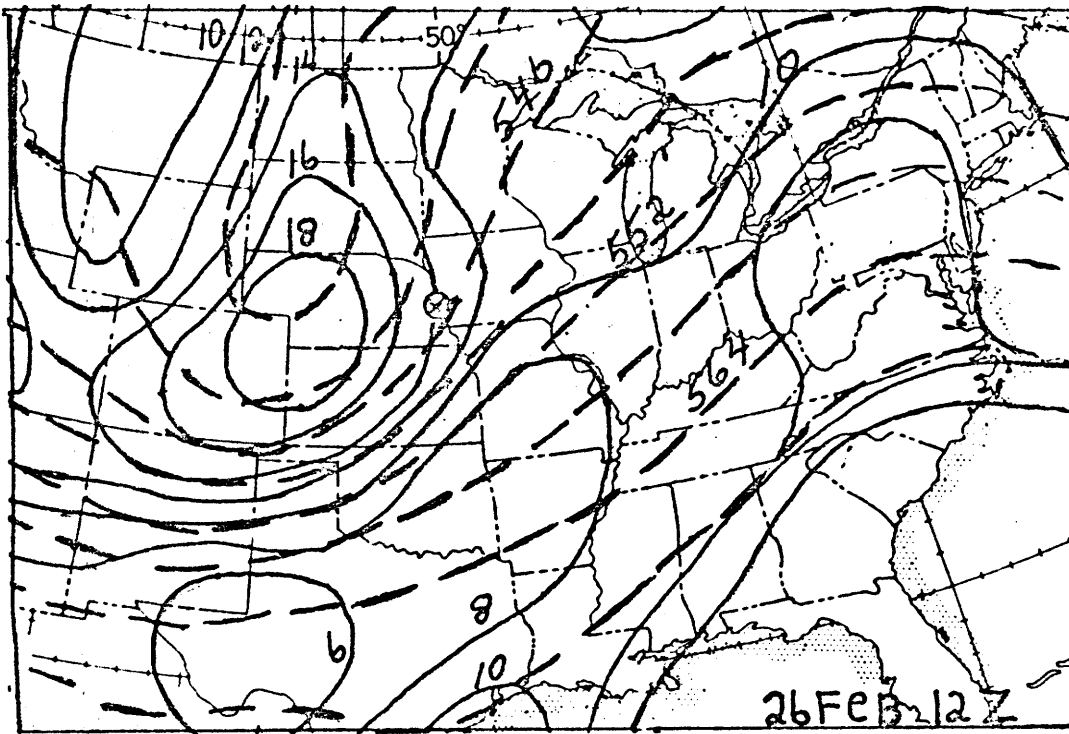


(a)

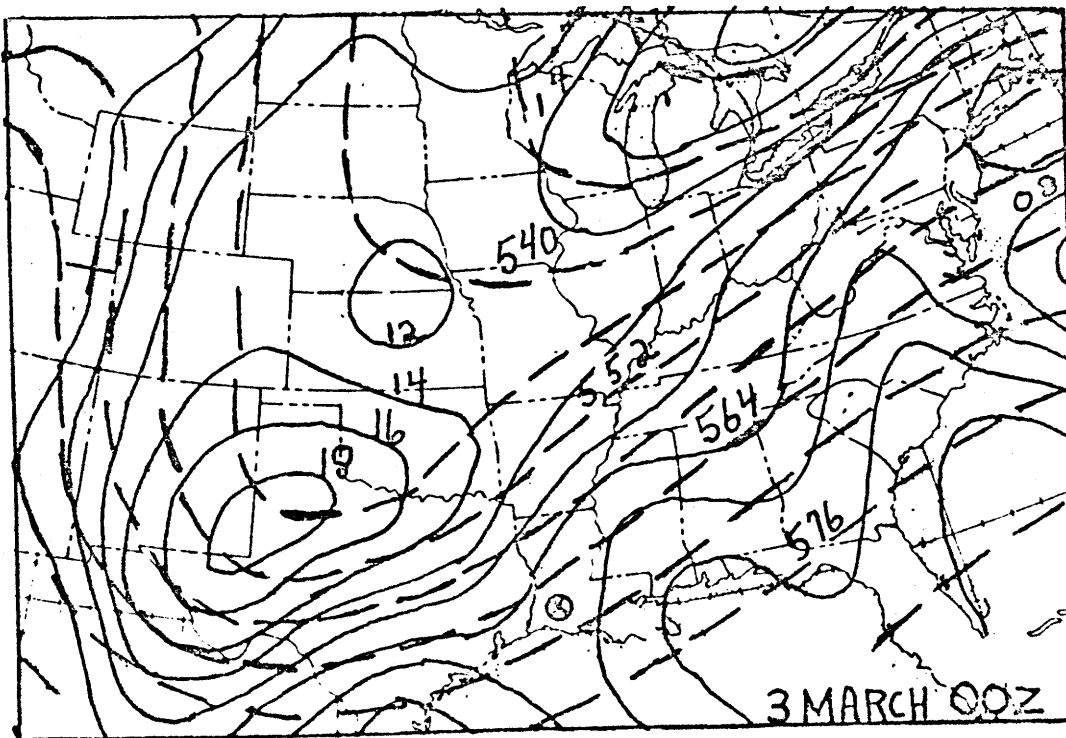


(b)

Fig. 64. Observed and forecast central pressure vs. time in terms of departure from initial values at 12Z 25 Jan. 1971 (a) and 00Z 26 Jan. 1971.



(a)



(b)

Fig. 65. 500 mb height and vorticity at time of initial development of Case VII (a) and Case IV (b).  $\otimes$  indicates position of incipient low center. Vorticity advection (geostrophic) is inversely proportional to size of quadrilaterals formed by the contours and isopleths. Note, vorticity advection over low in Case VII (a) is greater, qualitatively speaking, than in Case IV. The initial development of Case IV was accompanied by a significant outbreak of convection, while Case VII was not.



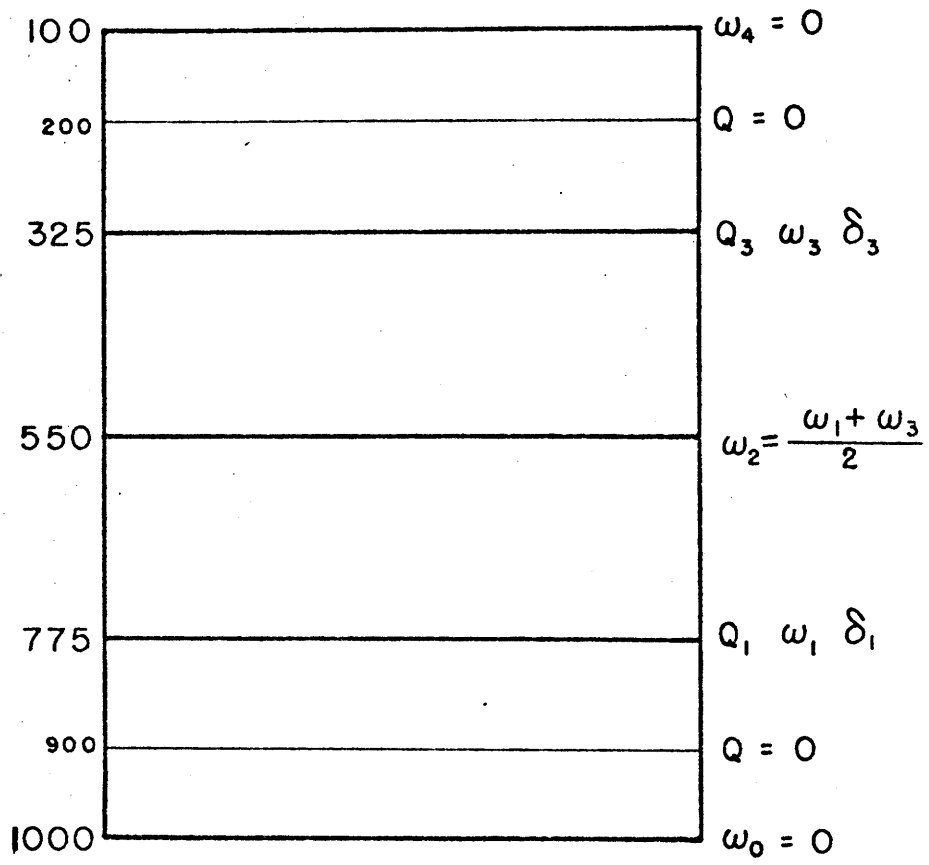
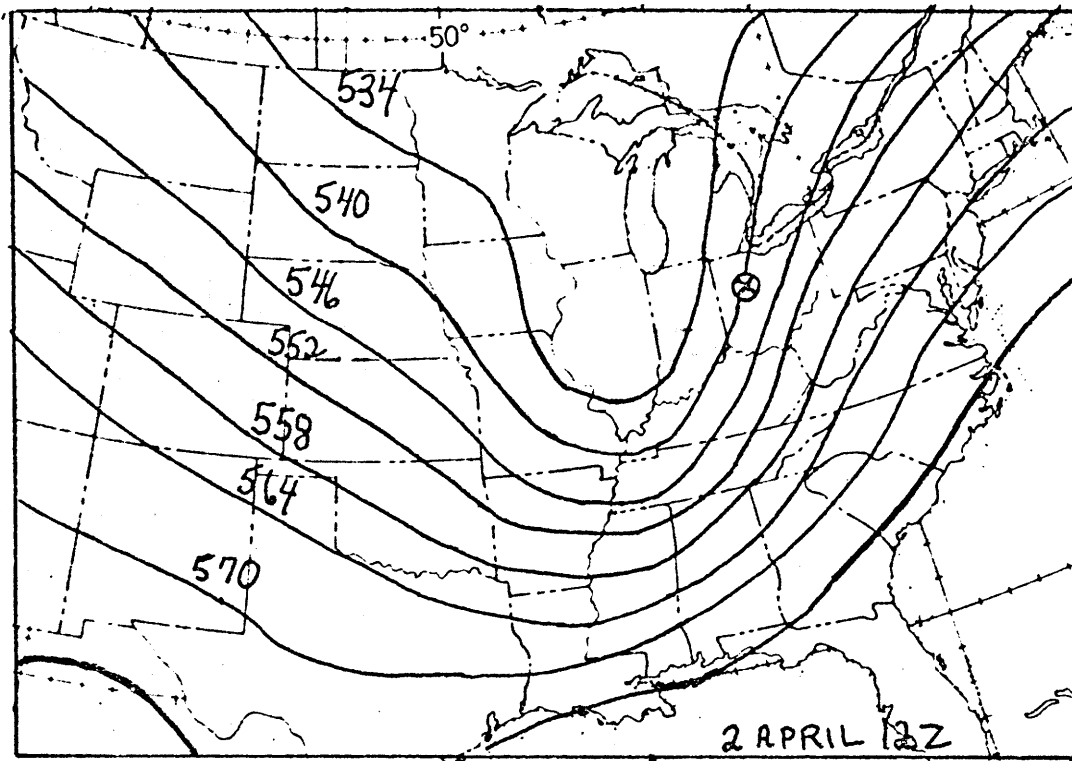
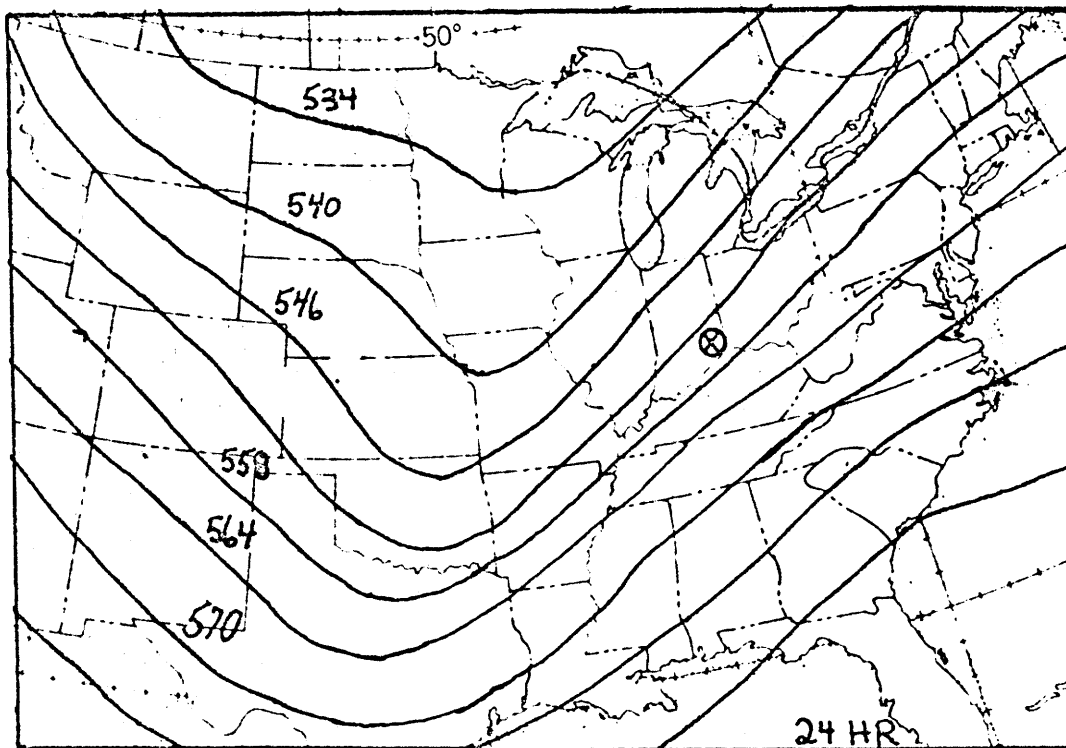


Fig. 66. Vertical structure of model utilized in solution of the omega and vorticity equations.

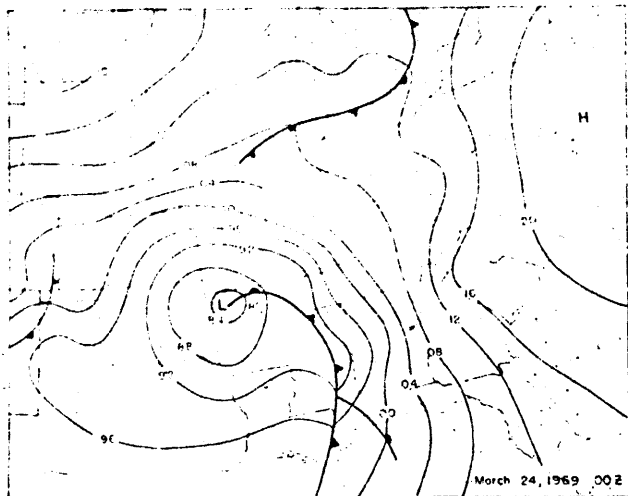


(a)

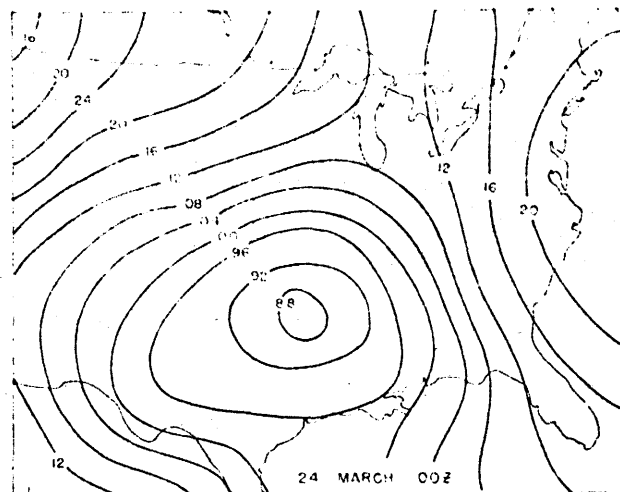


(b)

Fig. 67. - (a) 500 mb analysis for 12Z 2 April 1970; (b) NMC-PE 24-hour 500 mb forecast from 12Z 1 April 1970 (verifying at same time as "a"). ⊗ indicates respective positions of observed and forecast center of low pressure.



(a)



(b)

Fig. 68.- (a) Operational (NMC), manually drawn sea-level pressure analysis; (b) NMC objective analysis of field of sea-level pressure for same time as "a" (tracing of the contoured grid-point data). Central pressure of low in "b" as dictated by a grid point in low center, is 987 mb.

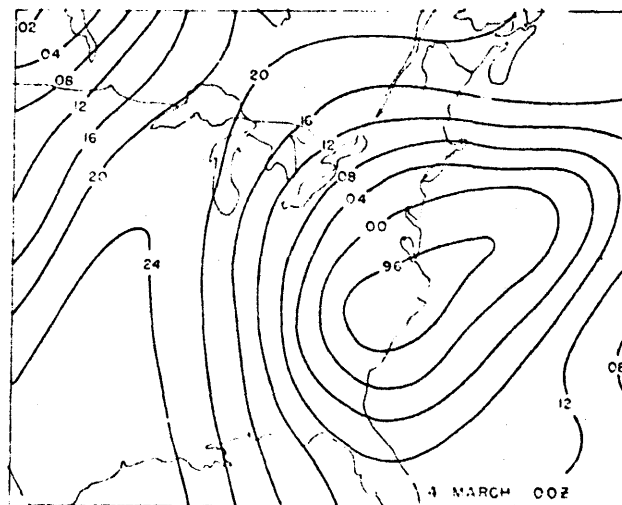
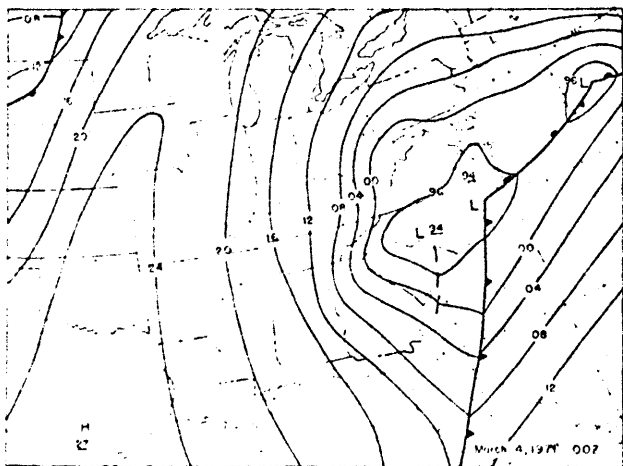


Fig. 69. Same as Fig. 68, except for time indicated. Central pressure of low center in "b" is 995 mb.

APPENDIX A

DETERMINATION OF THE INITIALIZED  
VALUES OF CENTRAL PRESSURE

In order to determine the initial 12-hour forecast change of central pressure, it is, of course, necessary to know the value of the initial state from which the prognosis is generated. This value, however, is not necessarily the same as that of the corresponding operational surface analysis (NMC) used to trace the actual storm development. The former is derived from an objective analysis of the surface data to an array of rather widely-spaced grid points, while the latter is obtained from a detailed manual analysis. Thus, since the objectively analyzed initial conditions are essentially a smoothed version of the operational surface charts, the value of central pressure from which a forecast is generated is generally somewhat greater than that of the corresponding manual analysis. The magnitude of the differences is primarily a function of the intensity of the system in question and the amount of data incorporated in each type of analysis. Fig. 68, for example, compares the manual and objective analyses (NMC-PE) of the field of sea-level pressure for 00Z 24 March 1969 (Case VI). The more detailed operational analysis indicates the intense low in Arkansas has a central pressure of 982 mb. The central pressure derived

from the objective analysis, on the other hand, is 987 mb. At this point, it should be noted that the NMC objective analysis scheme utilizes only "SM" surface observations, while the manually-plotted charts incorporate both "SM" and the more dense network of "airways" observations. In this particular example, the 982 mb value of central pressure is dictated by an observation that does not enter the objective analysis routine. If one, in fact, eliminated the airways observations from consideration, the manual analyses would indicate a 985 mb low, or 2 mb rather than 5 mb less than the objective analysis value.

As a further example, Fig. 69 presents the objectively and manually produced surface analyses for 00Z 4 March 1971. The lowest pressure indicated by the operational analysis for the East Coast system is 984 mb. The minimum of pressure derived from the objective analysis is 985 mb. In this situation, the gradient within the central region of the low is quite flat. Furthermore, the surface station reporting the lowest pressure is a "SM" station, and therefore, this observation is part of the input to the objective analysis scheme.

For several cases (see Table 2), the actual objective analyses were not available. On such occasions it was therefore necessary to estimate the initialized values of central pressure on the basis of experience gained from comparisons, as exemplified above, of the manually-produced surface charts with the corresponding objective analyses. In practice, surface analyses were constructed

utilizing only "SM" observations. The value of central pressure derived from these analyses was then subjectively adjusted upward by generally 1 or 2 mb, depending upon the gradient about the system in question.

It should be noted that the FNWC objective analyses were not available for the cases where the FNWC-PE forecasts were considered. It was inherently assumed, therefore, that the initialized values of central pressure from which the FNWC-PE forecasts were generated were the same as for the NMC-PE prognoses. Subsequent to completion of the case studies, however, it was learned that the FNWC objective analysis scheme does utilize the airways as well as the "SM" surface observations; however, careful re-examination of the pertinent initialized values of central pressure revealed that in no instance would incorporation of the airways observations have modified the subjectively estimated value by more than an insignificant 1 mb. (This is primarily because initial conditions of pertinent cases feature relatively flat gradients that are well-defined by "SM" observations alone). An additional point is that the estimated values of the initialized central pressure for the two detailed case studies in which LFM forecasts were considered were the same as the actual values derived by the LFM objective analysis scheme.

APPENDIX B

METHOD UTILIZED IN OBTAINING SOLUTIONS  
OF THE  
QUASI-GEOSTROPHIC OMEGA AND VORTICITY EQUATIONS

With vertical derivatives expressed in finite difference form (and  $\zeta \equiv P / p_0$ ), the omega equation (Eq. 1) applied to levels 1 and 3 (Fig. 66) becomes:

$$\nabla^2 \omega_1 + \frac{f_0^2}{\delta_1 p_0^2} \frac{(\omega_3 - 3\omega_1)}{2(\Delta \zeta)^2} = -\frac{R}{c_p p_0 \delta_1} \nabla^2 Q_1 \quad (I)$$

$$\nabla^2 \omega_3 + \frac{f_0^2}{\delta_3 p_0^2} \frac{(\omega_1 - 3\omega_3)}{2(\Delta \zeta)^2} = -\frac{R}{c_p p_0 \delta_3} \nabla^2 Q_3 \quad (II)$$

$Q_1$  and  $Q_3$  are related to each other and to the precipitation rate,  $P$ , as follows:

$$Q_3 = \gamma Q_1 = EP = E P_m e^{-[\kappa^2/A^2 + \eta^2/B^2]} \quad (III)$$

where

$$E \equiv \frac{2g L \rho_{H_2O}}{575 p_0 (1+\gamma)}$$

$\omega_1$ ,  $\omega_3$  and  $P$  can be expressed in terms of their Fourier transforms,  $\omega_1^*$ ,  $\omega_3^*$  and  $P^*$ :

$$\omega_1(x, y) = \iint_{-\infty}^{\infty} \omega_1^*(k, l) e^{i2\pi(kx + ly)} dk dl \quad (IV)$$

$$\omega_3(x, y) = \iint_{-\infty}^{+\infty} \omega_3^*(k, l) e^{i2\pi(kx+ly)} dk dl \quad (V)$$

$$P(x, y) = \iint_{-\infty}^{+\infty} P^*(k, l) e^{i2\pi(kx+ly)} dk dl \quad (VI)$$

When these expressions are substituted into Eqs. I and II, the following relations are obtained:

$$-(\delta_1 M^2 + 3N) \omega_1^* + N \omega_3^* = \frac{KEM^2 P^*}{\beta_1 \gamma} \quad (VII)$$

$$-(\delta_3 M^2 + 3N) \omega_3^* + N \omega_1^* = \frac{KEM^2 P^*}{\beta_3} \quad (VIII)$$

where

$$M \equiv 4\pi^2 (k^2 + l^2)$$

$$N \equiv \frac{1}{2} \left( \frac{b_0}{\rho_0 \Delta z} \right)^2$$

$$K \equiv \frac{R}{c_r \rho_0}$$

Elimination of  $\omega_3^*$  from Eqs. VII and VIII yields

$$\omega_1^* = - \frac{P^* K M^2 E [\beta_1 \gamma N + \beta_3 (\delta_3 M^2 + 3N)]}{\beta_1 \beta_3 \gamma [3NM^2 (\delta_1 + \delta_3) + \delta_3 \delta_1 M^4 + 8N^2]} \quad (IX)$$

while elimination of  $\omega_1^*$  from Eqs. VII and VIII yields



$$W_3^* = \frac{P^* K M^2 E [3_3 N + 3_1 \gamma (\delta_1 M^2 + 3N)]}{3_1 3_3 \gamma [3 N M^2 (\delta_1 + \delta_3) + \delta_1 \delta_3 M^4 + 8N^2]} \quad (X)$$

Eqs. IX and X represent the particular solutions of Eqs. I and II. With the boundary conditions  $W_0 = W_4 = 0$ , it can be shown that the homogeneous solutions are identically zero.

The Fourier transform of P can be obtained by application of the appropriate theorems of two-dimensional Fourier transforms to the tabulated expression of the Fourier transform of  $e^{-\gamma(x^2+y^2)}$  (see, e.g., The Fourier Transform and Its Applications, McGraw-Hill, 1965, pp. 244-248). The result is

$$P^* = A B \pi e^{-\gamma^2(A^2 k^2 + B^2 l^2)} \quad (XI)$$

Substitution of Eq. XI into Eqs. IX and X, followed by substitution of the results into Eqs. IV and V yields the following for  $W_1$  and  $W_3$  (real part):

$$W_1 = \frac{4AB\gamma^3 K E}{3_1 3_3 \gamma} \int_{l=-\infty}^{\infty} \left\{ \int_{k=-\infty}^{\infty} \frac{(k^2+l^2)[N(3_1 \gamma + 3_3) + 4\gamma^2 3_3 \delta_3 (k^2+l^2)]}{[12\gamma^2 N(k^2+l^2)(\delta_1 + \delta_3) + 16\gamma^4 \delta_3 \delta_1 (k^2+l^2) + 8N^2]} \times \right. \\ \left. \cos 2\gamma(kx+ly) e^{-\gamma^2 A^2 k^2} dk \right\} e^{-\gamma^2 B^2 l^2} dl \quad (XII)$$

$$W_3 = \frac{4AB\gamma^3 K E}{3_1 3_3 \gamma} \int_{l=-\infty}^{\infty} \left\{ \int_{k=-\infty}^{\infty} \frac{(k^2+l^2)[N(3_3 + 3_1 \gamma) + 4\gamma^2 3_1 \gamma \delta_1 (k^2+l^2)]}{[12\gamma^2 N(k^2+l^2)(\delta_1 + \delta_3) + 16\gamma^4 \delta_1 \delta_3 (k^2+l^2) + 8N^2]} \times \right. \\ \left. \cos 2\gamma(kx+ly) e^{-\gamma^2 A^2 k^2} dk \right\} e^{-\gamma^2 B^2 l^2} dl \quad (XIII)$$

With the substitution

$$R = A/A\pi$$

$$f = \pi/\beta\pi$$

Eqs. XII and XIII take on a form suitable for numerical evaluation via the 10-point Gaussian Hermite Quadrature Formulation described in the IBM manual Scientific Subroutine Package (p. 107).

In order to obtain a value of  $\partial w / \partial z$  at 1000 mb ( $\beta = 1$ ) and hence, enable solution of the vorticity equation,

$$\nabla^2 \frac{\partial \phi}{\partial t} = \frac{f_0^2}{f_0} \frac{\partial w}{\partial z},$$

(XIV)

for the 1000 mb geopotential tendency (or sea-level pressure tendency), a parabolic profile was fit to  $w_0 = 0$ ,  $w_1$ , and  $w_2$  ( $w_2 = \frac{w_1 + w_3}{2}$ ). That is, the equation for the parabola

$$w = (1-\beta)^2 a + (1-\beta)b + c$$

was applied to levels  $\beta_0 = 1$ ,  $\beta_1 = .775$  and  $\beta_2 = .55$  to obtain the coefficients a, b, and c in terms of  $w_0$ ,  $w_1$ , and  $w_3$ . Since  $c = 0$  ( $w_0 = 0$  at  $\beta = 1$ ),

$$\left. \frac{\partial w}{\partial \beta} \right|_{\beta=1} = -b$$

(XV)

so that all that is required is the coefficient b. Algebraic manipulation yields

$$b = 7.7w_1 - 1.1w_3$$

(XVI)

The geopotential tendency,  $\frac{\partial \phi}{\partial t} = \chi$ , can be written in terms of its Fourier transform:

$$\chi(x, y) = \iint_{-\infty}^{\infty} \chi^*(k, l) e^{i2\pi(kx + ly)} dk dl \quad (\text{XVII})$$

Substitution of Eqs. XV, XVI, and XVII (with  $W_1$  and  $W_3$  also written in terms of their Fourier transforms) into Eq. XIV yields:

$$\chi^* = \frac{\beta_0^2}{M^2 \gamma_0} [7.7 W_1^* - 1.1 W_3^*] \quad (\text{XVIII})$$

When Eq. XVIII is combined with Eqs. IX, X, and XI, the real part of the solution of Eq. XVII becomes:

$$\chi = -\frac{7.7 \beta_0^2 K \epsilon A B \gamma}{P_0 \beta_1 \beta_3 \gamma} \int_{l=-\infty}^{\infty} \left\{ \int_{k=-\infty}^{\infty} \frac{[N(\beta_1 \gamma + \beta_3 \delta_3) + 4\pi^2 (k^2 + l^2)] \cos 2\pi(kx + ly) e^{-\pi A^2 k^2}}{12\pi^2 N(k^2 + l^2)(\delta_1 + \delta_3) + 16\pi^4 \delta_3 \delta_1 (k^2 + l^2) + 8N^2} dk \right\} e^{-\pi^2 \beta_3^2 l^2} dl \quad (\text{XIX})$$

$$- 1.1 \frac{\beta_0^2 K \epsilon A B \gamma}{P_0 \beta_1 \beta_3 \gamma} \int_{l=-\infty}^{\infty} \left\{ \int_{k=-\infty}^{\infty} \frac{[N(\beta_3 + \beta_3 \gamma) + 4\pi^2 \beta_1 \gamma \delta_1 (k^2 + l^2)] \cos 2\pi(kx + ly) e^{-\pi A^2 k^2}}{12\pi^2 N(k^2 + l^2)(\delta_1 + \delta_3) + 16\pi^4 \delta_1 \delta_3 (k^2 + l^2) + 8N^2} dk \right\} e^{-\pi^2 \beta_3^2 l^2} dl$$

With the substitution

$$k = \rho / A \pi$$

$$l = \tau / B \pi$$

Eq. XIX can be solved via the 10-point Gaussian Hermite Quadrature Formulation.

BIOGRAPHICAL SKETCH

The author was born on February 9, 1945, in Brockton, Massachusetts. He attended Brockton public schools, graduating with honors from Brockton High School in 1962. Thereafter, he entered the University of Massachusetts, Amherst, where he majored in physics with the intent of studying meteorology at the graduate level. In June of 1966, he graduated from U of Mass. magna cum laude and was awarded a Bachelor of Science. He was elected to Phi Beta Kappa and Phi Kappa Phi.

The author married Bette L. Richman, also from Brockton, in June, 1966. In the fall of that year, he entered the Massachusetts Institute of Technology to pursue his studies in meteorology. The author received his Master of Science in February, 1969, and was elected to Sigma Xi.

REFERENCES

- Aubert, E. F., 1957: On the release of latent heat as a factor in large-scale atmospheric motions. J. Meteor., 14, pp. 527-542.
- Austin, P. M. and R. A. Houze, Jr., 1972: Analysis of the structure of precipitation patterns in New England. Accepted for publication, J. Appl. Meteor.
- Bullock, B. R. and D. R. Johnson, 1971: The generation of available potential energy by latent heat release in a mid-latitude cyclone. Mon. Wea. Rev., 99, pp. 1-14.
- Charney, J. G., 1947: The dynamics of long waves in a baroclinic westerly current. J. Meteor., 4, pp. 135-162.
- Charney, J. G., and A. Eliassen, 1964: On the growth of the hurricane depression. J. Atmos. Sci., 21, pp. 68-75.
- Danard, M. B., 1964: On the influence of released latent heat on cyclone development. J. Appl. Meteor., 3, pp. 27-37.
- Danard, M. B., 1966: On the contribution of released latent heat to changes in available potential energy. J. Appl. Meteor., 5, pp. 81-93.
- Eady, E. T., 1949: Long waves and cyclone waves. Tellus, 1, pp. 33-52.
- Fawbush, E. J., R. C. Miller, and L. G. Starrett, 1951: An empirical method of forecasting tornado development. Bull. Amer. Meteor. Soc., 32, pp. 1-9.
- Fawcett, E. B., 1967: A preliminary evaluation of the six-layer model's performance in winter. Note to Forecasters, Feb. 17, 1967, U. S. Dept. of Commerce, Weather Bureau, Weather Analysis and Forecast Division, 15 pp.
-

- Fawcett, E.B., 1969: Systematic errors in the operational baroclinic prognoses at the National Meteorological Center. Mon. Wea. Rev., 97, pp. 670-682.
- Howcroft, J.G., 1971: Local forecast model: Present status and preliminary verification. Office Note 50, U. S. Dept. of Commerce, National Oceanic and Atmospheric Administration, National Weather Service, 22 pp.
- Kasahara, A. and T. Asai, 1967: Effects of an ensemble of convective elements on the large-scale motions of the atmosphere. J. Met. Soc. Japan, Ser. 2, 45, pp. 280-290.
- Kesel, P. and F. Winninghoff, 1970: Fleet Numerical Weather Central's four-processor primitive equation model. Paper presented to Joint Technical Exchange Conference, U. S. Naval Academy, Annapolis, Md., September 1970, 23 pp.
- Kuo, H.L., 1965: On the formation and intensification of tropical cyclones through latent heat release by cumulus convection. J. Atmos. Sci., 22, pp. 40-63.
- Melvin, G.L., 1968: The development of thunderstorm complexes and their associated vertical transports. SM Thesis, Dept. of Met., MIT, Cambridge, Mass., 65 pp.
- Ooyama, K., 1967: Numerical simulation of the life cycle of tropical cyclones. J. Atmos. Sci., 26, pp. 3-40.
- Palmen, E. and C. W. Newton, 1969: Atmospheric Circulation Systems. Academic Press, New York, 603 pp.
- Petterssen, S., et al., 1954: Report on an experiment with forecasting cyclone development. Tech. Rept. No. 4, Univ. of Chicago, 21 pp.

Petterssen, S., 1956: Weather Analysis and Forecasting. McGraw-Hill Book Co., Inc., New York, 428 pp.

Phillips, N.A., 1963: Geostrophic motion. Reviews of Geophysics, 1, pp. 123-176.

Riehl, H. and J. Malkus, 1961: Some aspects of hurricane Daisy. 1958, National Hurricane Research Report No. 33, 63 p.

Shuman, F.G. and J. B. Hovermale, 1968: An operational six-layer primitive equation model. J. Appl. Meteor., 7, pp. 525-547.

Tracton, M.S., 1969: The role of cellular convection within an extratropical cyclone. SM Thesis, Dept. of Met., MIT, Cambridge, Mass., 51 pp.